الجمهورية الجزائرية الديمقراطية الشعبية
République Algérienne Démocratique et Populaire
وزارة التعليم العالي و البحث العلمي
Ministère de l'Enseignement Supérieur et de la Recherche Scientifique

المدرسة الوطنية المتعددة التقنيات
Ecole Nationale Polytechnique

École Nationale Polytechnique
Département d'Électronique
Département de Génie Mécanique
Institut catholique d'arts et métiers Nantes

End of studies project thesis

Submitted in partial fulfillment of the requirements
for the State Engineer Degree in Electronic / Mechanical Engineering

Nondestructive approach for pavement surface roughness assessment

Realized by:
Mr. BOUZIDI Abdelaziz
Ms. BOUMENDJEL Anfal

Supervised by:
Mr. Pinel Nicolas
Mr. Adnane Mourad
Mr. Sedjal Hamid

Publicly presented and defended on the 06th of July, 2022.

Jury members:

President	Mr. Yacine Belkacemi	Dr MAA	ENP
Examiner	Mr. Mohamed Oussaid Taghi	MAA	ENP

ENP 2022

الجمهورية الجزائرية الديمقراطية الشعبية
République Algérienne Démocratique et Populaire
وزارة التعليم العالي و البحث العلمي
Ministère de l'Enseignement Supérieur et de la Recherche Scientifique

المدرسة الوطنية المتعددة التقنيات
Ecole Nationale Polytechnique

École Nationale Polytechnique
Département d'Électronique
Département de Génie Mécanique
Institut catholique d'arts et métiers Nantes

End of studies project thesis

Submitted in partial fulfillment of the requirements
for the State Engineer Degree in Electronic / Mechanical Engineering

Nondestructive approach for pavement surface roughness assessment

Realized by:
Mr. BOUZIDI Abdelaziz
Ms. BOUMENDJEL Anfal

Supervised by:
Mr. Pinel Nicolas
Mr. Adnane Mourad
Mr. Sedjal Hamid

Publicly presented and defended on the 06th of July, 2022.

Jury members:

President	Mr. Yacine Belkacemi	Dr MAA	ENP
Examiner	Mr. Mohamed Oussaid Taghi	MAA	ENP

ENP 2022

الجمهورية الجزائرية الديمقراطية الشعبية
République Algérienne Démocratique et Populaire
وزارة التعليم العالي و البحث العلمي
Ministère de l'Enseignement Supérieur et de la Recherche Scientifique

المدرسة الوطنية المتعددة التقنيات
Ecole Nationale Polytechnique

École Nationale Polytechnique
Département de Génie Mécanique
Département d'Électronique
Institut catholique d'arts et métiers Nantes

Mémoire de projet de fin d'études

pour l'obtention du diplôme d'Ingénieur d'État en Électronique / Mécanique

Approche non destructive pour l'évaluation de la rugosité de la surface des chaussées

Réalisé par :
M. Bouzidi Abdelaziz
Mlle. Boumendjel Anfal

Supervisé par:
Mr. Pinel Nicolas
Mr. Adnane Mourad
Mr. Sedjal Hamid

Présenté et soutenue publiquement le 06 Juillet 2022.

Membres du jury :

Président	M. Yacine Belkacemi	Dr MAA	ENP
Examinateur	Mr Mohamed Oussaid Taghi	MAA	ENP

ENP 2022

‘To prosper, you must first build roads”, *Chinese proverbe*

ملخص

على مر التاريخ، اعتبرت الطريق واحدة من أكثر البنى التحتية أهمية للناس. ومع ذلك، فإن الأمر لا يتعلق فقط ببناءها، بل إن أهم شيء هو صيانتها والحفاظ عليها آمنة مع استخدامها بأكبر قدر ممكن من الكفاءة. لهذا نقترح طريقة جديدة، أسرع وأكثر دقة واقل طلبا لليد العاملة لتوصيف حالة سطح الطريق. في هذا السياق، ندرس طريقة يمكنها استبدال الوسائل التقليدية المستخدمة لتوصيف السطوح، والتي تتمثل في جهاز يمكنه توفير مقاييس حددتها المعاييرالدولية، مثل ال MTD (متوسط عمق القوام) باستخدام التثليث بالليزر، والذي يوفر معلومات قيمة عن حالة سطح الرصيف.

كلمات مفتاحية : توصيف السطوح, متوسط عمق القوام, التثليث بالليزر

Résumé

Tout au long de l’histoire, les routes ont été considérées comme l’une des infrastructures les plus importantes pour les populations. Néanmoins, il ne s’agit pas seulement de construire des routes, le plus important est de les entretenir, de les garder sûres et de les utiliser aussi efficacement que possible. C’est pourquoi nous proposons une nouvelle méthode, plus rapide, plus précise et moins coûteuse, pour caractériser la texture de nos routes. Nous étudions un cadre qui peut remplacer les méthodes traditionnelles utilisées pour la caractérisation de la surface, un instrument qui peut fournir des métriques définies par des organismes de normalisation internationaux, comme la PMT (Profondeur Moyenne de Texture), en utilisant la triangulation laser, qui offre des informations précieuses sur l’état de surface de la chaussée.

Mots clés : Caractérisation de la surface, Profondeur Moyenne de Texture, Triangulation laser

Abstract

Throughout history, roads have been considered one of the most critical infrastructures for people. Nevertheless, it is not only about building roads, the most important thing is to maintain them, keep them safe, and use them as efficiently as possible. That is why we are offering a new, faster, more precise, and labor-saving way to characterize our roads’ texture. We study a framework that can replace traditional methods used for surface characterization, an instrument that can provide metrics defined by international normalization organisms, such as the MTD (Mean Texture Depth), by using laser triangulation, which offers valuable information on the pavement surface condition.

Keywords : Surface texture characterization, MTD (Mean Texture Depth), laser triangulation.

Dedication

“

To my mother, who has always been my support system. Without her prayers, I would have never made it.

To my father, to my sister and best friend Nada, to my dear twin Rania, to the best siblings i can ask for Ahlam and Lokmane.

To my two cats Rocky and Silver, the delight of our home.

To my dearest friend Taki, who has never stopped helping and being there for me.

To everyone with whom I shared a happy memory in the past five years and made life a little easier.

To myself, for believing in me and never giving up even when it seemed like the easier option.

To Aziz, who became a dear friend during this journey.

”

- Anfal

Dedication

“

To my parents, my brothers and sisters and my family, those who give meaning to my life and whom I infinitely love.

To the memory of my grandfather, who always believed, supported, and encouraged me throughout his life, I wish I have made you proud.

To my uncle Hamza, who has been there for me whenever I asked and who helped with all of my struggles.

To my friends, Ouassim, Sabrinelle, Dina, and Malika whom I knew since my first day at the ENP and who have been with me since then.

To Sofiane, who's no longer a friend, he's actually a brother that had a tremendous impact in my life.

To all my classmates, who shared with me the Electronics department journey.

To Anfal who carried out this work with me and helped me get pass this challenge.

”

- Aziz

Acknowledgments

First of all, we thank God the Almighty for giving us the courage, the will and the patience to carry out this work.

We thank our parents, who supported us throughout our studies' journey.

We would like to express our gratitude to our supervisors from ENP, Mr.Sedjal Hamid and Mr.Adnane Mourad for their consistent support, guidance and clarifications during the running of this work.

We would like to thank Mr.Pinel Nicolas from Icam school of engineering, who accompanied us from the very beginning of this project, and was constantly helping us with his guidance and expertise, who also traveled all the way along from his mother country to Algeria to work with us, motivate our spirits, and push us to move forward.

We would like to thank Mr.Tahlaiti Mahfoud, the project manager for his help, availability and advice.

We would also like to thank in advance Mr. Yacine Belkacemi and Mr. Ouassaid Taghi Mohamed, for evaluating our work.

Each one of us would also like to thank the other, for having the courage to embark on such a complex project that ended up with creating a functional prototype, it was really a long journey filled with hardships and challenges, and we made it, together.

Contents

List of Figures

List of Tables

List of Abbreviations

MPD	*Mean Profile Depth*
MTD	*Mean Texture Depth*
TOF	*Time Of Flight*
ASTM	*American Society for Testing and Materials*
ISO	*International Organization for Standardization*
SMTD	*Sensor Mean Texture Depth*
ETD	*Estimated Texture Depth*
MSD	*Mean Segment Depth*
2D	*Two-Dimensional*
OFT	*Outflow Time*
IRI	*International Roughness Index*
RQCS	*Reference Quarter Car Simulation*
RMS	*Root Mean Square*
LCD	*Liquid Crystal Display*
3D	*Three-Dimensional*
Ssk	*Skewness*
Sku	*Kurtosis*
ASME	*American Society of Mechanical Engineers*
FDR	*False Discovery Rate*
GGD	*Genreralized Gaussian Distribution*
BRRC	*Belgian Road Research Centre*
SLAM	*Simultaneous Localisation and Mapping*
HD	*High Definition*

SSH *Secure Shell*

GPS *Global Positionning System*

IDRRIM *Institute for Roads, Streets and Infrastructures for Mobility*

General Introduction

Context and statement of the problem

Road surface texture has a significant influence on several traffic parameters related to the environment, economy, and safety since it has a direct relationship with tire/road interaction processes such as rolling resistance, friction, vehicle noise emission, and tire wear. As a result, the activity of studying pavement surface topography is a crucial part of their maintenance process to improve the conditions of travel for the drivers and passengers, and ensure their safety.

Current methodologies that describe pavements' roughness present several disadvantages that make them impractical and time-consuming. Current technologies for macro-texture evaluation rely either on two-dimensional (2D) methods using laser scanners to calculate the Mean Profile Depth (MPD), or volumetric methods, mainly the sand patch method as described in standards such as **NF EN 13 036-1** [1] in Europe, that measures the Mean Texture Depth (MTD). The MPD being a 2D parameter is not adequate to represent the texture and discards potentially useful information about the surface. As for the MTD, the method is manual and needs to be performed frequently, which makes it nonpractical, especially on roads that are open to traffic.

There is a need for a three-dimensional (3D) non-contact method to recover pavement surface texture, that can perform the task of characterizing and quantifying pavement surface texture, not only faster and safer, but also in a more accurate and reliable way, with calculating 3D texture indicators that are based on 3D cloud points.

Motivation and objectives

The urge of creating devices and instruments that are capable of performing on site surface characterization has been the motivation of multiple research and works in the last couple of decades, which is justified by the importance of these metrics with regard to drivers safety and the global road usage experience. Being able to characterize a surface with high accuracy without the need to put the roads out of service is a key factor in augmenting roads' effectiveness that highly affects sectors relying on transportation in general and that affect essential human beings needs.

This project aims essentially to provide and implement an affordable and innovative instrument that is based on a 3D non-contact method that can capture pavement surface texture at high resolution, and instantiate the needed metrics and information about pavement structures as defined in the various existing norms mainly the **NF EN 13 036-1** [1], as well as finding other parameters that can improve the characterization of the pavement. The information given by the different metrics can be used to monitor the road usage and identify problems that may occur in these excruciatingly important infrastructures. In addition to that, the 3D information provided with such an instrument can be used to simulate real world phenomena such as tire-road adhesion.

Work structure

The problematic is tackled following the steps:

- Setting the context of our work by presenting an overview of the importance of road surface characterization, explaining its most anticipated and observed effects and giving a summary on measurement practices and parameters described by different standardization organisms worldwide, as well as making a market research analysis on the instrumentation available on the market and its limitations.
- Listing the specifications of the device requested by the client, and finding the best non-contact technique for assessing the 3D texture height map of the pavement surface that fits our needs; the solution generation is done after studying the different non-destructive methods that are currently used such as: ultrasonic, photogrammetry and laser scanning. We find that the best technique that respects our specifications is the laser triangulation.
- Establishing the implementation approach of the laser triangulation, starting with the projective approach which consists of estimating a projection matrix that allows the transformation from pixels to real life coordinates, calibrating the system, and then detecting the laser line central axis for a better precision.
- Anticipating the different problems that can be found in the acquired point cloud based on data from previous work, such as the presence of a linear trend as well as outliers known as dropouts and spikes resulting from the data acquisition conditions. We develop a standard algorithm for data processing that applies the suitable and most efficient methods for treating the point cloud.
- Developing the design that respects our criteria and constraints, starting with choosing the adequate hardware, and then designing and manufacturing the mechanical part of the prototype, with respect to the characteristics of the camera and the laser. We describe the flowchart as well as the practical calibration process of the laser scanning system in this step.
- The final step of our work consists of testing and validating the prototype. We take and present various measurements; and a testing protocol to follow when conducting these measurements is described.

Chapter 1

Literature review

Introduction

This chapter presents an overview of the importance of road surface characterization, as well as measurement practices, technology, and instrumentation currently used worldwide.

It begins by presenting the terminology related to surface texture in general and pavement texture in particular, based mainly on the International Organization for Standardization, for a better understanding of the problematic.

It then presents the reasons that led engineers to pay extra attention to road surface quantification, as it details the most anticipated and observed effects of pavement texture and their relationship with its different ranges.

The chapter then presents the international standardization activities conducted by the different normalization organisms worldwide that aim to propose universal and reliable methods to quantify pavement texture, discussing the several disadvantages presented by these techniques, as they can be time-consuming and too general and proposing a larger range of surface texture parameters that can be calculated.

In the final section, the chapter presents an overview of the non-destructive techniques for distance measurements that can be used, and the different technologies that were developed in an attempt to automize and accelerate the process of characterization of the road surface texture.

1.1 Terminology with regard to pavement texture

Profile

A profile is a two-dimensional sample of the surface; it is generated when a sensor is continuously moved along the surface. Thus, it is described by two coordinates: one along the surface plane, called distance "x" (number 4 in figure 1.1), and the other in the direction normal to the surface plane "z" (number 1 in figure 1.1), called amplitude or vertical displacement.

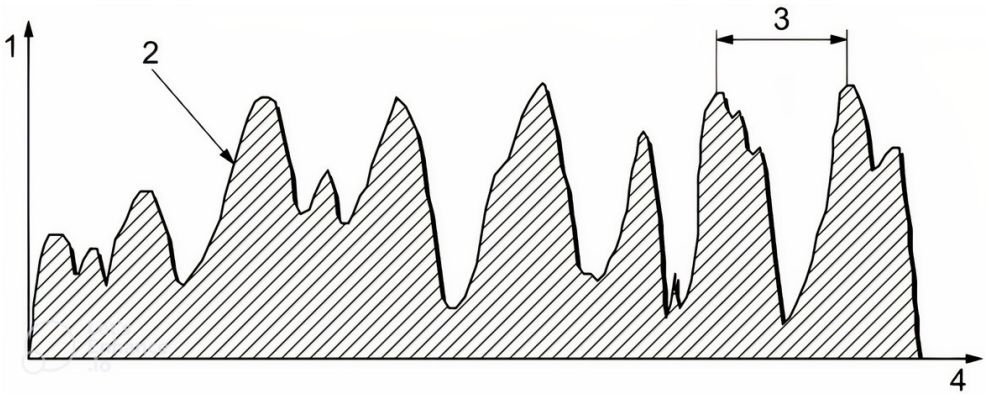

Figure 1.1: Illustration of some basic terms describing pavement surface texture 1- Vertical displacement 2- Profile 3- Texture wavelength 4- Distance

Texture wavelength

The texture wavelength is the spatial period of a wave (see number 3 in figure 1.1). It is given in meters or millimeters and uses a lambda λ as a symbol. The inverse of the wavelength gives the spatial frequency in cycle/m.

Surface texture

Surface texture is the repetitive or random deviation from a true planar surface [2]. Surface texture includes:

- **Surface roughness**: represents the highest frequency (short wavelength) components on the surface.
- **Surface waviness**: represents the next order of lower frequency (longer wavelength) components on the surface.
- **Surface form**: refers to the longest wavelength (the lowest frequency) components on a surface.

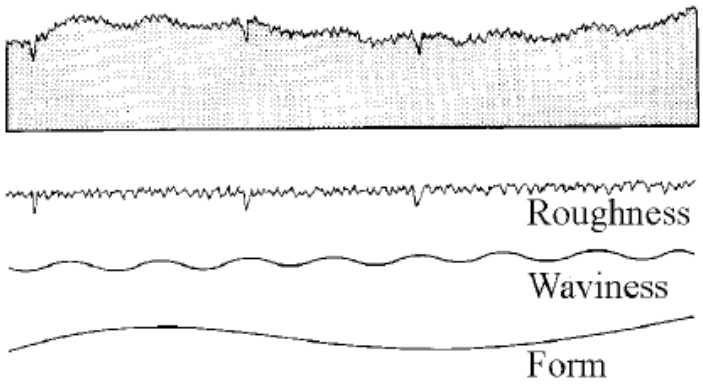

Figure 1.2: Schematic representation of the difference between roughness, waviness, and form [3]

The profile determined with a profilometer is generally a composition of roughness, waviness and form errors, the application of filters for separating these components of the surface roughness is mandatory. Figure 1.3 shows the decomposition of a measured profile in roughness (micro-roughness), waviness (macro-roughness) and form error (mega-roughness) according to their wavelengths.

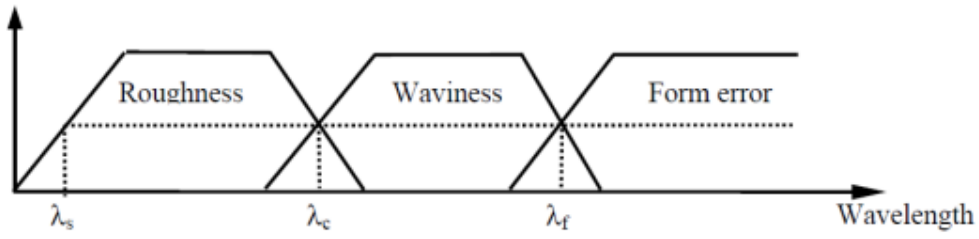

Figure 1.3: Separation of surface into frequency bands [4]

Pavement texture

Pavement texture is classified according to its wavelength and amplitude into four categories, which are:

- **Microtexture**: it is the equivalent of micro-roughness, it refers to the small-scale texture with wavelengths up to 0.5 mm. The microtexture is too small to be observed by the eye, and it depends on the surface properties of the individual chippings.
- **Macrotexture**: it is the equivalent of waviness, it refers to medium-scale texture with wavelengths that range from 0.5 to 50 mm. The macrotexture is primarily influenced by the size, shape, and gradation of the coarse aggregates.
- **Megatexture**: refers to the large-scale texture with wavelengths that range from 50 to 500 mm.
- **Unevenness**: it is the pavement texture with wavelengths longer than 500 mm.

Both megatexture and unevenness are the equivalent of form errors, their main source is construction or pavement distress. The distresses for pavement are: potholes, bleeding, cracking, transverse cracking, longitudinal cracking, block cracking, fatigue cracking, rutting, patches, and raveling.

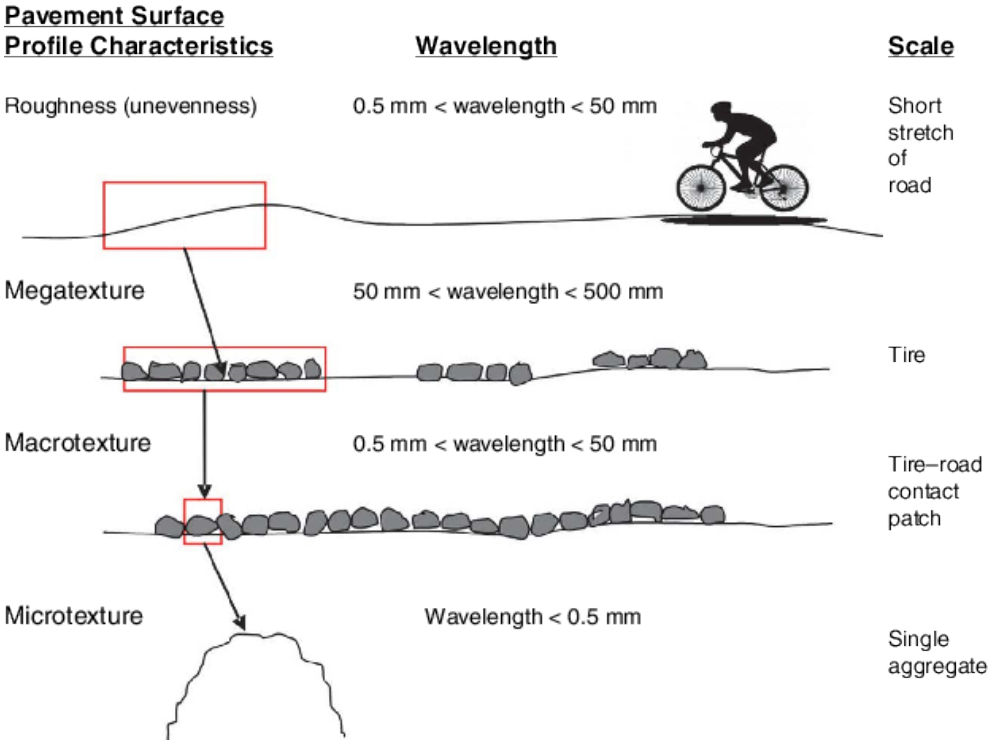

Figure 1.4: Pavement texture ranges [5]

Positive and negative textures

- **Negative texture**: When the deflections of the pavement surface are mostly directed downwards, meaning that the valleys are predominant, the pavement texture

is considered to be negative. Negative textures have fewer outliers.

- **Positive texture**: When the deflections of the pavement surface are mostly directed upwards, meaning that the surface asperities are predominant, the pavement texture is considered to be positive. Positive textures can quickly wear away when in contact with other surfaces.

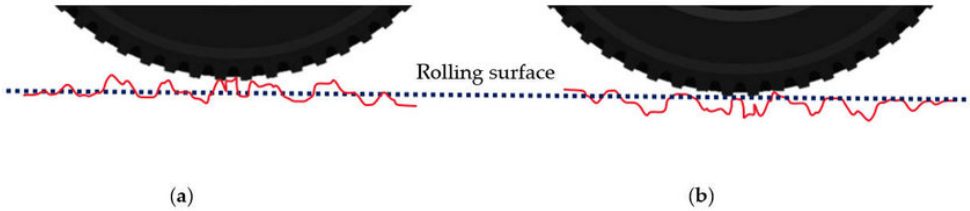

Figure 1.5: Schematic representation of a positive texture (a) and negative texture (b) [6]

Spatial variation of texture

ISO 13473-2 [7] defines the terms related to spatial variation of texture as follows:

- **Periodic texture**: surface texture that exhibits a repeated characteristic pattern or waveform, with a periodicity that may or may not be directional.
- **Random texture**: texture that does not exhibit a noticeable periodicity.
- **Isotropic texture**: texture that exhibits similar texture characteristics in all directions within the plane of the surface.
- **Anisotropic texture**: texture that exhibits some directional characteristics, such as, but not limited to, transversal and longitudinal grooves.

1.2 Effects of road surface texture

Dictionaries define tribology as the branch of science that studies interacting surfaces in relative motion. It applies operational analysis to problems of economic significance, namely, maintenance, and wear.

One of the most important concerns of pavements engineering is the study of tribological properties of pavement since its interaction with tires has a direct influence on friction coefficients, wear rates, and vehicle vibrations, affecting safety, economy, and comfort.

When conducting a tribological study, the first step is to define the tribosystem. The tribosystem in the study of tire/pavement consists of:

- **The body**: the first interacting surface, which is the pavement surface.
- **The counter body**: the second interacting surface, which is the tire surface.

- **The interfacial element**: a lubricating substance present at the surface contact area, mainly water.

The cost and complexity of friction and noise testing equipment have led transportation agencies to drop classic friction and noise testing. A special effort for finding a correlation between these parameters and surface texture, as an indirect approach, has been adopted instead. This section focuses on the effects of pavement surface texture on friction, water evacuation, noise, rolling resistance, and comfort.

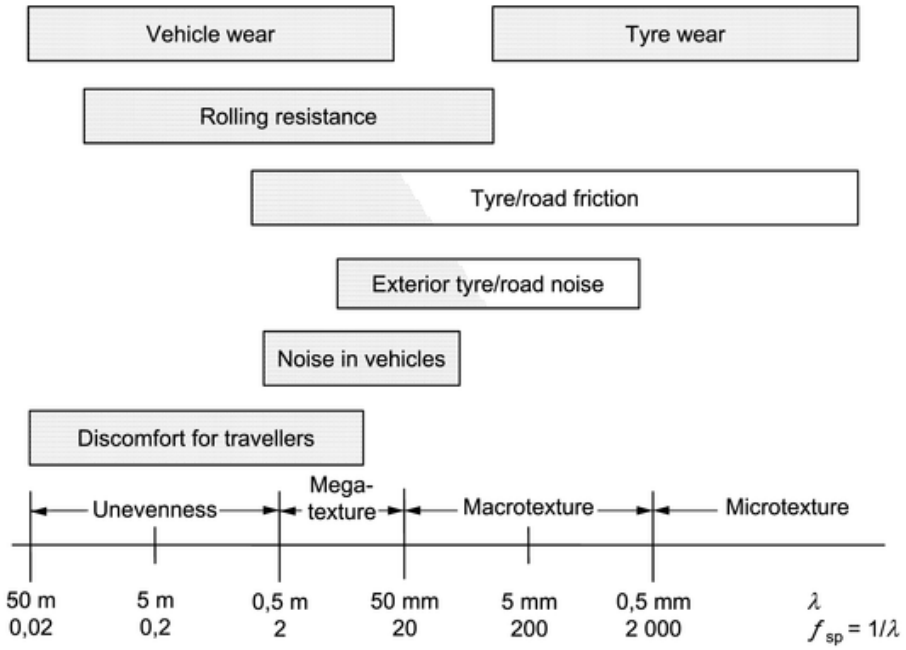

Figure 1.6: Ranges of pavement texture and their most significant, anticipated effects [8]

Water evacuation

The pavement's capacity to evacuate water has a direct relationship with its texture. Smaller grains, meaning lower macrotexture, lead to smaller voids and thus a smaller capacity for draining water and a smaller amount of water that can be held within it.

A deep macro-texture is preferable for taking care of the excess water to avoid hydroplaning (hydroplaning is a situation in which a vehicle tire rides up on a thin surface of water, losing contact with the pavement, resulting in a sudden loss of control).

Friction

Friction is described as the resistance to motion during sliding or rolling, it is experienced when one surface, that is in contact with another, moves tangentially over it. The friction force acts in the direction opposite to the direction of motion.

Friction forces can have both a positive and negative effect on the tire/road interaction. Without friction, it would not be possible to use automobiles with tires on a roadway.

However, due to the energy dissipation that it causes as well as the wear of the two surfaces in contact, friction can be pretty harmful.

There are mainly two frictional mechanisms to take into account in the study of tire/road interaction:

- **Adhesion**: Adhesion is the bonding of two materials when brought into contact, in our case the rubber and the pavement, resulting from the formation of adhesive bonds between the molecules of the two materials. A normal tensile force must be exerted to separate the surfaces [2].
- **Bulk hysteretic friction**: Hysteresis is a deformation component of friction. In the case of viscoelastic materials such as rubber, a deformation/displacement of the material after enveloping the surface texture occurs, which causes energy loss [2].

Generally, pavement texture has a positive effect on friction, which means that higher texture leads to higher friction between the two surfaces [9]. However, different ranges of texture have different effects on the two mentioned mechanisms. While adhesion is mostly affected by microtexture, hysteretic friction is mostly affected by macrotexture.

Studies have shown that the adhesion force is the most influential mechanism in dry conditions and low speed, which means that microtexture becomes the major determining surface feature. However, in wet conditions and due to the presence of an interfacial element, there is a risk of separating the two surfaces, thus breaking up the adhesive bonds, leading to an important decrease in friction. In this case, macrotexture becomes an important feature since it allows water drainage.

Megatexture that is present as bumps in the road surface, leads to a loss of contact between tire and pavement since the vehicle bounces in the presence of deviations of long wavelengths. It also leads to energy loss due to hysteretic friction. Which makes megatexture an undesired range of the pavement texture.

Noise

Driving a vehicle produces several contaminants, and one important contaminant that is often overlooked is the noise emitted from the interaction of the vehicle with the road. Noise can be classified into two categories:

- **Exterior tire-road noise**: A study was conducted as a joint effort by research institutes in Denmark, Norway, and Sweden, aiming to establish a relation between road surface texture and tire/road noise. After studying data from previous research as well as newly collected data, it was not possible to establish perfect correlations between noise emission levels and pavement texture parameters, however, it was found that low megatexture was associated with low noise emission, and high texture levels at small wavelengths are also associated with low noise levels[10].

  Another study was conducted in Sweden on the effects of positive and negative texture on noise emission. It was found that grinding the surface, and thus giving a more negative texture profile, appeared to reduce noise emissions [11].

- **Interior noise (noise in the vehicle)**: Noise levels inside the vehicle is related to both the exterior noise and the transfer of vibrations from the tires to the body of the vehicle. The vibrations are found to be a consequence of the bigger wavelengths of macrotexture and megatexture [9].

Vehicle and tire wear

The quality of the road surface on which a vehicle travels has an undeniable influence on its rate of wear. For instance, both megatexture and unevenness produce important vibrations that contain many frequencies, occur in several directions (bounce, pitch, and roll), and change over time, which causes various patterns of oscillatory motions and forces within the vehicle, causing fatigue, and as a result, defects in the vehicle's body start appearing after a certain time.

Also, the constant contact between the road's surface and the tires leads to the abrasion of the tread. The wearing rate of the tread is accelerated with greater micro and macrotexture.

Rolling resistance

Rolling resistance is the force resisting the motion when the wheels roll on a surface. Rolling resistance is a parameter that affects both the economy and the environment, since an increase in rolling resistance results in an increase in fuel consumption, as well as an increase in air pollution due to greenhouse gas emission.

Mega and macrotextures are mainly responsible for rolling resistance. It was also found that a negative texture presents lower rolling resistance coefficients than positive textures.

Discomfort and health

As it was already established, both megatexture and unevenness produce important mechanical vibrations, and the constant exposure to these vibrations causes great discomfort to the travelers.

Apart from discomfort, they also present a great risk to the travelers' health. The effects of the Whole-Body vibration (a term used to describe the transmission of mechanical vibration to the human body when in contact with a vibrating surface [12]) are similar to the effects on the vehicle's body. It was found that professional drivers are at high risk for back disorders as well as cardiovascular diseases. Many studies have been made on the relationship between certain diseases and mechanical vibrations from tire/road interaction.

1.3 Overview of pavement texture measurement standards

Various standards have been established regarding pavement texture measurement by different standardization organisms.

1.3.1 The volumetric method

The volumetric method also known as the sand patch is a method that uses a known volume of a material to determine the MTD of the pavement. The volume is spread evenly on the surface in a circular shape in a way that it fills the hollows of the surface while flushing with the top of the asperities. The value of the texture depth is obtained by dividing the volume of the used material by the area it covers. This technique is commonly used worldwide with slightly different material specifications.

EN 13036-1 [1] is a European standard that describes the detailed specifications of the material used as well as the procedure for measuring the MTD.

For this version, solid and fully spherical glass beads are used. These beads must be calibrated so that 90% at less of the mass passes through the 0.25 mm sieve and is retained by the 0.18 mm sieve [1]. Which makes this method insensitive to the microtexture of the pavement.

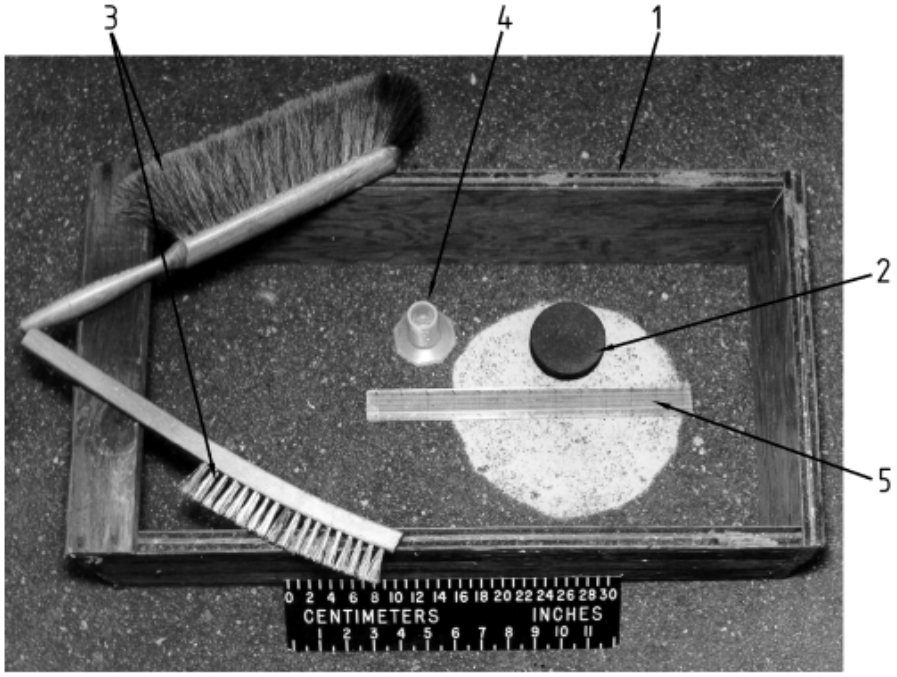

Figure 1.7: Apparatus for measuring the surface macrotexture depth [1]

1. Portable windshield: used for shielding the area from the wind that could displace the beads.

2. Stripper disc: used for distributing the material on the surface.
3. Brushes: used for cleaning the surface, since the measurement must be done on a clean and dry area.
4. Calibrated cylinder: for measuring the exact volume of the beads.
5. Graduated ruler: used for measuring the diameter of the surface, the diameter is measured at 4 evenly spaced locations, the average diameter is the diameter that would be used for calculating the mean texture depth in the following equation:

$$MTD = \frac{4V}{\pi D^2} \tag{1.1}$$

MTD: mean texture depth in millimeter (mm).
V: the volume of the beads (mm^3).
D: the diameter of the circular spot (mm).

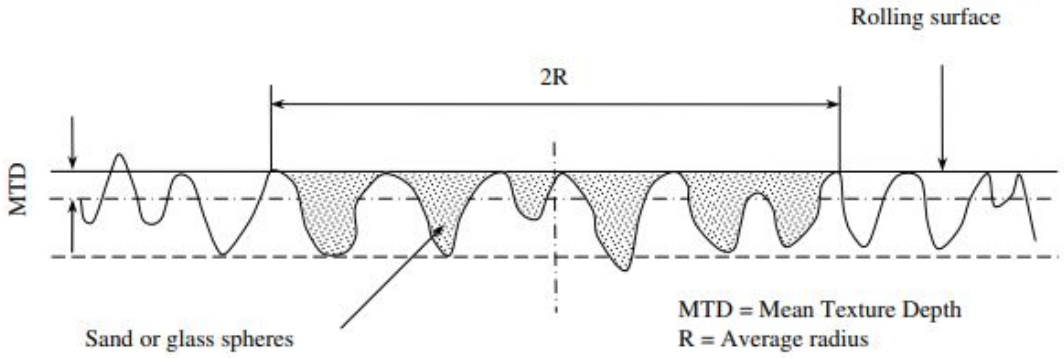

Figure 1.8: Illustration of the MTD [13]

Even though the sand patch method is widely popular; it presents different limitations. Apart from being very time-consuming because it is manual, it also presents a risk to the employee's safety since the measurements are made on pavements that are open to traffic. To reduce the risk to safety, it is important to control traffic which leads to important traffic delays.

1.3.2 Profilometry

In light of the limits that the volumetric method presents, many devices that estimate pavement's texture at traffic speed were developed. These devices however use a different approach, since they estimate texture using profiles instead of surfaces. The profiles produced are used to compute various parameters, such as the MPD, the Estimated Texture Depth (ETD), and the Sensor Mean Texture Depth (SMTD).

Mean Profile Depth

The standard **ISO 13473-1:2019** [8] which has the title: **"Characterization of pavement texture by use of surface profiles — Part 1: Determination of mean**

profile depth" describes a test method to determine the average depth of pavement surface macrotexture by measuring the profile of a surface and calculating the texture depth from this profile. The technique only takes into consideration the pavement macrotexture and is considered insensitive to pavement microtexture and unevenness characteristics.

Capturing the profile data is usually done using laser equipment, the minimum baseline of the profile is 100 mm. The minimum recommended vertical resolution is 0.05 mm. The sampling interval should not be greater than 1.0 mm, and the samples should be sampled at fixed intervals in the horizontal direction [8].

This method generates measurement errors and erroneous values that must be treated. The treatment technique of the data is described in detail in the text of the standard, it generally consists of removing outliers and remodeling the profile, the next step would be filtering by applying firstly a high-pass filter to eliminate the large wavelengths in the profile, and then a low-pass filter to remove components of frequencies that lie above a given texture wavelength.

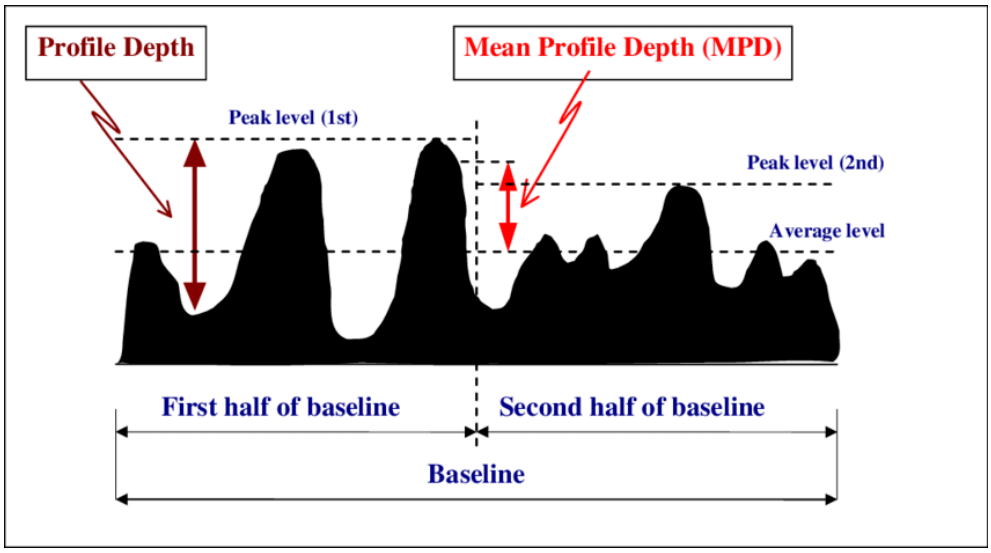

Figure 1.9: Schematic of Mean Profile Depth Computation [14]

After treating the data, the scanned profile is divided into 100 mm segments. Each segment is divided into two halves; in each half, we identify the maximum value. The Mean Segment Depth (MSD) is calculated as described in the following equation:

$$MSD = \frac{\text{peak level (1st)} + \text{peak level (2nd)}}{2} - \text{avergae level} \tag{1.2}$$

The mean value of calculated MSDs gives the MPD.

Even though this method presents the advantage of continuously determining the MPD at normal traffic speed, thus not causing traffic delay, the MPD is judged to be a too general 2D parameter of the road surface texture, it fails to describe the detailed surface texture characteristics.

Sensor Mean Texture Depth

The sensor mean texture depth is a parameter that is widely used in the United Kingdom. The process of determining the SMTD is simple, it consists of fitting the pavement's surface profile over a $300mm \pm 15mm$ with a 2nd-order polynomial using a quadratic least square regression, this step helps remove the effects of vehicle bounce [13]. The SMTD is then calculated using equation 1.3.

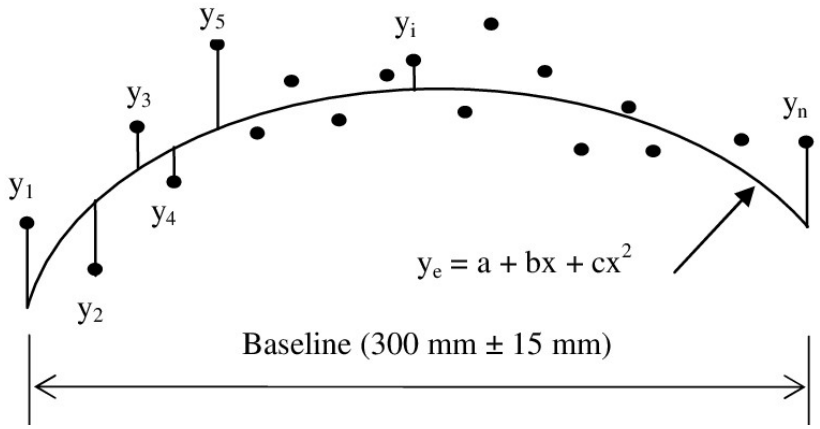

Figure 1.10: Illustration of concepts related to the procedure calculation of the SMTD [13]

$$SMTD = \sqrt{\frac{\sum_{i=1}^{n}(y_i - y_e)^2}{n}} \tag{1.3}$$

Estimated Texture Depth

The **ISO 13473-1(2019)** standard provides an equation, obtained from a linear regression, that relates the texture depth to the mean profile depth:

$$ETD = 1.1MPD \tag{1.4}$$

The standard specifies that the equation is only valid for **0,3 mm < MPD < 3,0 mm** in dense surfaces. It is however important to note that individual studies of this relationship give different results, with a coefficient that ranges between 0.9 and 1.3 [8].

The large range of the coefficient obtained can be explained by the fact that the given equation is the result of an average of several collected data, which makes it general and does not take into consideration several factors, among which:

- Repeatability of the sand patch method.
- Types of coating: in a study that was conducted by the Institute for Roads, Streets and Infrastructures for Mobility (IDRRIM) that aims to assess the possibility of updating the MPD/MTD relationship, it was found that different types of coating give different correlations between the two parameters.

- The range of macrotexture: the pavement macrotexture ranges from low to high (macrotexture is classified as Low when the MPD is less than 1.5 mm, and High when the MPD is above 1.5 mm). A series of research were conducted for studying the relationship between the MTD and the MPD of asphalt pavements, the results show that there is an evident divergence from linearity in the domain of high macrotexture [15].
- Types of profilometers: every profilometer has its specifications, which leads to different results from different devices, studies show that different correlations were obtained using different profilometers [16].

We can conclude that the MPD measurement and the MTD are two types of measurement that do not use the same principle, so there can only be imperfect correlations between the results.

1.3.3 Outflow time

As was already mentioned in previous sections, the pavement's texture has a direct relationship with its drainage capacity. The American Society for Testing and Materials, an international standards organization, established a standard test method for measuring pavement texture using an outflow meter **ASTM E2380/E2380M-15(2019)** [17].

The outflow meter consists of a cylinder filled with water, the bottom of this cylinder is equipped with an orifice and a circular rubber ring. The procedure consists of measuring the time it takes for a known quantity of water, under the gravitational pull, to disperse through the gaps that appear between the circular rubber ring of the outflow meter and the pavement's surface. This method quantifies the interconnected nature of the voids on the surface.

Figure 1.11: The outflow meter

A faster escape time indicates a greater capacity of drainage and so a greater macrotexture.

The following equation is used for calculating the mean texture depth:

$$MTD = \frac{3.114}{OFT} + 0.636 \tag{1.5}$$

MTD is the mean texture depth (mm) and OFT is the outflow time (sec) [18].

Similar to the sand patch method, the outflow method presents safety concerns since the study is conducted on roads that are open to traffic, and the standard fails to address these concerns. It is also time-consuming because it is manual. One other limitation of this method is that it gives erroneous results for highly porous surfaces (surfaces that allow water to penetrate) and gives a too general description of the texture.

1.3.4 International roughness index

The International Roughness Index (IRI) is an indicator for characterizing the longitudinal road roughness. Even though this indicator is used worldwide, different regions use different standards, the most common ones are:

- **ASTM E1926-08(2021)** [19]: a standard for computing the international roughness index of roads from longitudinal profile measurements, it is used mainly in America.
- **EN 13036-5:2019** [20]: a standard for calculating and reporting estimates of road evenness from digitized longitudinal profiles, it describes the calculation procedure for the IRI in Europe. It is obtained by measuring the vertical movement of a standard theoretical dynamic model called the quarter-car model, traveling on a road, using equation 1.6. The model has standard parameters known as the Golden-car parameters.

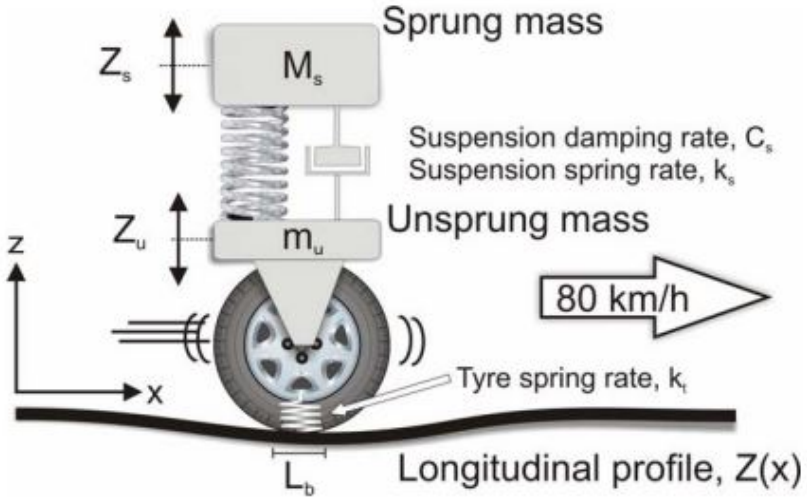

Figure 1.12: The quarter car model [21]

- The vehicle sprung mass (vehicle body mass) (M_s).
- The suspension spring (k_s).
- The suspension damper (C_s).

- The unsprung mass (m_u) (axle mass).
- The tire spring (k_t).

$$IRI = \frac{1}{L}\int_0^T |\dot{z}_s - \dot{z}_u| dt \tag{1.6}$$

The measurement time: $T = \frac{L}{V}$ with $V = 80\ km/h$

The procedure consists of simulating the theoretical vehicle on the pavement's profile at a constant speed (80 km/h), this operation is called the Reference Quarter Car Simulation (RQCS). The vertical movements of the vehicle and the axle mass are recorded. The IRI is obtained by the summation of the vertical movements along a base length of the profile[21].

The quarter-vehicle model can be studied by considering the forces and accelerations of the two masses. A free body diagram for each of the masses is constructed, which gives two differential equations. An algorithm is used for solving the differential equations numerically.

IRI is sensitive to the longer wavelengths in profiles of 10 m or 100 m in length. It does not take into account the effects of micro and macro textures, as the procedure requires that a high-pass filter at 250 mm is first applied to profiles whose sampling interval is less than 167 mm [22].

1.4 Surface texture characterization parameters

As we already saw in previous sections, road surface texture has a significant influence on several parameters that are related to the driver's safety. This makes the characterization of road surface texture based solely on the MTD and the MPD, which are predominantly used, too general to describe pavement surface's true characteristics. While the MTD and the MPD remain useful as a general guide, their limitations lead us to think beyond them.

The development of a device that would recover a texture height map of the pavement would give us the possibility to measure 3D surface quality parameters, and consequently a more accurate study of the road's quality.

Both the International Organization of Standardization (ISO) and the American Society of Mechanical Engineers (ASME) give a range of 3D parameters. A number of these parameters, their mathematical context as well as the information they provide about spatial structure will be described in this section. The parameters are classified into three types:

1.4.1 Height

Height parameters define properties of the surface that are related to the amplitude.

Sa (arithmetical mean height)

Sa is a widely used dispersion parameter. It expresses the arithmetic mean of the difference between the absolute values of height of the surface and the arithmetical mean of the surface. It is given by the following expression:

$$S_a = \frac{1}{A} \int \int_A |z(x,y) - \bar{z}| dxdy \tag{1.7}$$

with:

$$\bar{z} = \int \int_A z(x,y) dxdy \tag{1.8}$$

The continuous function $z(x,y)$ represents the physical surface, with x et y being independent variables.

When measuring a surface, it is digitized into a point cloud, which makes it necessary to define the discrete form of the equations.

$$S_a = \frac{1}{N.M} \sum_{i=1}^{N} \sum_{j=1}^{M} |z(x_i, y_j) - \bar{z}| \tag{1.9}$$

N: number of points in the x-direction.
M: number of points in the y-direction.

$\bar{z}$ in this case, is given by:

$$\bar{z} = \frac{1}{N.M} \sum_{i=1}^{N} \sum_{j=1}^{M} z(x_i, y_j) \tag{1.10}$$

Sq (Root mean square height)

Sq is a dispersion parameter, it is also referred to as the Root Mean Square (RMS). It is given by the following expression:

$$S_q = \sqrt{\frac{1}{A} \int \int_A |(z(x,y) - \bar{z})^2| dxdy} \tag{1.11}$$

The discrete form:

$$S_q = \sqrt{\frac{1}{N.M} \sum_{i=1}^{N} \sum_{j=1}^{M} |(z(x_i, y_j) - \bar{z})^2|} \tag{1.12}$$

It represents the standard deviation of the surface's height. The mathematical expression of Sq makes it more sensitive to extreme values than the arithmetical mean height.

Ssk (Skewness)

The skewness is a coefficient that measures the asymmetry of the distribution of a random variable, in our case the surface height.

$$S_{sk} = \frac{1}{S_q^3} \left[\frac{1}{A} \int \int_A |(z(x,y) - \bar{z})^3| dxdy \right] \tag{1.13}$$

The discrete form :

$$S_{sk} = \frac{1}{S_q^3}\left[\frac{1}{N.M}\sum_{i=1}^{N}\sum_{j=1}^{M}|(z(x_i,y_j)-\bar{z})^3|\right] \tag{1.14}$$

Ssk=0: A Gaussian surface (Symmetric surface height distribution).
Ssk>0: The distribution has a longer tail at the lower side of the mean plane.
Ssk<0: The distribution has a longer tail at the upper side of the mean plane.

This parameter indicates the nature of the pavement texture. A positive Skewness means that we are dealing with a positive texture, whereas a negative Skewness means that we are dealing with a negative texture.

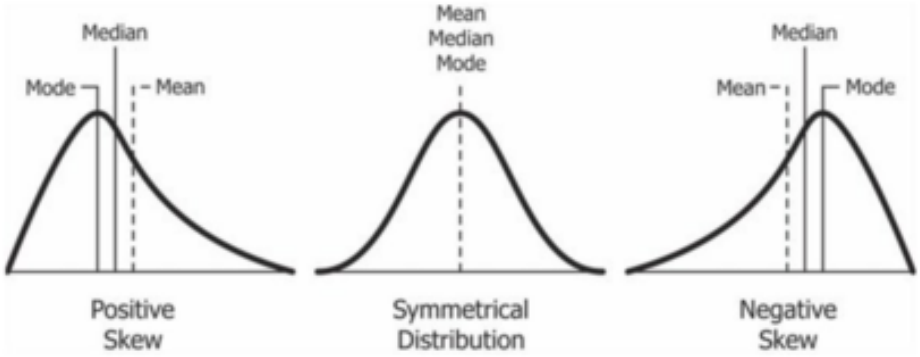

Figure 1.13: Illustration of skewness a) Negative skewness; b) Zero skewness; c) Positive skewness [23]

Sku (Kurtosis)

The kurtosis is a coefficient that measures the peakedness or sharpness of the distribution of a random variable, in our case the surface height. It is a suitable parameter for analyzing the degree of contact between two objects.

$$S_{ku} = \frac{1}{S_q^4}\left[\frac{1}{A}\int\int_A |z(x,y)-\bar{z})|^4 dxdy\right] \tag{1.15}$$

The discrete form :

$$S_{ku} = \frac{1}{S_q^4}\left[\frac{1}{N.M}\sum_{i=1}^{N}\sum_{j=1}^{M}|z(x_i,y_j)-\bar{z}|^4\right] \tag{1.16}$$

Sku=3: A Gaussian surface.
Sku>3: A centrally distributed surface.
Sku<3: A well-spread height distribution.

1.4.2 Spatial

Spatial parameters define the spatial properties of the surface texture.

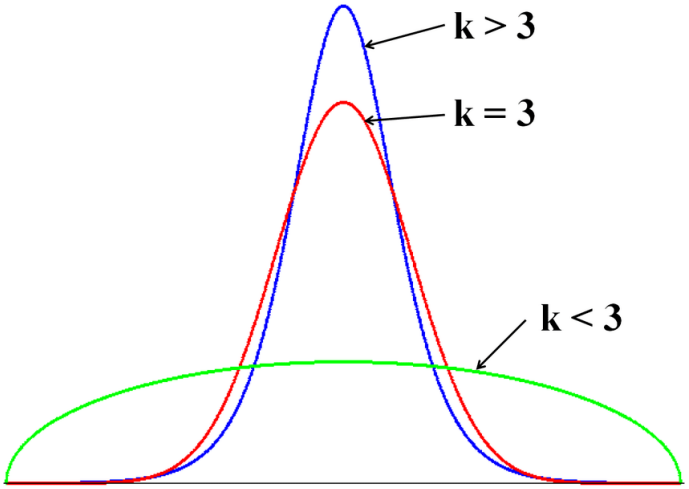

Figure 1.14: Illustration of Kurtosis [24]

Sal (The Fastest Decay Auto-correlation length)

Sal is the horizontal distance in the direction in which the autocorrelation function decays to a certain value (0.2 by default) the fastest.

$$S_{al} = min(\sqrt{t_x^2 + t_y^2}) \qquad where : R = \{(t_x, t_y) : f_{ACF}(t_x, t_y) \leq 0.2\} \tag{1.17}$$

with f_{ACB} being the auto-correlation function, and t_x and t_y being the autocorrelation lengths in the x and y directions respectively.

A large value of Sal means that the surface is dominated by low frequency (or long wavelength) components.

Str (Texture aspect ratio)

Str measures the uniformity of the surface texture. It is obtained by dividing the fastest decay auto-correlation length by the slowest decay of the autocorrelation function to the same value.

The texture aspect ratio varies from 0 to 1, with 1 indicating a perfectly uniform texture.

In the case of a small portion of the surface, the slowest decay may not reach 0.2, so when taking a sample, it is important to have important dimensions.

1.4.3 Hybrid

The hybrid parameters define properties that are related to both the amplitude and the spatial distribution.

Sdq (root mean square gradient)

The root means square gradient is given by the following equation:

$$S_{dq} = \sqrt{\frac{1}{A}\int\int_{A}\left[\left(\frac{\partial z(x,y)}{\partial x}\right)^2 + \left(\frac{\partial z(x,y)}{\partial y}\right)^2\right]dxdy} \tag{1.18}$$

The discrete form :

$$S_{dq} = \sqrt{\frac{1}{(M-1)(N-1)}\sum_{i=2}^{N}\sum_{j=2}^{M}\left[\left(\frac{z(x_i,y_j)-z(x_{i-1},y_j)}{\Delta x}\right)^2 + \left(\frac{z(x_i,y_j)-z(x_i,y_{j-1})}{\Delta y}\right)^2\right]} \tag{1.19}$$

A Sdq that is equal to zero refers to a perfectly flat surface, the value of Sdq becomes larger with larger amplitudes and spacing.

1.5 Overview of existing pavement texture measurement technologies

The conventional methods used for characterizing pavement's texture require manual handling and present safety risks to the operators. This led scientists into developing technologies to replace the traditional methods, their main focus was automating the systems while providing precise calculations. This section presents an overall review of several existing and innovative technologies for measuring pavement surface texture.

Circular Track Meter (CTMeter)

The circular track meter is a stationary apparatus for measuring a road's macrotexture. The device is equipped with a laser sensor that is mounted on an arm that rotates clockwise on a circular track of 284 mm in diameter at a fixed elevation from the pavement's surface. The profile is segmented into eight equal parts of 128 samples each. The CTMeter is connected to a notebook computer that saves and processes data. The software developed for the CTMeter calculates the MPD and the RMS values.

The device is small and portable (approximately 13 Kg), it also allows a rapid (under 1 minute) dense and precise data sets acquisition (it has a vertical resolution of 3 μm and a sampling spacing of 0.87 mm). It is however not fully automated.

TM2 – Texture Meter

The TM2 surface texture meter is a device developed by WDM USA. It projects a thin continuous beam of light onto the road surface transversely to the direction of travel, over a width of 100 mm every 2 to 5 mm (depending on the required data density). The device operates at an ideal walking speed of 3.5 km/h. It calculates the MPD according to **ISO 13473**. Data is stored on the tablet pc connected to the device, it is then analyzed using the standalone TMView software.

The technology provides a good resolution for the profile depth measurement (0.05 mm), it however requires an operator on site.

Road Surface Profilometer MK IV

The MK IV is a road surface longitudinal profile measurement device developed by Dynatest. The technology can be attached to any vehicle and is capable of providing measurements at traffic speed. It is equipped with:

- Two Laser sensors for capturing height data.
- An accelerometer that is placed in the wheel path to track the vertical motion of the laser.
- A distance encoder, that is mounted on one of the vehicle's wheels, produces 2000 counts per 1 revolution of the vehicle for tracking the vehicle motion with precision.

It has a built-in analysis software reporting the IRI and the MPD according to **ISO 13473**. It has a resolution of 1 mm in the travelling direction.

9400 Laser Texture Scanner

The 9400 laser texture scanner is a stationary apparatus for measuring the road's macro and microtexture. The laser sensor scans an area of 104.00 mm*72.00 mm. The data is stored in an internal flash; it can be exported to a computer for viewing the surface texture using the Ames Texture Scanner software. The software application can segment the original scans into smaller areas. The values of the MPD, ETD, RMS, Ra, Rq, Skewness, and Kurtosis are displayed on a sunlight readable (LCD).

The device provides dense and precise data sets acquisition (Vertical Resolution: 0.015 mm, Maximum Length Resolution: 0.015 mm, Maximum Width Resolution: 0.0635 mm), it is also small and light (approximately 4.2 Kg) which makes it easily portable.

Conclusion

When taking into consideration all of the anticipated effects, we can conclude that pavement texture has a complex relationship with several parameters, as it has negative and positive effects. Texture parameters should be optimized so that noise levels and wearing rates are reduced without compromising safety aspects, which means that friction levels should be acceptable.

The different standards that are available present different limitations. The volumetric and the outflow methods are both manual, which makes them time-consuming; the standards related to these methods fail to address the safety concerns related to operating on roads that are open to traffic. As for the profilometry method, and even though it presents a solution for the disadvantages of the volumetric and outflow methods, the 2D parameters are judged to be too general as they fail to describe the properties of the surface from a 3D point of view.

To replace the conventional methods used for characterizing pavement's texture that require manual handling, scientists developed technologies that are currently available in

the market, these technologies rely mainly on 2D methods that capture texture with a spot-laser to create a texture profile with the travel direction.

We can finally conclude that there is a need for developing a three-dimensional and non-contact method to capture pavement surface topography, that provides precise results and can work in traffic speed. The 3D point cloud data also provides the advantage of calculating other surface texture parameters such as skewness and kurtosis in order to have a better characterization of the pavement.

Chapter 2

Project specifications and chosen approach

Introduction

Nondestructive or noncontact techniques might be used to assess previously stated parameters, such as the MPD, MTD and Ssk by evaluating distances. The idea is to create a numerical replica of the actual scanned surface and which can be used to estimate the needed parameters that lead to a precise description of the surface.

The created replica is presented in a cloud points with a resolution in the 3 axis, which allows the study of the given surface.

There are many ways to estimate distances without direct contact using some physical principles such as waves propagation in its different types.

2.1 Overview of nondestructive techniques for distance measurements

2.1.1 Ultrasonic

Ultrasonic technology, as its name suggests, uses an emitted modulated sound wave generated by a transmitter and receives its echo signal while calculating the time of flight, resulting in a value for the distance between the detected object and the sensor. This technology is widely used due to its availability, price, and ease of implementation.

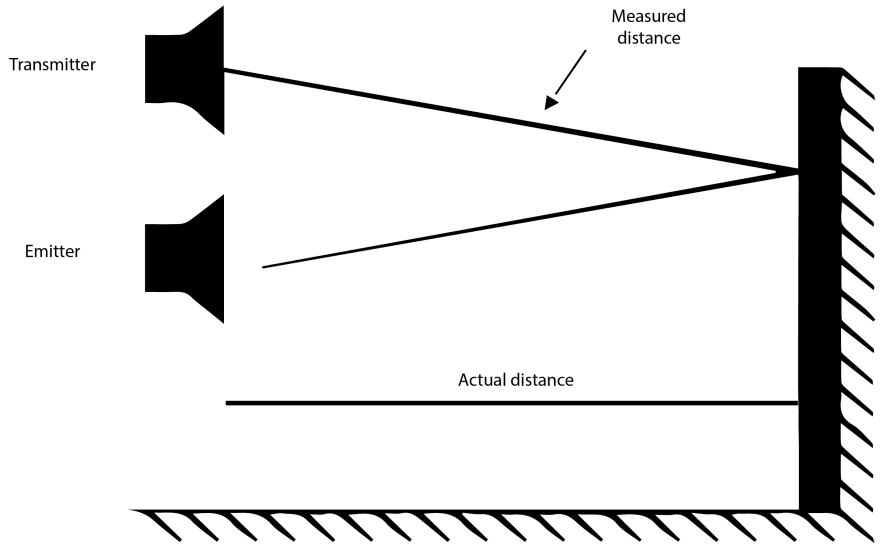

Figure 2.1: Ultrasonic working principle

Nevertheless, its application in our study scenario is impossible, since typically localizing with precision which part of the pavement reflected the sound wave is unachievable in view of the fact that the distances between measurements needed to be done is about 0.25 mm. The relatively high sensor size causes distance estimation errors, as figure 2.1 shows, because the sensor estimates the **measured distance** instead of **actual distance**.

While this problematic is fairly easy to address by using the distance between the transmitter and the receiver, it can introduce a huge of error in the distance measurement that can be neglected in some application, but since the range of distances tackled by our system is in micro meters it might be drastically affected with the introduced error. Also, the problematic shown in figure 2.3 is applied to ultrasonic systems either, therefore this distance measurement technique will be out of scoop for our 3D surface reconstruction task due to its low resolution. Although some research is being conducted in order to increase the resolution of ultrasonic instruments such as [25] where they achieved a 0.6 mm which is revolutionary with regard to this kind of instrument, it is still far from the resolution needed by our application which is 0.25 mm.

2.1.2 Photogrammetry

According to [26], photogrammetry is a passive scanning technique i.e. it doesn't need a separate light source, it works by using multiple pictures (hundreds to thousands) of the same object from different angles and then combining them in order to get a 3D representation of the object, photogrammetry systems normally use multiple cameras or one camera that has multiple degrees of freedom.

Figure 2.2: A 3D model of a statue reconstructed using photogrammetry

Photogrammetry 3D resolution intuitively depends on the images' resolution, while the precision depend on the amount of information provided by the multitude of images. This technique is still immature and considered as an open problem. On the other hand, scanning objects using this technique, as well as processing the data it provides, takes a lot of time due to the different poses of the object that need to be taken.

2.1.3 Laser scanning

Laser technology provides multiple methods to measure distances with high resolution, usually clustered into three different categories: time of flight, phase shift, and laser

triangulation.

2.1.3.1 TOF (Time-Of-Flight)

Time of flight (TOF) is an active laser scanning technique, it works by calculating the time it takes for the laser beam to travel in a round trip from the emitter to the detected object and reflecting back to the laser detector [27], the distance is then calculated such as follows:

$$d = \frac{ct}{2}$$

where c is the speed of light and t is the time of flight.

The resolution of such an instrument is derived from how precise we can measure the time, and since the speed of light is extremely high (in vacuum it takes approximately 3.3 picoseconds to travel 1 mm), it is quite difficult to measure the time that it takes to travel short distances; which makes its employment in our application very complicated and costly. In addition to that, using the so-called Range Finders is time-consuming, since the emitter needs to be rotated with precision in order to take measurements of multiple points. These systems are still in development and are not very accessible through public markets. Lately, this technology started to emerge in the form of low-cost sensors such as **VD55H1** which is not yet available in the market. In addition to that, irregular surfaces present an irritating challenge for TOF systems since the reflection of light will be complicated to analyze, mainly because it is hard to identify the source of the reflection as shown in figure **2.3**. While this can be resolved using multiple modulated light source, double reflections as in **C** is still an active problem in what concerns TOF Systems.

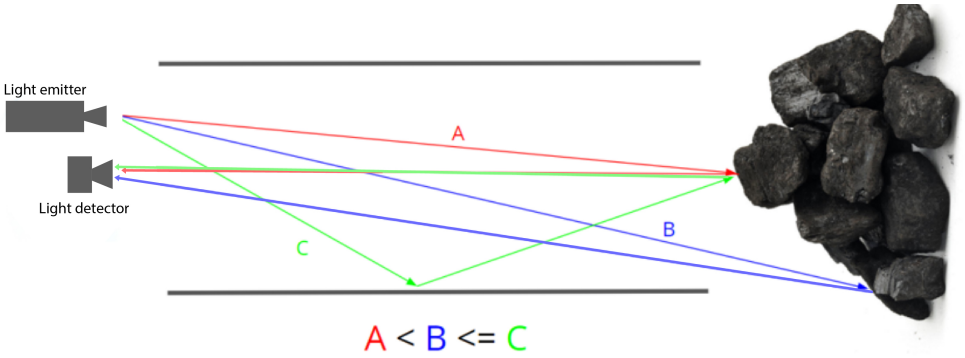

Figure 2.3: Irregularities effect on TOF Systems

2.1.3.2 Phase shift

A phase-shifting laser uses the shift occurring in the reflected laser beam to determine the distance by comparing it to a standard phase, the process is quite similar to the TOF method in the sense of using the reflection to calculate the distance. Even though phase-shift lasers are more accurate and more reliable than standard TOF, it makes them even more expensive and difficult to manufacture and use. Calculating phases is not straightforward and requires advanced hardware.

The maximum range that can be achieved can be estimated using the modulation frequency. A higher frequency modulation results in a high precision but a small maximum range. Exceeding the maximum range will result in an ambiguity [28], that's being said, using this technology requires a compromise between range and precision.

2.1.3.3 Triangulation

Laser triangulation devices are also active devices. The measurement is achieved by projecting laser light in a specific form (line, dots ...) into the subject of interest and capturing the reflection of this latter using a camera. The position of the laser in the camera depends on the distance between the projector and the subject, and the camera position, a geometrical relationship between real distances and camera distances can be achieved by a Homography projective matrix that depends on the camera angle and position, focal length and resolution. Figure 2.4 shows the basic components that form a laser triangulation system.

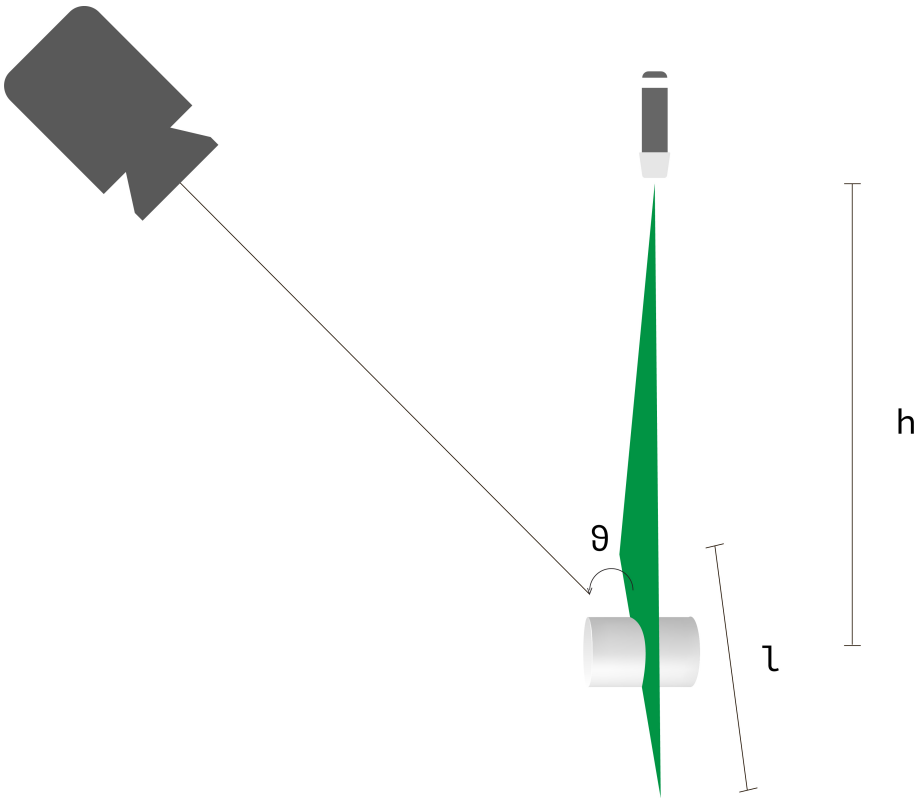

Figure 2.4: Basic laser triangulation components

The 3D image after being projected into the camera plane undergoes a vertical and a horizontal distortion, research shows that the original image can be reconstructed using linear or nonlinear transformations [29], to approximate the transformation appearing in the image.

2.2 Client specifications

From the beginning of the project, a dialogue was established with the client to determine expectations of the finished product. These were formulated in the form of constraints, presented in the following initial specifications. As we will see in the following parts, this one was used as a basis for building the prototype.

The initial specifications imposed the following constraints:

- The device must be able to measure the roughness of the road surface.
- The device must provide an output value of the MTD.
- The minimum accuracy (size of the smallest correctly defined length) must be 0.25 mm in all three axes (to obtain an accuracy similar to the MTD measurements using the current sand height technique).
- The device shall perform a non-destructive surface measurement.
- The capture area must be at least of the same order of magnitude as the contact area between the pavement and a tire (about 140 cm^2).
- The device must be tolerant of ambient vibrations from the interior of a moving vehicle.
- The device must be resistant to humidity (possible water splashes), dust as well as to possible splashes of gravel.
- The device must be connected to a computer for measurements.
- The device must be fast enough to make measurements at a speed of the order of 30 km/h in order to be able to make measurements on a stretch of highway without having to slow down traffic too much.

  Ideally, the tool should have the following features (these features are optional):

  - The device should be functional both day and night.
  - The device should be easily repairable and modifiable by the operator.
  - The device shall be capable of providing skewness and kurtosis values which can provide a better characterization of pavement texture.

2.3 Fitting the problematic needs

Our application relies on two fundamental constraints, the data acquisition needs to be highly precise, and the resolution needs to be around 0.25 mm or less. That said, if an error of 1 per cent is tolerated, it means that we need to have a system that gets information about every 2.5um of the pavement surface.

2.3.1 Choice process

Under the stated circumstances, we can directly exclude ultrasonic methods, since it is practically impossible to generate sonic waves that can respect the needed precision (capturing information about every 2.5 micrometers of the pavement surface). Similarly, photogrammetry, and even though it seems to be a promising solution, is highly affected by the brightness of the scanned structure, usually this technique is practiced indoors using special lights in order to achieve a considerable precision. Although photogrammetry can now be used outdoor mainly to scan buildings and different infrastructures, it is performed using special airborne cameras and dedicated material, we also argue that a huge number of pictures of the same surface need to be done which complicates the task of dynamic surface scanning.

Laser scanning offers a variety of techniques that can be used for our application. In order to break down our laser triangulation choice, let's first recall how laser shifting works. The idea is to modulate an optical wave and then reflect it into the desired object to scan, which leads to estimating the distance between the emitter and the reflecting object by estimating the phase shift. In order to have a high resolution the scanning range needs to be narrowed down, which forces the system to be extremely close to the object in order to operate in the desired resolution, which might be quite of an issue when dealing with pavement structures that can have a broad range of elevations. In order to achieve the desired resolution within the scanned surface, we need to make about 1 million and half measurement which makes the process of using a punctual laser beam very slow, making measuring at high speed impossible. One possible solution to this problem is to create a system with multiple phase-shifting laser detectors in order to cover the desired surface. However, such systems are quite complex to monitor, they are also costly.

Concerning TOF systems, the technology uses the time of flight to estimate distances, which means that it is in direct relationship with the speed of light. If the distance is small (in the order of millimeters), and knowing that the speed of light is extremely high while the height variations of the pavement are small, we need to have a time estimator that is pretty robust and extremely precise in order to have a decent resolution. The problem is, having such a system is quite costly and the use of a sensor array is needed to cover the studied surface. Currently, there are no available sensors on the market that are both affordable and easy to use to meet our requirements, which put the TOF systems out of our scoop either.

2.3.2 Laser triangulation

The chosen approach is laser triangulation. A laser line is projected on the pavement, giving a profile in the transverse direction. The laser is captured by the camera, and the system moves in the longitudinal direction to get multiple scans of the laser strip in order to cover the whole 14 cm* 10 cm surface as shown in figure 2.4.

In order to have a resolution of 0.1 mm in the vertical axis, the camera needs to be able to capture 1000 pictures of the pavement surface which is approximately equivalent to having 1 million and half cloud points and by using a high speed camera we can achieve that within a second. By having a resolution of 1920 * 1080 for example, the horizontal

axis resolution should be $\frac{100}{1920} = 0.052\,mm$ i.e. 50 micrometers, the better the resolution is the higher is the acquisition precision.

After capturing the pictures, they need to be triangulated and then converted to the 3D surface representation. Our choice was also motivated by other research, such as [29], where they achieved a resolution of 0.25 mm/pixel and a maximum error of 0.5 mm by only using a 640*480 resolution camera, whereas we expect better results by using better camera resolution. In [30], where the laser triangulation technique was used for 3D high resolution scanning of the pavement texture.

2.3.2.1 Light structure choice

In laser triangulation, a pattern of light is projected to the scene and then a relationship between the patterns' deformation in the picture and the real world object dimensions is established. In our study case we aim to scan an $140cm^2$ area with a precision of 0.25 mm in the 3 axis, in order to achieve that we make the choice of scanning the road portion with a thin linear laser beam (around 0.8 mm) and reconstruct the whole surface using the captured profiles. We argue that the use a more complex structure of light such as a grid or multiple laser lines isn't possible in our application since, first we can't practically generate a grid or set of laser lines that are spaced in a way that allows us to do a one picture acquisition with the needed resolution, for example in order to have a resolution of 0.1 mm in the vertical axis and being able to scan the area by using single shot and multiple laser lines, we need to ensure that the distance between the lines is the same as the resolution and the laser line width is smaller than 0.1 mm which is difficult or even impossible to reach. It is also complex to create such a system, since the resolution varies at each part of the laser line, which makes it difficult to obtain a coherent acquisition. Thus, a system that scan the road profile by profile as presented on 2.4 is adopted in our application.

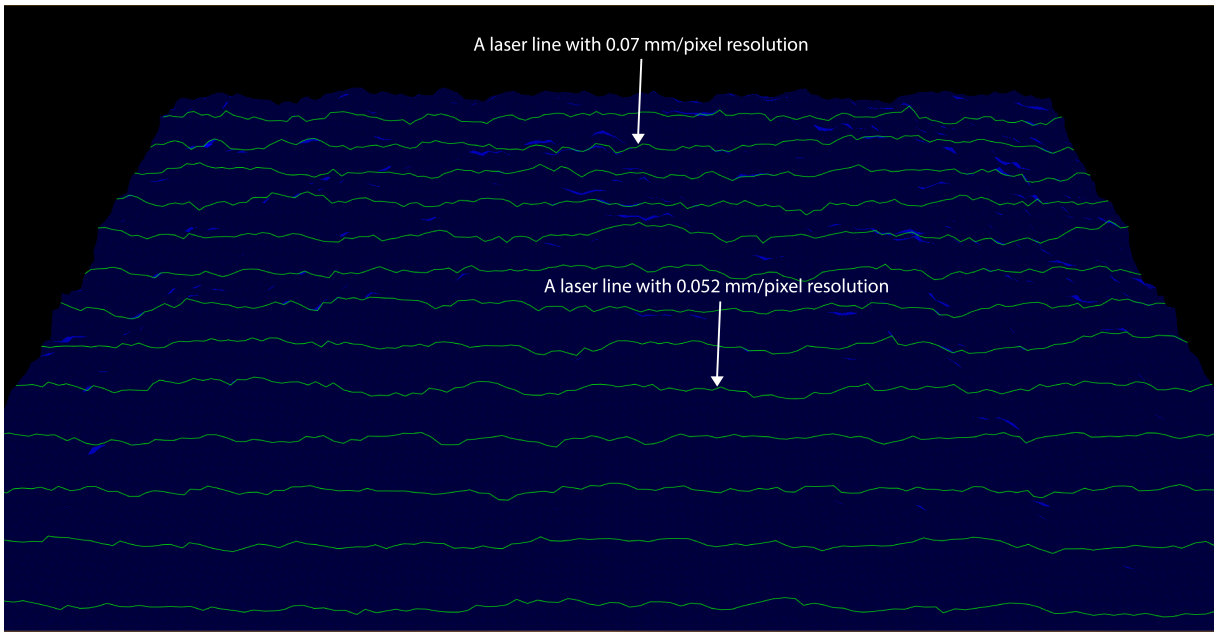

Figure 2.5: A generated rough surface with multiple projected laser lines

Figure 2.5 shows the effect of having multiple laser lines on the global resolution (acqui-

sition incoherence) on a simulator by using OpenGL. We generate a random surface by using a statistical model, and then laser lines are projected to simulate a real world situation. Note that the vertical resolution is defined as $\frac{\text{laser line real length}}{\text{laser line length equivalent on the image}}$mm/pixel.

2.3.2.2 Setting up the system parameters

A laser triangulation system is usually composed of a CCD camera, a laser line projector and the object to scan, figure 2.4 shows the most crucial parameters in terms of system performances:

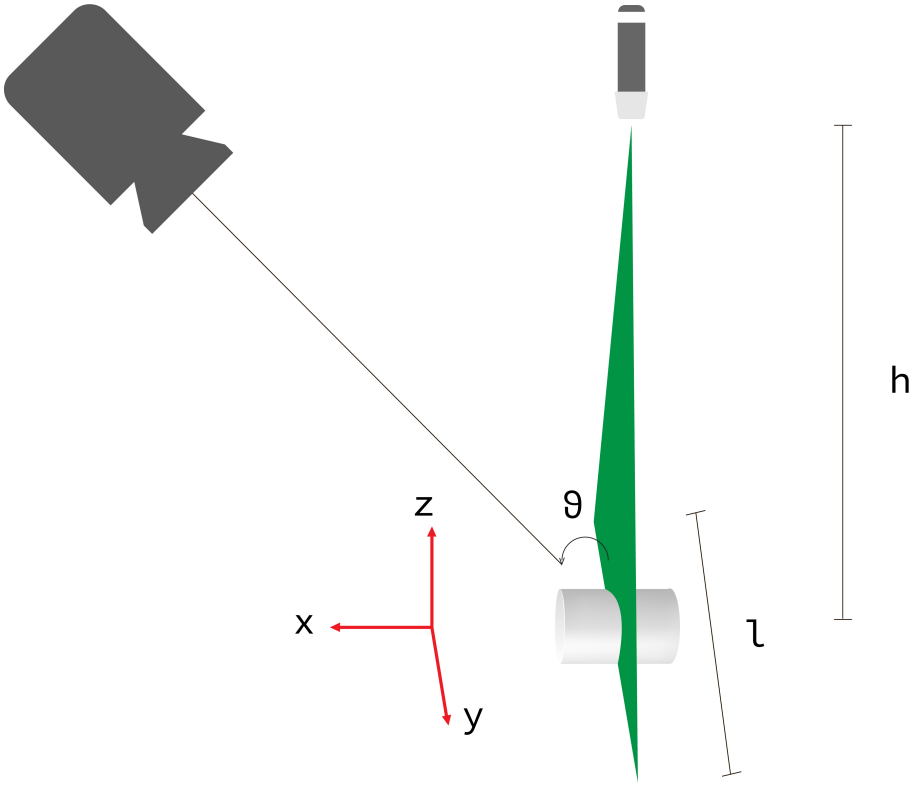

Figure 2.6: Systems parameters

Incidence angle θ

This parameter defines the angle between the vertical of the camera's field of view and the laser projector, which is oriented vertically. It is proportional to the acquired elevation resolution, which means that the greatest θ is, the better resolution we have in the z axis, which is the elevations' axis (see figure 2.6). Nevertheless, while this parameter seems to be better for the system if maximized, a higher incidence angle causes a problematic known as shadowing that causes occlusion of the protruding surfaces, so portions of the laser line can be out of sight because of the pavement texture. A compromise needs to be made in order to get the better resolution without loosing so much information from the scan.

Laser length l

The laser length defines the length of the scanned profile at each scanning step, it needs to be set with respect to the dimension of the scanned surface as presented in the previous section (about $140mm$).

Laser width w

The laser width is an important parameter that defines how precise we can be in the data acquisition: the thinner the laser line, the better is the detection. Nonetheless, it must not exceed a certain threshold in order to be correctly detected by the camera, commercial laser lines width varies between 0.5 and 2 mm.

Laser height (working distance) h

The height of the laser line needs to be set with respect to the laser projector fan angle and the line's length.

Laser color

Laser color plays a crucial role for the task of daylight scanning, a laser wavelength that is less prone to sunlight interference needs to be employed.

Laser intensity

Also called optical power and measured in mW, it plays an important role in laser visibility.

Conclusions

There are many ways to generate the 3D cloud points needed in our application in order to perform the pavements' characterization, the conducted analysis shows that ultrasonic systems are by far excluded from this task due to their poor resolution which is about 0.6 mm in the best existing ultrasonic systems [25].

On the other hand, TOF systems are more suitable for scanning wide areas such as buildings or different infrastructures with a range of kilometers, but when it comes to resolution and precision it is outperformed with phase shifting lasers and triangulation due to the difficulties caused by estimating the time flight of light in short distances [27].

Contrastingly, Phase shifting laser and laser triangulation fail when it comes to scanning long distanced objected, but can achieve an extremely precise scan up to the range of micrometers [31]. Lastly, in the current state-of-the-art, laser triangulation outperforms phase shifting lasers in the scan speed, which is a very important factor in the project approach choice.

Chapter 3

Implementation, from theory to practice

Introduction

Laser triangulation gives the possibility of translating the visual information contained on the camera projection plan to real world cloud points. A geometrical relationship between the two coordinates systems is usually called a correspondence problem, which can be established such as explained in this chapter.

3.1 From a captured image to real world coordinates

In this section, we first start with an explanation of what homogenous coordinates are and how they help building the projection model without approximations, since they present an analytical approach for doing various transformations.

3.1.1 Projective approach

Projective geometry has always been used historically especially in the renaissance era by famous painters, it was a technique that allowed them to precisely paint 3D objects into a 2D plane, it was recently developed and applied in various machine vision applications such as Simultaneous Localization and Mapping (SLAM), it is now applied for images taken by cameras so that we can represent the object in real world coordinates.

Researchers developed a system that requires the light projector and the camera orientations to be invariant. It uses a transformation matrix that maps between the image coordinates in pixels and the real world coordinates, and it is defined by using different intrinsic and extrinsic parameters, starting from the absolute position of the laser projector, the camera position, the focal length and the camera projection plane dimensions [32].

3.1.1.1 Homogeneous coordinates

Before heading into solving the correspondence problem, Some needed mathematical tools are explained.

In projective pinhole cameras model, the light is projected into the camera plane passing by the focal point (see figure 3.1). Homogeneous coordinates are the basic building block of our projective representation, a point in the projective plane $\mathbb{P}^2$ is represented with three coordinates in the Cartesian coordinates $\mathbb{R}^3$.

According to [33], In homogenous coordinates, all points laying in the same line are equivalent as in equation 3.1, correspondence of a point in the homogenous representation to the corespondent euclidean representation is done as in equation 3.2.

$$[X, Y, T]^T \sim [\lambda X, \lambda Y, \lambda T]^T \tag{3.1}$$

$$[x, y, 1]^T = [\frac{X}{T}, \frac{Y}{T}, 1]^T \tag{3.2}$$

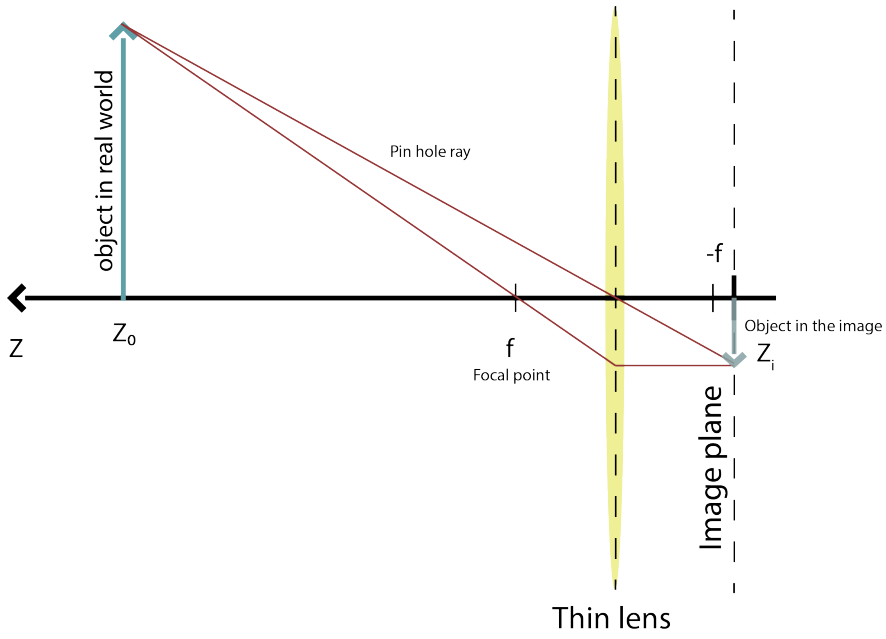

Figure 3.1: Camera pinhole model

3.1.1.2 Projective space properties

- **Duality** in a projective space points and lines are dual and respect the equation below, as l a line $[a, b, c]$ and p a point $[X, Y, T]$:

$$l^T p = aX + bY + cT = 0 \tag{3.3}$$

- **Line construction** with two points p_1 and p_2:

$$l = p_1 \cdot p_2 = 0 \tag{3.4}$$

- **Lines' intersection point** with l_1 and l_2:

$$p = l_1 \cdot l_2 \tag{3.5}$$

3.1.1.3 Projection Matrix C

Research proved that the transformation occurring to a 3D object on the camera plane when expressing the points on homogenous coordinate can be done using a projection matrix [34]:

$$\begin{bmatrix} X \\ Y \\ Z \\ T \end{bmatrix} = \begin{bmatrix} C_{11} & C_{12} & C_{13} \\ C_{21} & C_{22} & C_{23} \\ C_{31} & C_{32} & C_{33} \\ C_{41} & C_{42} & C_{43} \end{bmatrix} \begin{bmatrix} U \\ V \\ 1 \end{bmatrix} \tag{3.6}$$

where $[X, Y, Z, T]^T$ and $[U, V, 1]^T$ are the homogenous representation of the point in real world coordinates and camera projection plane, respectively. $[\frac{X}{T}, \frac{Y}{T}, \frac{Z}{T}]^T$ are the real world points coordinates in the euclidean space, this model allows the transformation from pixels coordinates in the camera to real world position in a predefined reference.

Figure 3.2 shows the transformation occurring to real world objects in the camera projection plane due to the pinhole effect where parallel lines for example are no longer parallel in the projected image. One of the advantages of the homogeneous coordinate is to define lines tending towards infinity rigorously, simply by writing $[U, V, 0]^T$.

Figure 3.2: An image showing the distortions occurring in an object after being projected to the image plane

Moreover, the matrix C is the multiplication of 3 other matrices that depend on the intrinsic parameters of the system, such:

$$\begin{bmatrix} C_{11} & C_{12} & C_{13} \\ C_{21} & C_{22} & C_{23} \\ C_{31} & C_{32} & C_{33} \\ C_{41} & C_{42} & C_{43} \end{bmatrix}^{-1} = \begin{bmatrix} \frac{1}{\rho_u} & 0 & 0 \\ 0 & \frac{1}{\rho_v} & 0 \\ 0 & 0 & 1 \end{bmatrix} \begin{bmatrix} f & 0 & 0 & 0 \\ 0 & f & 0 & 0 \\ 0 & 0 & 1 & 0 \end{bmatrix} \begin{bmatrix} R_{11} & R_{12} & R_{13} & \delta X \\ R_{21} & R_{22} & R_{23} & \delta Y \\ R_{31} & R_{32} & R_{33} & \delta Z \\ 0 & 0 & 0 & 1 \end{bmatrix} \tag{3.7}$$

where we define:

- ρ_u the horizontal pixel size in µm
- ρ_v the vertical pixel size µm
- f the camera lens focal distance µm
- R matrix elements $\begin{bmatrix} R_{11} & R_{12} & R_{13} \\ R_{21} & R_{22} & R_{23} \\ R_{31} & R_{32} & R_{33} \end{bmatrix}$ define the rotations applied to the camera with respect to the real world coordinates system.
- $[\delta X, \delta Y, \delta Z]$ are the camera translation with respect to the real world coordinates system.

in our study case, as shown in figure 3.3 and 3.4, the laser line occupies only the vertical plane to the floor, which means that the points constituting it, might be represented using only 2 dimensions X and $Z \subset \mathbb{R}^2$. Which justifies the following simplification of our projection matrix:

$$\begin{bmatrix} C_{11} & C_{12} & C_{13} \\ C_{21} & C_{22} & C_{23} \\ C_{31} & C_{32} & C_{33} \\ C_{41} & C_{42} & C_{43} \end{bmatrix} \rightarrow \begin{bmatrix} H_{11} & H_{12} & H_{13} \\ H_{21} & H_{22} & H_{23} \\ H_{31} & H_{32} & H_{33} \end{bmatrix} \tag{3.8}$$

Another simplification is granted by equation 3.1, so we can write:

$$\begin{bmatrix} H_{11} & H_{12} & H_{13} \\ H_{21} & H_{22} & H_{23} \\ H_{31} & H_{32} & H_{33} \end{bmatrix} \rightarrow \begin{bmatrix} H_{11} & H_{12} & H_{13} \\ H_{21} & H_{22} & H_{23} \\ H_{31} & H_{32} & 1 \end{bmatrix} \tag{3.9}$$

This simplified matrix **H** contains 8 unknowns that depend on the system itself as presented in 3.7. In the next section, we will discuss the process of estimating these constants for a given system.

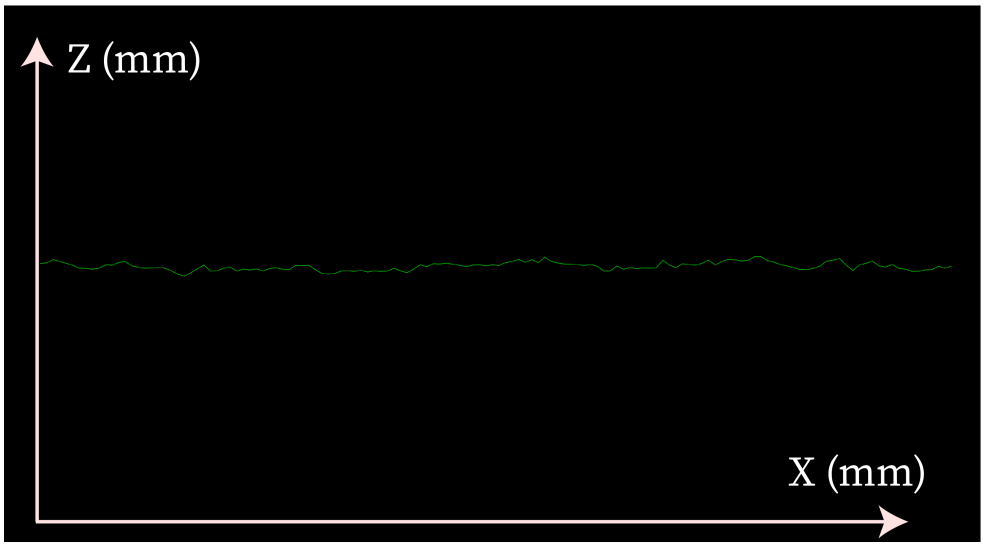

Figure 3.3: Laser line variations on a universal coordinates system

3.1.2 Estimating the projection matrix parameters

We have already established that a given triangulation system can be modeled by using a projective matrix that can be used with homogeneous coordinates to map between real world points and the points we can perceive on the image. Therefore, our system projection matrix needs to be estimated by using a calibration process.

Our system as presented in figure 2.6 has one degree of freedom, where the camera and the laser orientation are invariant. Accordingly the only variant parameter is the X coordinates, therefore the system projection matrix needs to be estimated only once and can be used to estimate the elevations of any given profile, while of course the X coordinates get saved in real time and used to generate a 3D surface.

Some advanced and high precise lasers, such as the **OKIO-FreeScan X5**, can scan a 3D object even if the system orientations and positions are variant, thanks to a system

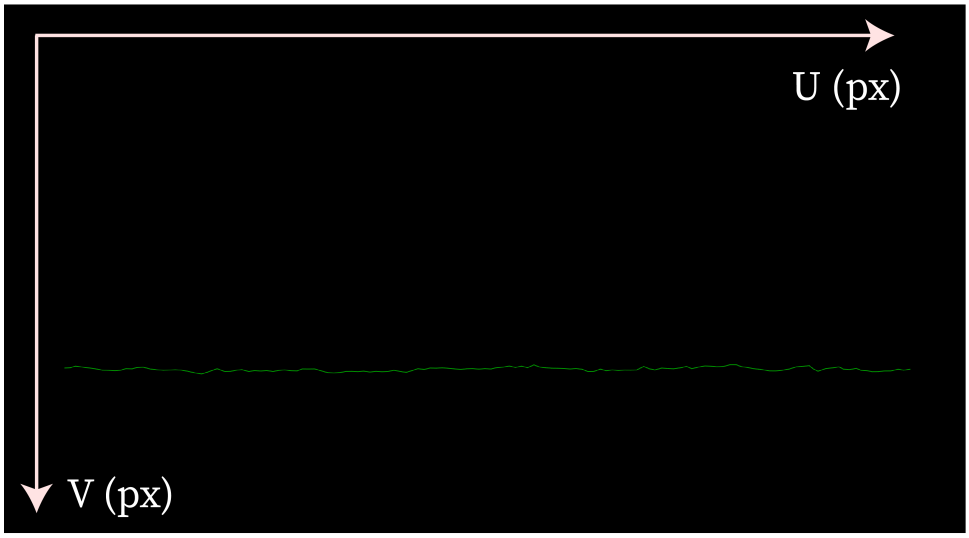

Figure 3.4: Laser line variations as perceived in the camera projected image

based on landmarks that are plugged into the wanted object for the scan. These landmarks are used as references to estimate the projection matrix in real time. While this technique is very effective, it cannot be adopted for our application, since we are scanning portions of a large pavement surface at high speed.

3.1.2.1 Calibration process

In the simplified matrix (see equation 3.9), eight unknowns need to be estimated, and therefore we need pairs of 4 points in both real world coordinates and their equivalent in the distorted image after the camera projection. Figures 3.5 and 3.6 show the corners of the grid that will be used for calibrating the camera, we use a grid with known dimensions, we get the corner points with their equivalents on the camera plan, solving the given linear system gives the constants of the matrix **H** (3.9), that we need for our acquisition

3.1.2.2 Generating the linear system

The linear system to be established in this section, will be our way to fully estimate the projection matrix (also called the homography matrix) **H** without specifically studying all the system parameters that were previously mentioned (incidence angle of the camera, focal length...). In figures 3.5 and 3.6 there are four pairs of points that represent the same points in both real world coordinates and the projected image, we write:

$$\begin{bmatrix} X_1' & X_2' & X_3' & X_4' \\ Y_1' & Y_2' & Y_3' & Y_4' \\ T_1' & T_2' & T_3' & T_4' \end{bmatrix} = \begin{bmatrix} H_{11} & H_{12} & H_{13} \\ H_{21} & H_{22} & H_{23} \\ H_{31} & H_{32} & 1 \end{bmatrix} \begin{bmatrix} U_1 & U_2 & U_3 & U_4 \\ V_1 & V_2 & V_3 & V_4 \\ 1 & 1 & 1 & 1 \end{bmatrix} \tag{3.10}$$

Also, according to equation 3.2, the real world coordinates are calculated by dividing by the third dimensions **T**, which gives:

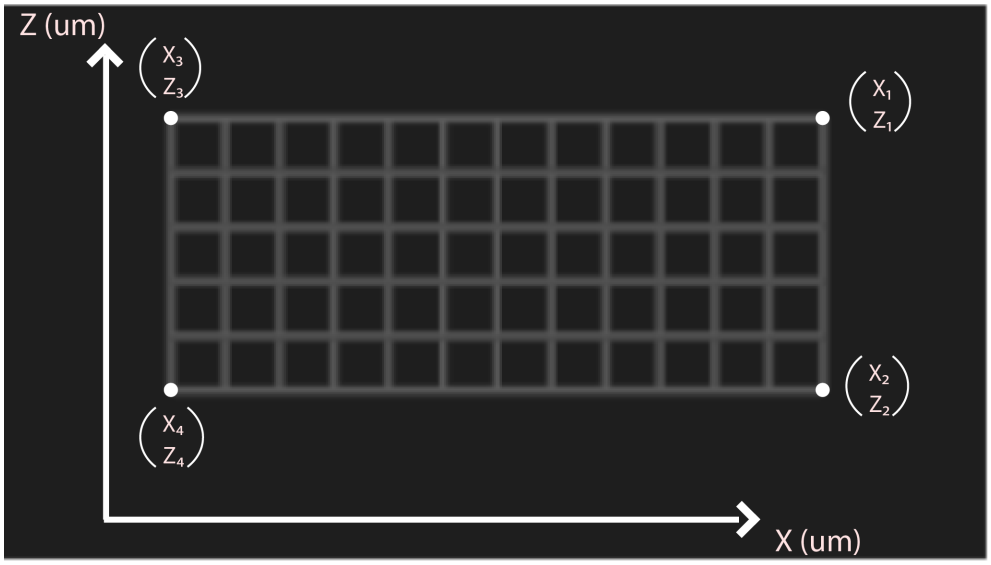

Figure 3.5: Image of the grid with the real coordinates

Figure 3.6: Image of the grid as seen from the tilted camera

$$X_n = \frac{X_n{}'}{T_n{}'} (3.11)$$

$$Y_m = \frac{Y_m'}{T_m'} (3.12)$$

we get the direct relationship between real world points and projected points:

$$X_n = \frac{H_{11}U_n + H_{12}V_n + H_{13}}{H_{31}U_n + H_{32}V_n + 1} \tag{3.13}$$

$$Y_m = \frac{H_{21}U_m + H_{22}V_m + H_{23}}{H_{31}U_m + H_{32}V_m + 1} \tag{3.14}$$

Finally, the linear system is established. The matrix **H** elements as a solution are written as follows:

$$\begin{bmatrix} U_n \\ V_n \\ U_m \\ V_m \\ 1 \\ -X_nU_n - Y_mU_m \\ -X_nV_n - Y_mV_m \end{bmatrix}^T \begin{bmatrix} H_{11} \\ H_{12} \\ H_{21} \\ H_{22} \\ H_{13} + H_{23} \\ H_{31} \\ H_{32} \end{bmatrix} = \begin{bmatrix} X_n + Y_m \end{bmatrix} \tag{3.15}$$

So that this linear system is solvable the chosen points need to be unaligned so that vectors defining the linear system are orthogonal, otherwise the needed constants will not be defined. This justifies the chosen points that represent the grid corners.

3.2 Laser line central axis detection

Usually, a linear laser line emitter has an important width that ranges between **0.5 mm** to **2 mm**. Therefore, being capable of detecting the central axis with the highest possible precision delivered by the camera is crucial in order to increase the system precision. In this section, we will discuss the approach we have chosen to implement this task, it is directly derived from a previous research present in [29].

3.2.1 Vertical laser line derivative

The laser lines' energy pattern is usually Gaussian [29]. Therefore, if we can estimate the derivative of the laser line energy vertically we can identify the position where the derivative is null, which means that we can identify the center of the projected laser line. In figure 3.7 we can see how the energy (intensity) of the laser line evolves with respect to its width.

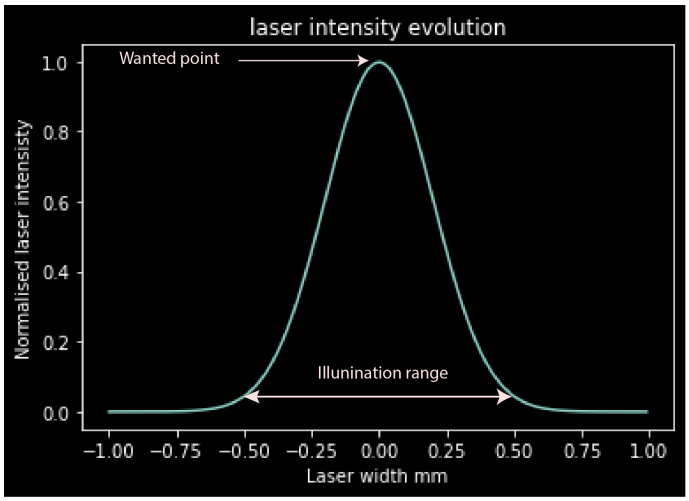

Figure 3.7: Vertical laser projection pattern

In our case, the laser line is presented in a grid of pixels, i.e. an image. Calculating the derivative along each column of pixels will allow us to identify the points where the derivative goes from being positive to negative, therefore we can estimate the pixels representing the thinnest laser line present on the image. This step allows a better estimation of the elevations at each profile.

Figure 3.8 shows the evolution of laser intensity in an image, since it's a simulation the laser projection pattern isn't quite Gaussian, but it follows a similar pattern. One might argue that there is no need to calculate the derivative of the laser energy pattern, since we can simply identify the max value of its intensity and therefore determine the pixel position representing the central axis point of the laser at a given column, while this's true when simulating an image totally filtered in a way that it represents only the laser line intensities in the whole frame. In practice, it is not quite the case since the image will most probably be full of parasites, so in order to ensure that the maximum point we are spotting belongs to the laser line central axis, which is the aim of using a derivative, we follow the pattern of the derivative and ensure that it is increasing and then decreasing in a short interval of space, this allows us to spot the maximum point with more certitude.

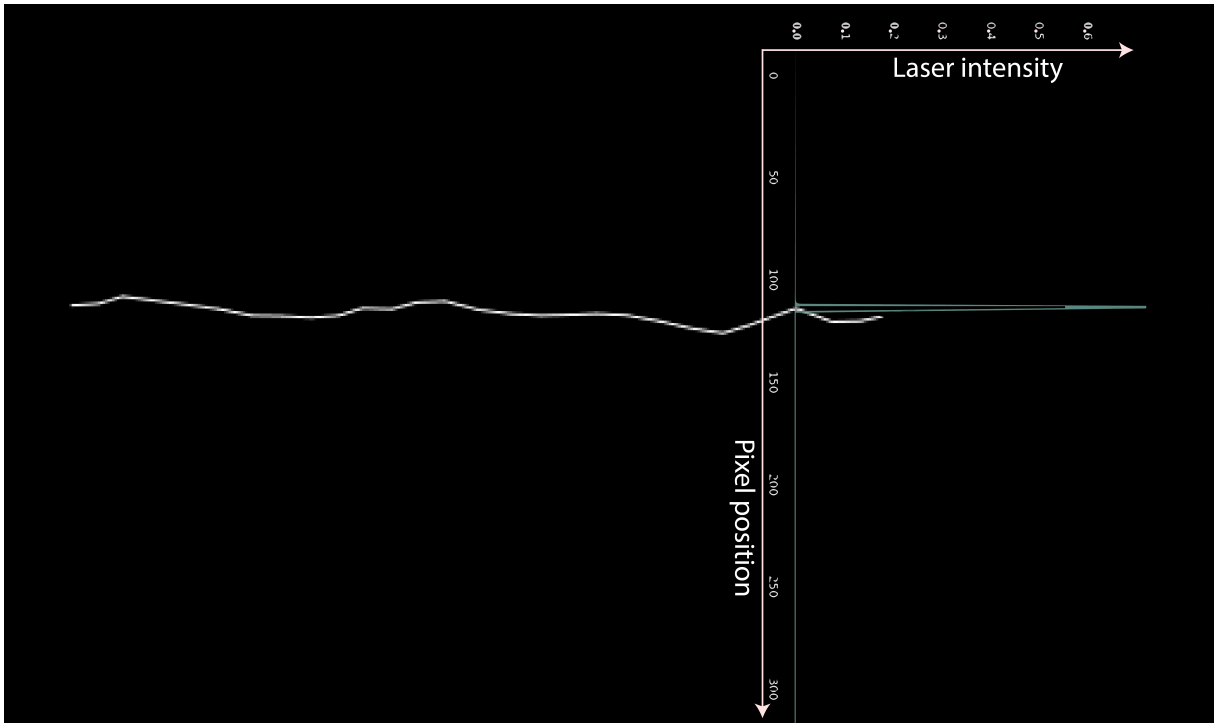

Figure 3.8: Laser line projection as seen from the camera (OpenGL simulation), along with the pixels' intensity evolution graph in green

Running the derivation process in all the columns will result in the presentation in figure 3.9, where every column has the Gaussian pattern we aim to capture.

3.9 shows the observable pattern of the laser line energy, positive, null and then negative derivative. In order to automate the central line detection, we propose a filter that maximizes the central points values, and we define:

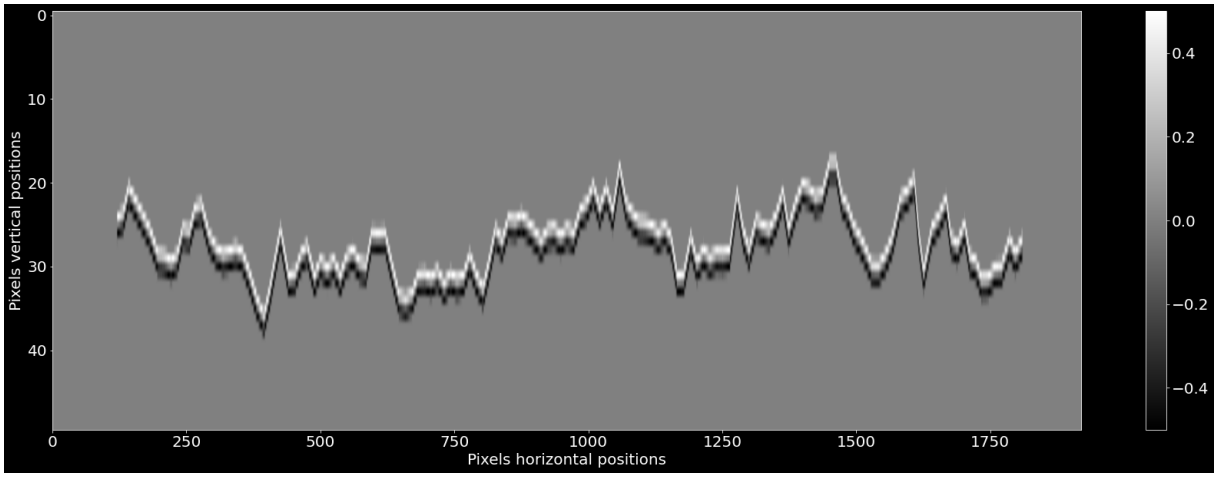

Figure 3.9: Laser line derivative at each column

$$\begin{bmatrix} 0 & 0 & 0 & 1 & 0 & 0 & 0 \\ 0 & 0 & 0 & 1 & 0 & 0 & 0 \\ 0 & 0 & 0 & 1 & 0 & 0 & 0 \\ 0 & 0 & 0 & 0 & 0 & 0 & 0 \\ 0 & 0 & 0 & -1 & 0 & 0 & 0 \\ 0 & 0 & 0 & -1 & 0 & 0 & 0 \\ 0 & 0 & 0 & -1 & 0 & 0 & 0 \end{bmatrix} \tag{3.16}$$

the null values in the left and the right-hand side of the central column are only used to respect the definition of a filter, which states that a filter size must be a $n * n$ matrix.

Convolving equation 4.6 with figure 3.9 resulting in figure 3.10 where we can simply identify the central line position by taking the coordinates of the maximum values at each column.

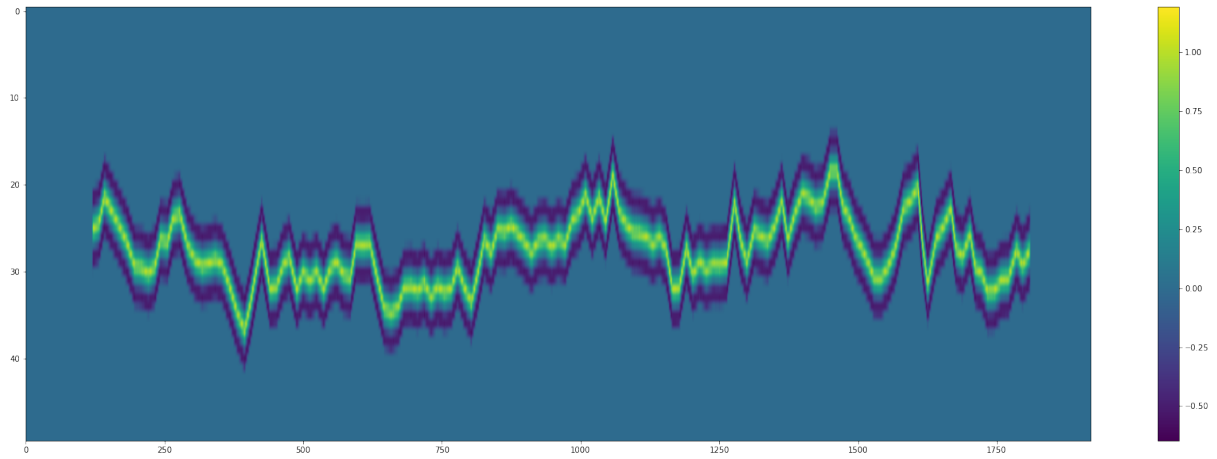

Figure 3.10: Convolution between the line derivative and the proposed filter result

This allows a precise estimation of the central line position. The precision is given by pixels, which means that the thinnest point we are detecting will be the camera pixels' dimension.

Conclusion

In this chapter, we discussed the approach we have chosen to conduct the data acquisition process, we start from a raw image that represent the observed variation of the laser line projected into a rough surface, we discussed the needed calculus to obtain the real world coordinates that are needed to proceed to the surface reconstruction. We recall that the geometrical transformation isn't an approximation, it represents the real geometrical changes occurring in the camera plane, this particular property give it the upper hand in comparaison with other methods such as interpolating the points which is not exact.

Chapter 4

Data processing

Introduction

As it was stated in previous chapters, our goal in the long term is to introduce a practical high speed device that can capture pavement surface texture at traffic speed in order to estimate the desired parameters to characterize pavement texture. However, when dealing with the collected data, we are generally faced with several problems that need to be treated in order to have precise measurements.

The produced errors are related to the measurement process, calibration and external factors. Apart from the vibrations that are present in data due to the movement of the device, the errors can take the form of spikes or drop outs that are inevitable when using laser sensors. The presence of outliers leads to an overestimation of the texture parameters and an erroneous characterization of pavement surface texture.

Our main goal in the short term is to implement a device that can successfully collect data and present reliable measurements, and to do so it is important to correct the problems that are produced, making the step of data processing a very crucial part of our study.

This chapter focuses on the measurement process as well as the different kinds of errors that are present and the different methods that are adopted to treat the data.

4.1 The measurement process

In 3D surface assessment, a certain number of parallel profiles, perpendicular to the direction of travel, are collected. In the x-direction, there are N points, the distance between the points is noted Δ_x; it depends on the image resolution provided by the camera. In the y-direction, the profiles are separated with a certain distance, this distance is noted Δ_y; it depends on the speed of travel and the camera's speed of collecting data. There are M profiles. The surface is presented with a matrix made up of $N * M$ points.

The measurement process can be done following two approaches:

4.1.1 Static collection of data

Static collection means that the data is taken one profile at a time. For better precision, it is necessary to precede each reading with an idle time in order to allow the stabilization of the device after displacement [35].

This procedure presents the advantage of acquiring data without any displacement noise. It is however very time consuming and doesnt align with our requirements.

4.1.2 Dynamic collection of data

Dynamic collection means that data is collected when the sensor is moving. The displacement of the sensor must be synchronized with the camera's speed of collecting data in order to have regularly spaced profiles.

An electronic system manages the synchronization between the displacement of vehicle and the data acquisition. The collection of data begins when the vehicle's speed is somehow stable, in order to minimize the vibrations caused by the acceleration and deceleration phases of the vehicle on which the device is mounted.

Ideally, the device should possess one degree of freedom, in the direction of travel, perpendicular to the profiles. However, due to the vehicle's movement, the device possesses a second degree of freedom in the y direction, and a third degree of freedom in the z direction. This movement in the z direction is mainly caused by the external vibrations; it will be recorded along with the true deviations of the surface.

For this chapter, two samples of collected point clouds that define two different zones of the pavement were used, the data was collected as a part of last year's internship at ICAM, the measuring device being the LJ-X8200 laser profiler.

The LJ-X8200 laser profiler has the following specifications:

- Width accuracy (X axis): 80-100 µm.
- Length accuracy (Y axis): 80-100 µm.
- Height accuracy (Z axis): 0.27 mm.
- Height measurement range: ±34 mm.
- The projected laser line's length (axe X): 64-80 mm.
- Nominal working distance: 245 mm.
- Repeatability: dZ = 1 micron, dX = 3 microns.

The following parameters were fixed:

- Camera viewing angle: 21.7°.
- Laser line thickness stain: e = 140 microns.
- Laser line length: $L_x = 80$ mm.
- N=3200 points / profile ($\Delta_x = 0.025mm$).
- The distance between the profiles: $\Delta_y = 0.025\ mm$.

4.2 Surface levelling:

The reference from which the point cloud is assessed is called a datum plane. The movement of the vehicle defines the datum from which the measurements are made, which means that the data is highly affected by external vibrations.

A misalignment of the nominal surface plane and the data collection datum leads to a linear trend in the assessed surface data, the aim of this step of data processing is the removal of the linear trend.

Levelling is performed by a least squares plane. The plane is then subtracted in order to adjust the datum value to zero, meaning that the data will be centered about zero.

The least squares mean plane is defined in mathematics as "a plane such that the sum of the squares of asperity departures from this plane is a minimum"[36]. Each surface has a unique least squares plane.

The linear or first order least squares mean plane for a z(x,y) may be defined by:

$$f(x, y) = a + bx + cy \tag{4.1}$$

The sum of the surface asperity departures from this polynomial plane was given by [36]:

$$\epsilon^2 = \sum_i^N \sum_j^M \left(z(x_i, y_j) - f(x_i, y_j)\right)^2 = \sum_i^N \sum_j^M \left(z(x_i, y_j) - (a + bx_i + cy_j)\right)^2 \tag{4.2}$$

The coefficients a,b,c are determined by minimising equation (4.2), we differentiate the equation with respect to the three coefficients:

$$\begin{cases} \dfrac{\partial \epsilon^2}{\partial a} = -2 \displaystyle\sum_i^N \sum_j^M \left(z(x_i, y_j) - (a + bx_i + cy_j)\right) \\ \dfrac{\partial \epsilon^2}{\partial b} = -2 \displaystyle\sum_i^N \sum_j^M \left(z(x_i, y_j) - (a + bx_i + cy_j)\right) x_i \\ \dfrac{\partial \epsilon^2}{\partial c} = -2 \displaystyle\sum_i^N \sum_j^M \left(z(x_i, y_j) - (a + bx_i + cy_j)\right) y_j \end{cases} \tag{4.3}$$

When rearranging equation (4.3), we obtain a system of linear equations, by solving them we find the coefficients of the mean squares plane:

$$\begin{bmatrix} MN & \sum_i^N \sum_j^M x_i & \sum_i^N \sum_j^M y_j \\ \sum_i^N \sum_j^M x_i & \sum_i^N \sum_j^M x_i^2 & \sum_i^N \sum_j^M x_i y_j \\ \sum_i^N \sum_j^M y_j & \sum_i^N \sum_j^M x_i y_j & \sum_i^N \sum_j^M y_j^2 \end{bmatrix} \begin{bmatrix} a \\ b \\ c \end{bmatrix} = \begin{bmatrix} \sum_i^N \sum_j^M z(x_i, y_j) \\ \sum_i^N \sum_j^M x_i z(x_i, y_j) \\ \sum_i^N \sum_j^M y_j z(x_i, y_j) \end{bmatrix} \tag{4.4}$$

The levelled surface is obtained by subtracting the least squares datum plane from the original surface.

4.3 Handling outliers

High-speed laser data acquisition presents the issue of the dense presence of erroneous values called "outliers" in the form of "spike errors" and "drop out errors".

The presence of spikes and drop outs results in inaccurate measurements and erroneously characterized texture. Therefore, in order to accurately calculate texture indicators, there is a pressing need for methods to minimize measurement noise, especially with the presence of surface parameters that have 2nd, 3rd, or even 4th-order dependence with respect to surface Z(x,y) values.

Finding the most suitable methods for filling up dropouts and the removed spikes is considered to be one of the most challenging steps of data processing.

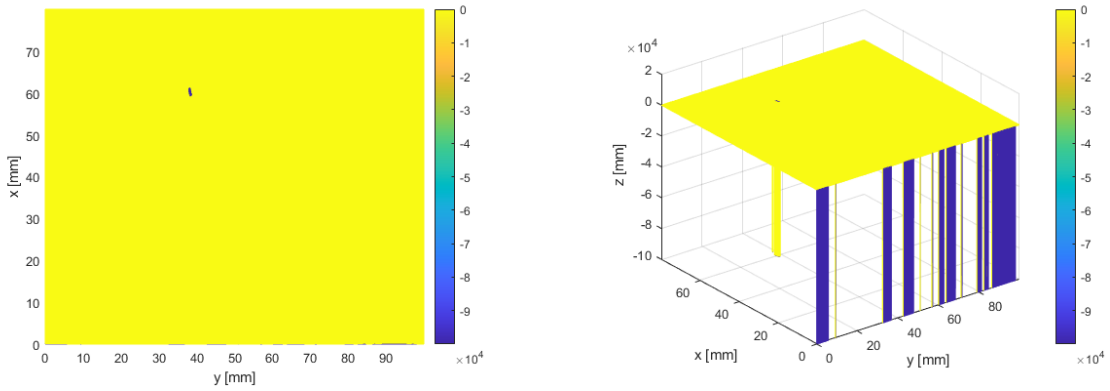

Figure 4.1: The drop outs in the scanned surface (zone 1)

4.3.1 Drop outs

A drop out is defined as an invalid reading or an intermittent missing value along the texture profile [37]. Drop outs originate from what we call "a dead zone" which is a zone of the laser line that can't be identified correctly.

Drop outs are formed because of two main reasons:

- When the object is located right under the emitter (in the center of the laser line), the laser has the minimum incidence angle. Moving along the laser line from the center to the left and right side, the incidence angle increases; the increase of the incidence angle leads to an increase in the the reflection angle. When the incident angle reaches a certain treshold where the corresponding reflex angle cannot be received by the optical camera, drop outs are produced [38]. This could explain the increase of drop outs percentile in the edge of the sample in the case of keyence measurements.

- When the object we are scanning is not smooth, which is the case of pavement surface, the presence of peaks blocks the irradiation of the laser light emitted to the surface from reaching the camera, creating dead zones and resuling in drop outs. This phenomena is called "shadowing", also known as "masking/hiding".

4.3.1.1 Drop outs detection

Drop outs usually take very extreme values, which makes the process of detecting these outliers less challenging. The identification of drop outs may be achieved by setting them a particular value within the data range. The points that exceede this value will be eliminated.

Another method that can ensure a more precise detection of drop outs is the False Discovery Rate method (FDR). This method will be discussed later on.

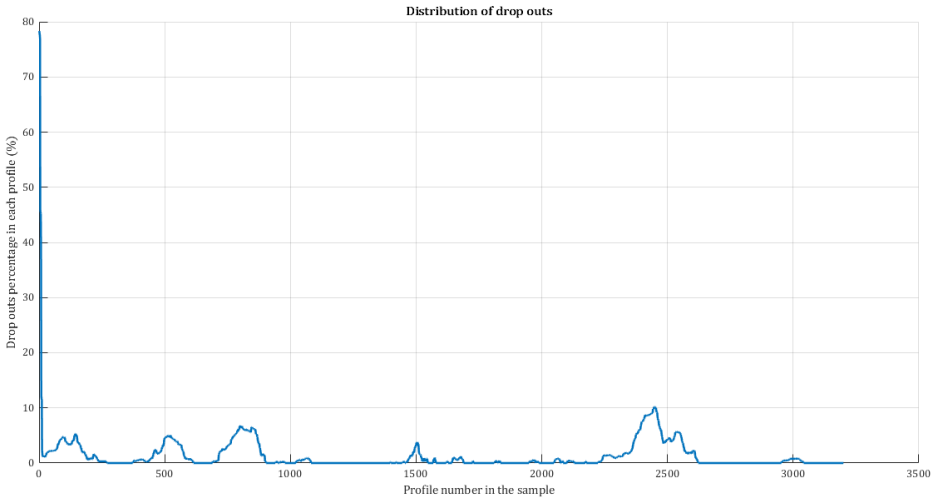

Figure 4.2: Distribution of the dropout percentage in the profiles of the surface (zone 1)

4.3.1.2 Drop outs filling

The presence of drop outs is moderate in the middle of the surface, and it can be very dense in the borders of the surface for being in the limit of the ineffective scan coverage of the laser. Figure 4.2 shows the distribution of the drop outs percentage in each line in the longitudinal direction that constitutes the surface in the first set of the keyence data.

For the areas where the drop outs percentage is low, they can be filled using the non-dropout points neighboring it. When the drop outs percentages is very high, it becomes impossible to replace these values using the neighboring points. For this reason, the profiles with important drop outs percentage should be dismissed.

When treating a sample of the data, we can observe that the percentage of the drop outs in the profiles is generally below 10%, the profiles with a percentage that exceedes 10% will be dismissed.

A method to address the problem of drop outs is proposed in [38]. An algorithm was developped to predict appropriate values assigned to the dropout points.

$$\begin{cases} z_i = \dfrac{1}{5}\displaystyle\sum_{j}^{5} z_{i-j} & (i \geq 6) \\ z_i = \dfrac{1}{5}\displaystyle\sum_{j}^{5} z_{i+j} & (1 \leq i \leq 5) \end{cases} \tag{4.5}$$

with i and j being the longitudinal position of point i or j of each profile.

According to [38], this solution doesn't give perfectly accurate profile geometries since it uses the points either after or before the drop out, leading to a presence of right angles in the profile, but the method is judged to be very simple to implement as well as being efficient in its operation, which led us to adopt it for our study. Figure 4.8 shows the result of the adopted filling procedure, the profile is then smoothed using a moving-average filter.

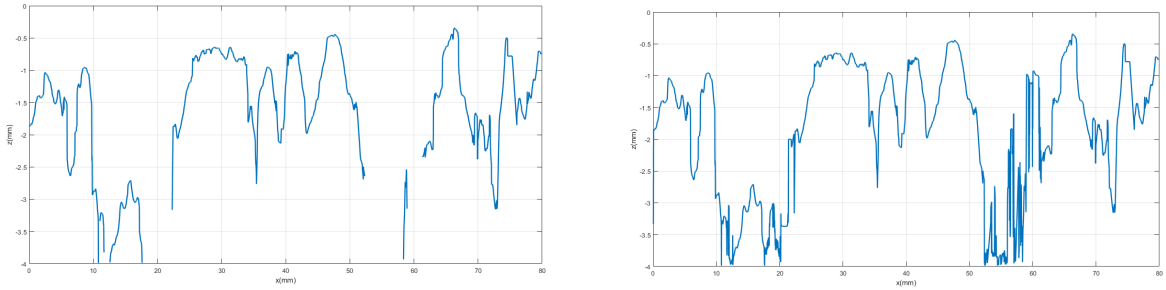

(a) Before filling (b) After filling

Figure 4.3: The result of the filling procedure on a given profile of the scanned surface (zone1)

The moving-average filter slides a window along the data, computing averages of the data contained in each window.

The following difference equation defines a moving-average filter of a vector z:

$$z'(n) = \frac{1}{WindowSize}(z(n) + z(n-1) + ... + z(n-(Windowsize-1))) \tag{4.6}$$

This method is chosen for its easy implementation and its effectiveness, concretely it served to remove the noise caused by the mobile device vibrations, on the other side it allowed cleaning the data from all possible artifacts.

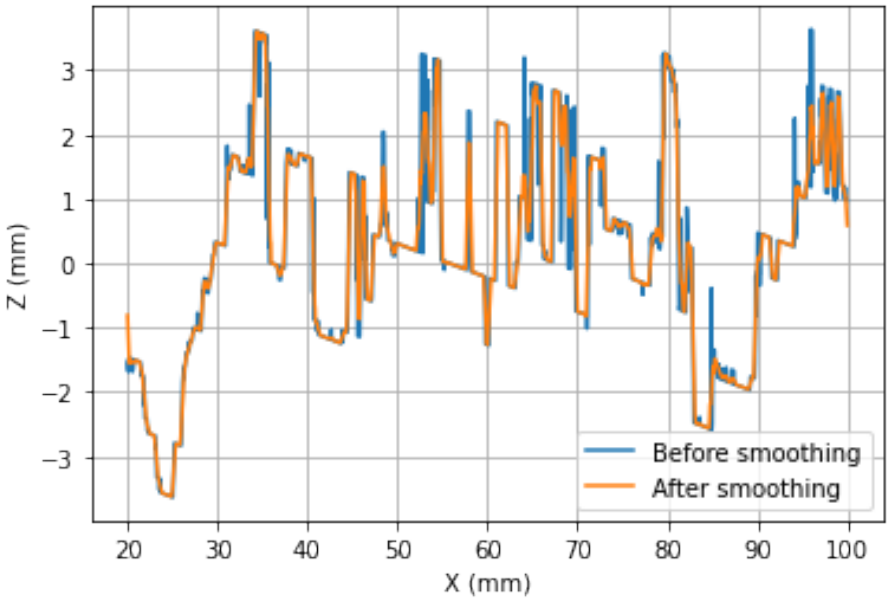

Figure 4.4: The smoothed profile

4.3.2 Spikes

Spikes originate from a change in the amount and direction of light reflected to the receiving lens, this can be due to the sharp edge of aggregate, the presence of shiny materials such as silica, water, pavement markings and polished aggregates. Fresh asphalts being

black and shiny present the problem of scattering only a small part of the incident light as it absorbs a portion of it, and deviates another portion [38].

Other factors, such as temperature, geometry, secondary reflections, bandwidth, and sampling rate, are potential sources of noise in the measurements [38].

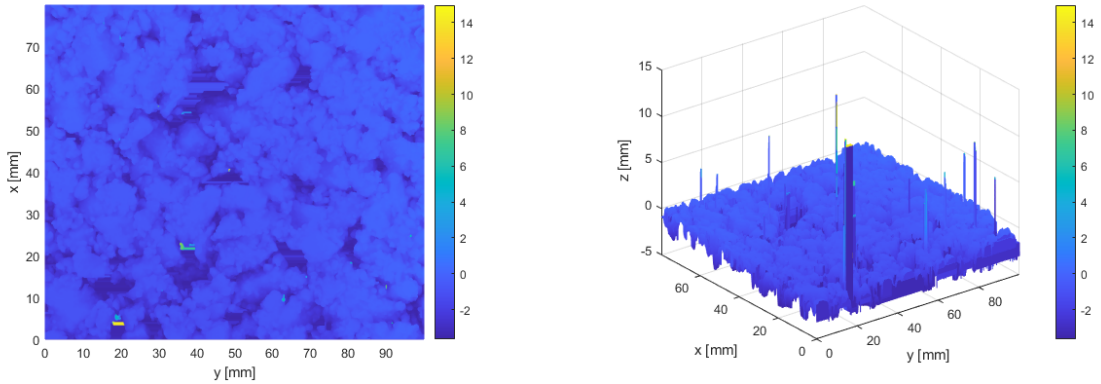

Figure 4.5: The spikes in the scanned surface (zone 1)

4.3.2.1 Spikes detection

Spikes detection is a very challenging step of data processing since the range of spikes height values is large. They can have both small values and very large values, these are easier to treat since they are easily identifiable.

The use of preliminary identified thresholds such as 2-sigma, meaning that 5% of the data will be eliminated, or 3-sigma, where 0.3% will be eliminated, can lead to an overestimation or an underestimation of the spikes' percentage, especially that the percentage of spikes in each sample can be different, since it is directly related to the conditions in which the data acquisition step took place.

When spikes are not properly treated, they can seriously bias the calculation of texture parameters. The FDR method was used to detect spikes.

The false discovery rate procedure is a statistical method that controls the proportion of wrongly identified spikes among all identified spikes [37]. The FDR control allows us to have an adaptive threshold selection for any data sample, this threshold differentiates between valid measurements and invalid measurements. This presents the advantage of being able to develop a standard algorithm that can work on any data sample.

The FDR method consists mostly of two steps:

- Determining the probability density function.
- Determining the outlier detection threshold.

In practice, the pavement surface texture is not normally distributed; the distribution is asymmetrical, as shown in figure 4.7. In previous studies regarding the study of

pavement texture a Generalized Gaussian Distribution (GGD) which is a more flexible 3 parametric density function that allows for the tail of the distribution to be larger or thinner, was used to fit the data. However, the use of a GGD calls for dividing the data into two parts and using two different sets of parameters for each part in order to have a better fit, this method does not always give the best results as shown in figure 4.6.

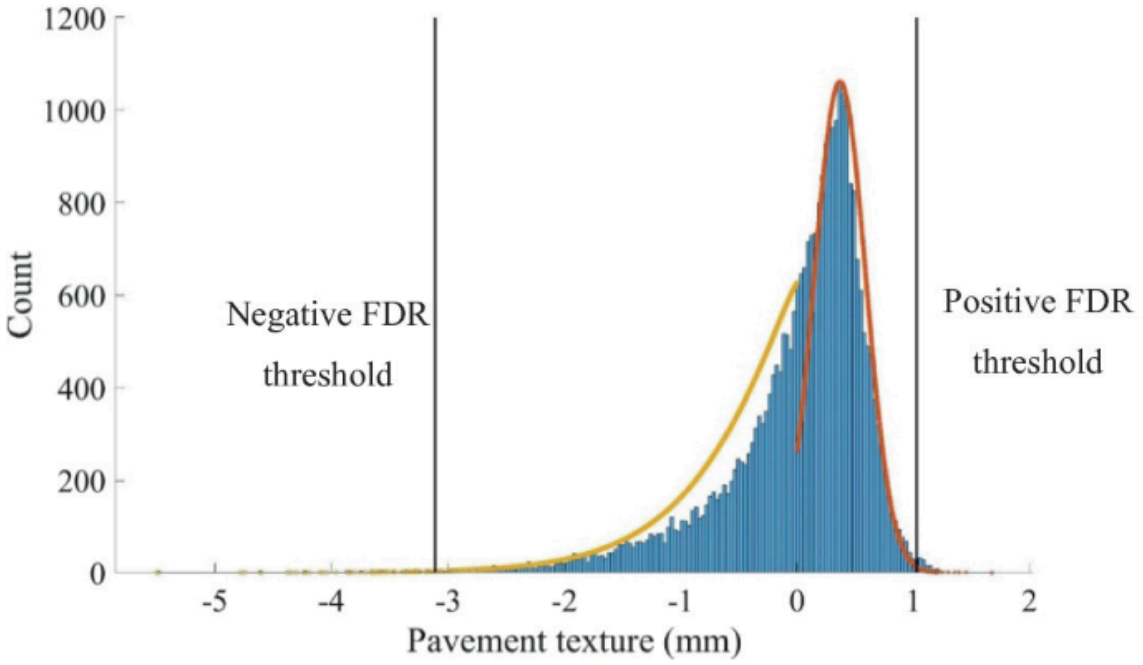

Figure 4.6: The GGD of pavement texture data [39]

Other parametric density functions were considered, such as the Weibull distribution. However, the use of such functions calls for a manipulation of the data, in order to respect the characteristics of the functions. For instance, the 2-parameter Weibull distribution, which is characterized by the shape and scale parameters, is defined only for positive values. Adding a third threshold parameter allows us to work with negative data, but this makes the process of estimating the parameters more complicated.

Taking into consideration the shape of the pavement texture measurements distribution and all the limitations of the parametric functions which result in an improper description of the data, a non-parametric Kernel probability density function estimation was used instead. Kernel-based estimators can uncover important patterns in the data while filtering noise and ignoring irrelevant details, which makes the estimated function smooth [40]. The use of a non-parametric solution is very practical in our application, since it does not require making an assumption about the distribution of the data.

The Kernel density estimation is implemented in Matlab through the ksdensity function, the estimate is based on a normal kernel function. Once the density probability is defined, the next step consists in calculating the positive threshold corresponding to our data that allows us to detect spikes using the FDR method, the method can also be used for calculating a more precise negative threshold to detect non-treated dropouts. The FDR was applied following the steps explained below:

- Separate the p-values of the positive and negative texture measurements.

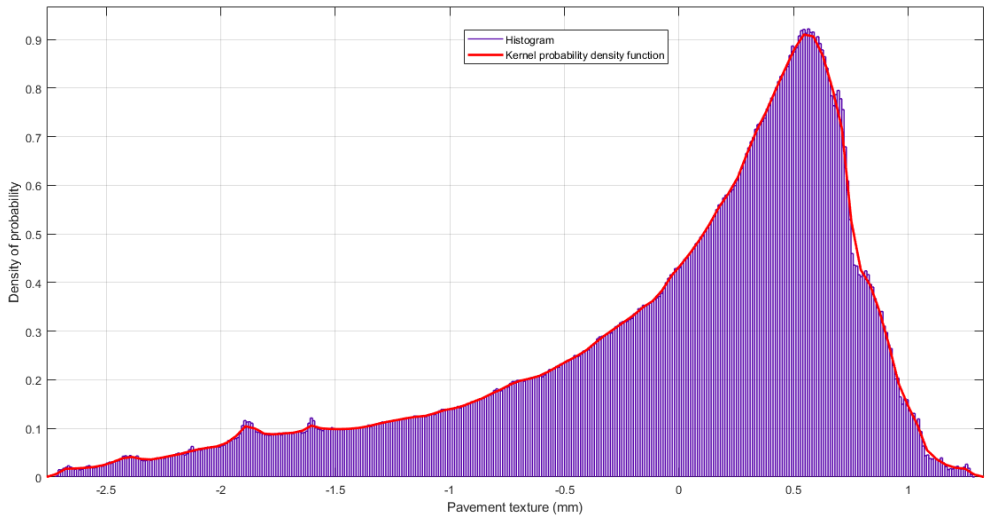

Figure 4.7: The Kernel density estimation applied on zone 1

N1: the number of the positive values.
N2: the number of the negative values.
N=N1+N2 : the total number of the p-values.

- Reorder the two different sets of the p-values in an increasing order.

$$P_1 \leq ... \leq P_i \leq ...P_{N1}$$

$$P_1 \leq ... \leq P_i \leq ...P_{N2}$$

- Select a q value at which to control the FDR. According to both [37] [39], the ideal value of q to control outliers in pavement surface texture is 0.1, this value was established by conducting a sensitivity analysis, the analysis aims to maximize the correctly identified outliers and minimizing the wrongly identified outliers.

- Find k which presents the maximum i that respects equation 4.7.

$$P_i \leq \frac{i}{N} q \tag{4.7}$$

  This equation is applied to the two different sets of p-values, which gives us k1 for the positive values and k2 for the negative values.

- Outliers are identified as all measurements whose p-value is inferior to P_{k1} for the positive values and P_{K2} for the negative values.

When treating the data we observe the presence of curve in the surface, these forms need to be removed in order to ensure a better spikes processing. The simplest and most effective way to do so is by fitting the curved surface with the least squares polynomial plane.

In general, the least square fitted polynomial plane of n-th order is given by:

$$f(x,y) = \sum_{k=0}^{n} \sum_{l=0}^{k} a_{(k-l)l} x^{k-l} y^{l} \tag{4.8}$$

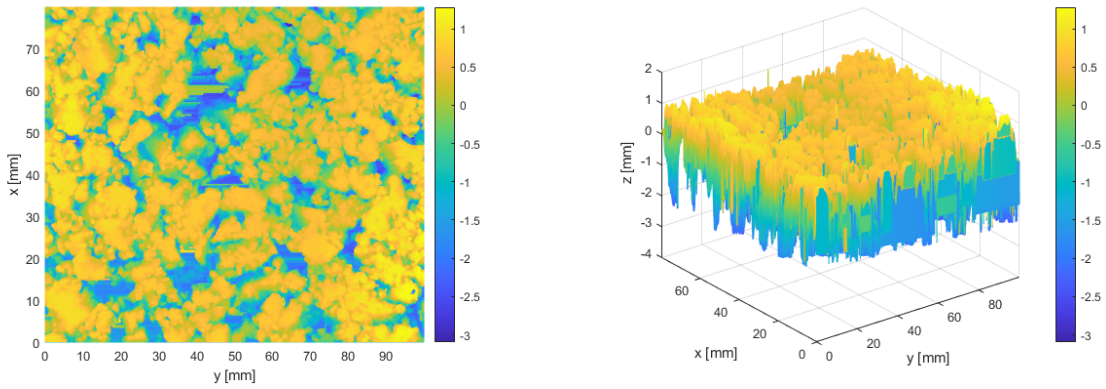

Figure 4.8: The surface with a curvature (zone 1)

Using the same method that was used previously, we establish the sum of the surface asperity departures from the polynomial.

$$\epsilon^2 = \sum_i^N \sum_j^M \left(z(x_i, y_j) - f(x_i, y_j)\right)^2 = \sum_i^N \sum_j^M \left(z(x_i, y_j) - \sum_{k=0}^{n} \sum_{l=0}^{k} a_{(k-l)l} x_j^{k-l} y_i^l\right)^2 \quad (4.9)$$

The same procedure that was explained in detail for the first order polynomial plane was followed, meaning that the coefficients a_{kl} were determined by minimizing equation 4.9. Therefore, by differentiating the equation with respect to the coefficients and equating them to zero [36].

$$\frac{\partial \epsilon^2}{\partial a_{kl}} = 0 \quad , \quad (k = 0, 1, ...; l \leq k) \quad (4.10)$$

the obtained equations are rearranged in a matrix form, the system is then solved.

Since this step aims to eliminate the curve form and not complex forms such as waviness, a second-order quadratic is judged to be enough for a sample of the pavement surface. In this case, the polynomial is given by:

$$f(x, y) = a_{00} + a_{10}x + a_{01}y + a_{20}x^2 + a_{11}xy + a_{02}y^2 \quad (4.11)$$

Additionally, to the FDR method, another criterion was proposed by [8] to detect spikes, the procedure is called the "overslope" procedure, it consists of assigning read error status to the i-th data point that satisfies 4.12.

$$|z_i - z_{i-1}| \geq \alpha.\Delta x \quad (4.12)$$

with Δx being the distance between two points in one pavement texture profile, and α being a constant factor.

A series of research conducted by Belgian Road Research Center (BRRC) found that a value of $\alpha = 3$ is recommended. However, this method is better applied "in both directions" of the profile, in order to make it symmetrical [41].

4.3.2.2 Spikes filling

The removed spikes are replaced with an interpolated value by using the neighboring values, simple linear interpolation was adopted. The procedure of spikes filling is proposed by [8], and equation 4.13 is used.

$$z_i = \frac{z_n - z_m}{n - m}(i - m) + z_m \tag{4.13}$$

with:

- i is the number of the sample whose value is invalid;
- m is the number of the closest sample before i having a valid value;
- n is the number of the nearest sample after i having a valid value;
- zi is the interpolated value for sample i;
- zm is the sample m value;
- zn is the sample n value.

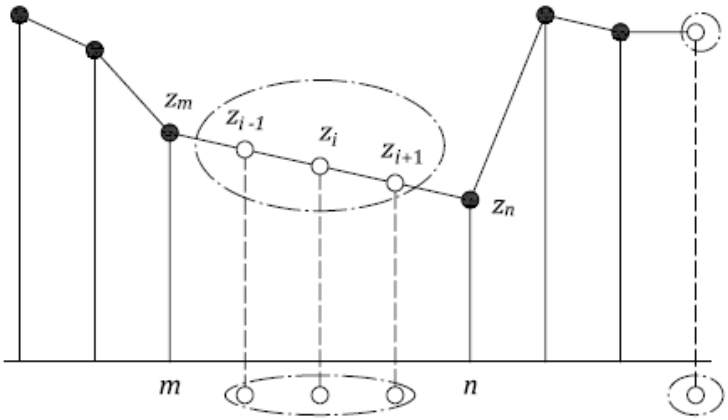

Figure 4.9: Illustration of the filling spikes process [8]

The points on the borders are replaced using the closest non-outlier value.

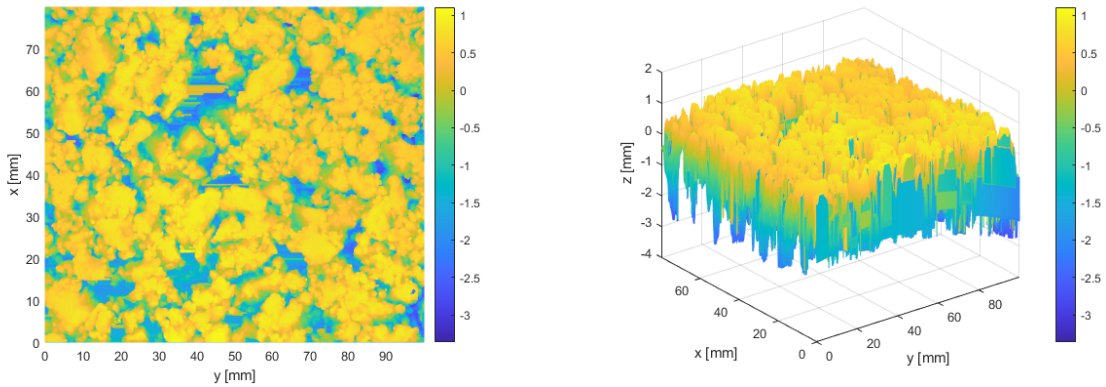

Figure 4.10: The result of the final treatment of the surface (zone 1)

4.3.3 Mean texture depth calculation procedure

Apart from finding more representative 3D texture parameters to replace the current ones, the main objective of this work remains to be finding a method that estimates the MTD from the captured point cloud, in order to replace the sand patch method.

The difficulty of this step is to find the best approach to estimate the MTD from a digitized surface that simulates and correlates with the sand patch method, which is a purely manual technique.

According to its definition, the MTD corresponds to the average distance of the object surface to a plane deliminated by the highest peaks.

As a first reflex, the determination of the parameter MTD using 3D point clouds could be performed in a similar way to the arithmetical mean height, with the difference that the reference plane is placed on the uppermost points of the point cloud [42]. The distances between the points and the plane have to be summed and divided by the total number of points. Even though, this calculation procedure is easy to implement, it presents certain limitations since it does not correspond perfectly to the definition of the MTD.

Another more adapted approach consists of calculating the volume between a plan, and the recovered surface. The plan, as described in [8], is defined by the three highest points of the surface. The problem with this method is that the plan is not horizontal and has a certain linear trend that can take important values, as shown in figure 4.11.

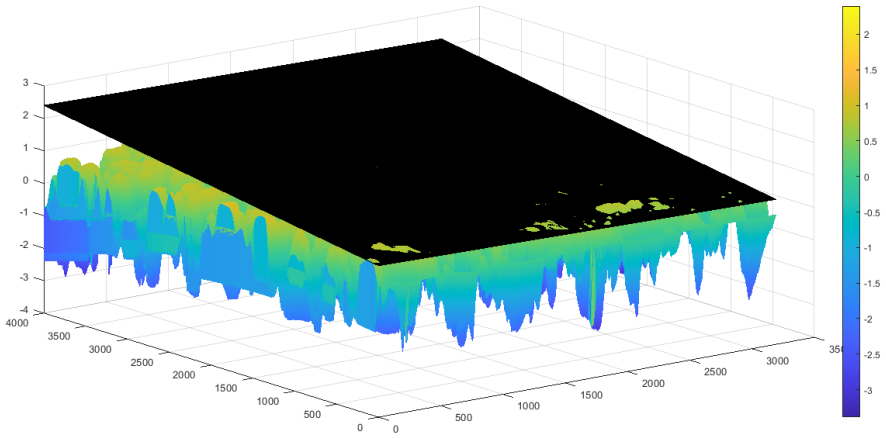

Figure 4.11: Illustration of the limitation of the first proposed method

A method for simulating the MTD is proposed by [43]. The MTD is obtained based on the recovered 3D texture height map, with the assumption that the sand will fill in all the hollow space up to the highest elevation of the recovered surface[43]. The material volume is calculated using a squarebased pyramid for any pixel of the recovered surface. The equation is given by:

$$MTD = h_{max} - \frac{1}{A}\sum_{i=1}^{M}\sum_{j=1}^{N}\frac{1}{3}ah_{ij} \tag{4.14}$$

with:

MTD : Simulated texture depth of the recovered surface texture.
h_{max} : the highest elevation of the recovered surface texture.
h_ij : the elevation of any pixel of the recovered texture.
A : the area of the recovered surface.
a : the area of each pixel of the recovered texture.
M,N : number of points in each direction.

Even though this equation corresponds better to the sand patch method, the assumptions that were made lead to an overestimation of the parameter. In practice the hollows on the border of the patch are not filled completely, also the calibrated beads don't fill up to the highest elevation and the abnormally large chippings are ignored when levelling the beads as shown in figure 4.12.

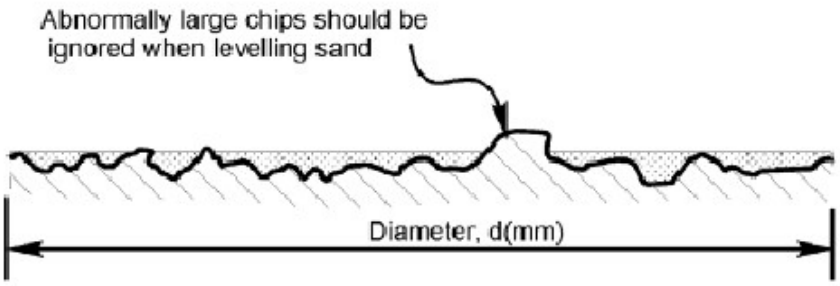

Figure 4.12: Illustration of the sand circle test [44]

In order to avoid this problem, a solution is proposed. The volume is calculated between the horizontal plan that passes through the mean of the highest elevation of each line and the recovered surface. Equation 4.16 becomes:

$$MTD = h'_{max} - \frac{1}{A}\sum_{i=1}^{M}\sum_{j=1}^{N}\frac{1}{3}ah_{ij} \tag{4.15}$$

with:

$$h'_{max} = \frac{1}{M}\sum_{i=1}^{M} max(z_j) \quad with: \quad j = 1:N \tag{4.16}$$

4.4 Results

The results that are obtained using the developed algorithm are compared to the results obtained using the sand patch method on the same surface, as well as the results given by the algorithm that was used during last year's project. The results are summarized in table 4.1:

We conclude that the results given are satisfactory, as the values of MTD are very close with the values given by the sand patch method. The error is reduced in comparison with the results that were given by the previous study.

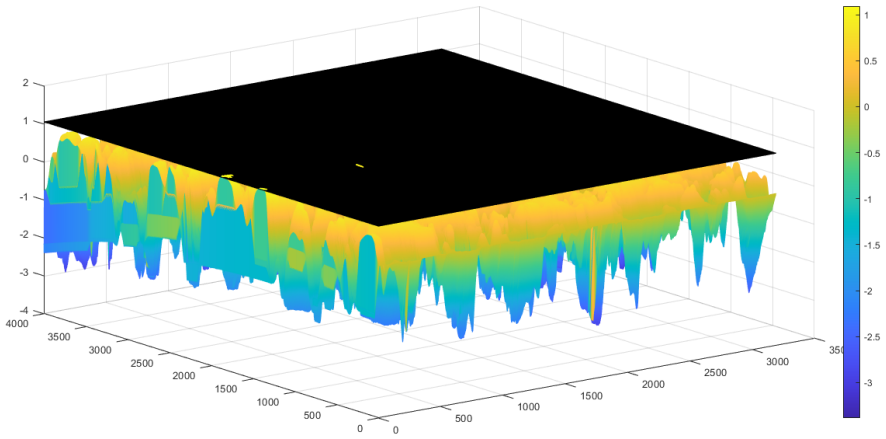

Figure 4.13: Illustration of the adopted method for calculating the MTD

Region	Sand patch MTD (mm)	Our results		Previous results	
		MTD (mm)	error (%)	MTD (mm)	error (%)
1	1	1.02	2	1.19	19
2	0.54	0.60	11.11	0.98	81

Table 4.1: Summary of the data processing results

Conclusion

In this chapter, we developed a method for processing the captured data of the pavement surface in order to eliminate the various errors that can influence the characterization of surface texture. The used methods were mainly inspired by previous research conducted by the different entities. The objective was to develop a standard automated algorithm that can treat any sample of data in an efficient and reliable way.

The method consists of eliminating any present linear trend in the data by levelling the surface using the least squares plane, and then removing the outliers that are present in the form of dropouts and spikes and controlling their percentage in each line using mainly the false discovery rate method that was presented in detail. The eliminated data was then replaced using the neighboring points.

When comparing the results given after treating the surface, with the results that were obtained by the sand patch method, we find that the error is acceptable.

Chapter 5

Prototyping

Introduction

In this chapter, we discuss the prototyping process of our scanner described earlier. After having all the building blocks and the technical knowledge needed to satisfy the requirements of our surface scanning application, we describe the electrical scheme and the mechanical system holding our required hardware. This prototype needs to respect certain constraints that we have argued in a previous chapter, such as the incidence angle of the camera and the distance between the pavement and the laser projector.

5.1 General system functioning process

The device is a four wheeled robot designed to hold the camera and the laser projector, two wheels are motorized and use the differential robot system principal, the prototype moves in straight lines to translate the laser line and the camera simultaneously while scanning the full wanted surface, the motors aim to stabilize the system speed, so we can scan the area profile by profile with equal distances in between each. The distance depends on the camera frequency.

5.2 Used hardware

5.2.1 Triangulation materials

5.2.1.1 The camera: *Raspberry Pi High Quality Camera*

Figure 5.1: Raspberry HQ camera

The HQ Raspberry camera is the latest generation of the existent PI cameras, it uses **Sony IMX477R stacked** with a 12.3 megapixels resolution, 7.9 mm sensor diagonal which makes it very small and lightweight and suitable for our prototype. It has a very high resolution with 1.55 um × 1.55 um pixel size, also it is affordable compared to other commercial cameras since it doesn't need a dedicated processing system neither a memory

management system since it is directly connected to a raspberry which takes care of the latter.

The camera comes with a variable focal length in addition to the focal length caused by the lens that we will present later. it has a software that runs on a Raspberry Pi and in which we can tune the parameters of the camera, such as the shuttering speed and the sensitivity of the sensor, the resolution and the frame taken per second.

5.2.1.2 The lens:*16 mm 10 MP Telephoto Lens*

A compatible C or CS mount lens is needed for the camera to properly work, it comes with an adjustable focal length for far and near sight.

The focal length plays a major role in defining the image inside the camera projection plan, it is the one responsible for defining the visual areas as well as the blurred spots on the image, it is adjusted so that the parts representing the laser ine are clear and not blurred.

Figure 5.2: Raspberry HQ camera lens

5.2.1.3 The laser projector: *Line Laser Diode - 5mW 650nm Red*

The laser line projector is used to illuminate the part, where the triangulation is performed. This type of laser projectors comes with a variable focus, that allows tuning the laser width with respect to the projection height.

The intensity of the laser is very crucial, since it dictates the possibility of doing scans in daylight. The color is also very important, where green light lasers are preferable, only the red one was available in local markets.

5.2.2 Power systems, movements handler and control circuits

As already mentioned, the prototype movement is handled using two DC motors supplied with integrated encoders. The motors are driven using an H bridge and the principal energy suppliers is a LIPO battery.

Figure 5.3: Laser line projector

5.2.2.1 DC Motors : *Metal DC Geared Motor w/Encoder CQGB37Y001*

With a 7.5:1 gear ratio supplied with an integrated encoder that delivers 64 ticks per revolution which means that a full rotation of the motor shaft will generate 480 ticks per revolution which gives us a resolution of 0.75 degrees.

The pair of motors is controlled with an H bridge module capable of controlling two motors at once with a variable speed and rotation direction.

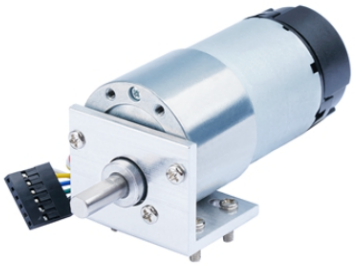

Figure 5.4: Metal DC Geared Motor w/Encoder CQGB37Y001

5.2.2.2 H bridge : *LM298n*

This piece is a DC motor controller capable of driving 2 different motors separately in both directions (clockwise and counterclockwise) and with a variable speed.

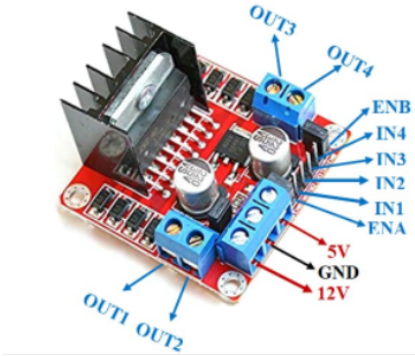

Figure 5.5: LM298n with its associated connections

5.2.3 Control systems

5.2.3.1 Data acquisition from the camera : *Raspberry Pi 3 B+*

The Raspberry Pi is a mini computer that has 1 GB of ram supplied with an embedded OS, usually a dedicated Linux distribution called RaspbianOS or Bullseye.

In our prototype, the Raspberry Pi is the principal component, it takes care of capturing the needed frames representing the profiles of the laser line at each time step with a full High Definition (HD) resolution with a speed of 30 frames per seconds, it is connected to a computer where it is controlled using a wireless connection with the Secure Shell protocol (SSH).

The Raspberry Pi, since it is powered with an operating system it is very complicated to work with in real time applications such as driving motors and regulating the speed, the reason is that each command isn't executed directly, but it goes through a scheduler that favors the operating system functions which results in unwanted delays, therefore the motors control is handled using another control system that we will present later on, additionally the Raspberry Pi GPIOs set doesn't contain analogue pins which are needed to control the H-bridge that takes care of motors controls.

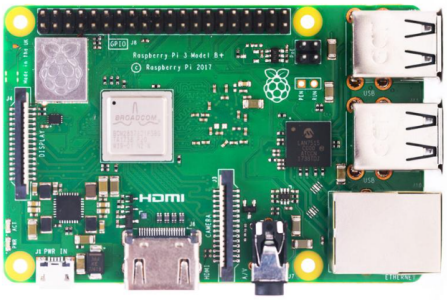

Figure 5.6: Raspberry Pi 3 B+

5.2.3.2 Motors control : *ESP32 Devkit V1*

The ESP32 is a fast and low cost microcontroller with a clock frequency up to 240MHz, and it has a 512 Kb of RAM. It is used to drive the motors and read from both motors encoders, we supplied a program running each 20 ms to check the motors' speed and make the necessary changes to the command to keep it constant.

5.2.4 The overall schematic

The discussed hardware is assembled so that the ESP32 take care of the motor control we ensure the data acquisition by the Raspberry Pi and the communication between the two agents, the resulted scanned surface resolution as discussed in the previous chapter depend on 3 factors, the camera pixels density, the frames per seconds furnished by the camera and the speed of the system itself, these 3 factors combined results in the final digitized surface resolution and precision, therefore the two principal agents need to be synchronized so that the overall cloud points will not be biased.

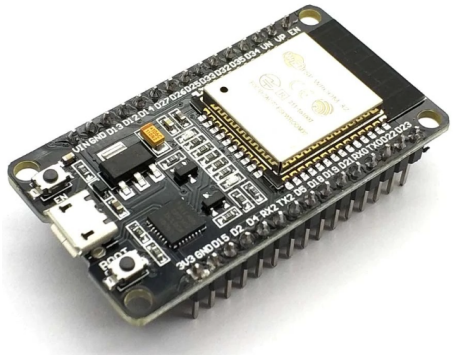

Figure 5.7: ESP32 Devkit V1

The system is assembled based on the 5.8

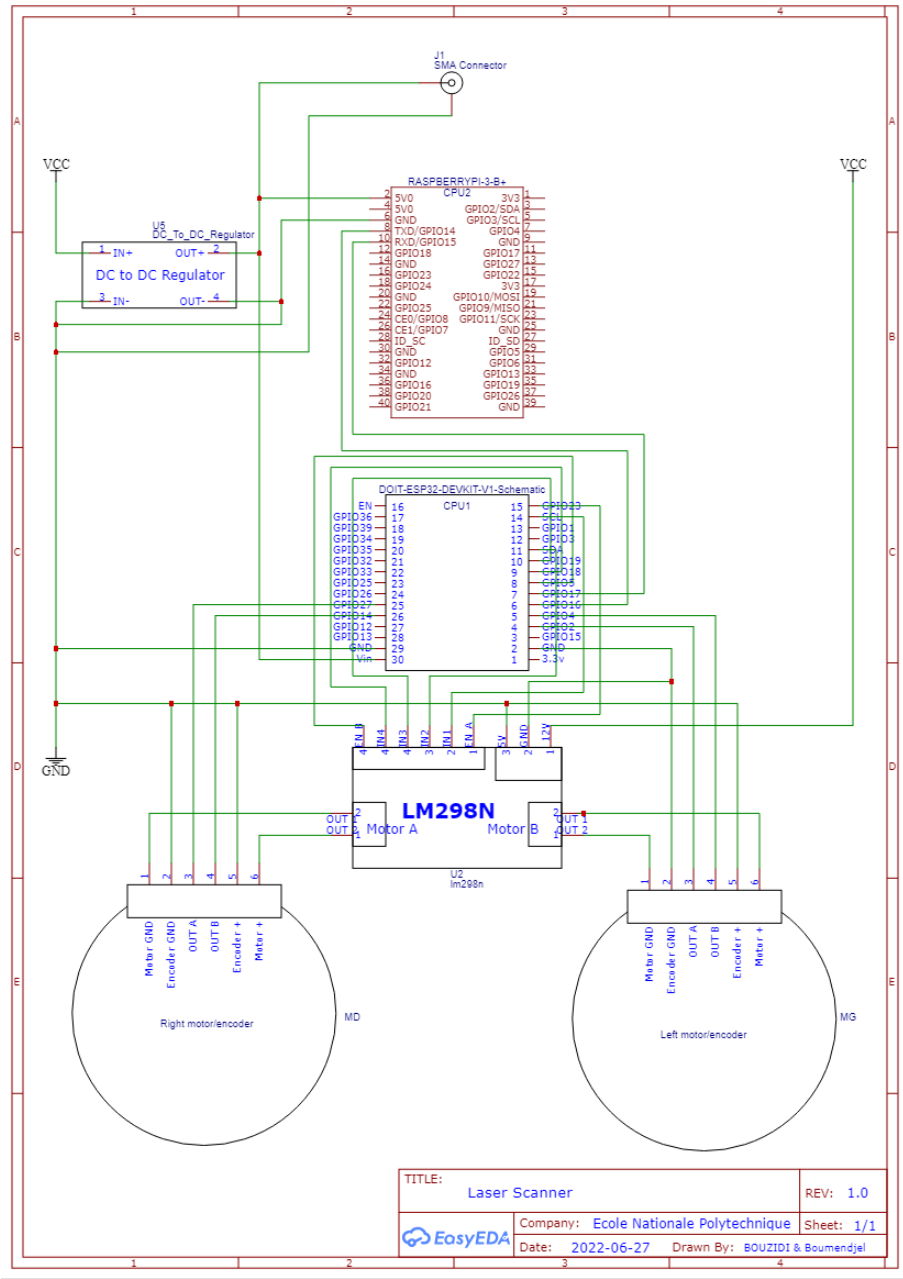

Figure 5.8: Electrical scheme of the system

5.3 Mechanical description

The mechanical part of the prototype is built according to the hardware specifications. The main characteristics that were taken into consideration, and on which the design was based, are:

- It holds the laser at a certain elevation. The distance between the laser projector and the ground depends on its fan angle.
- It holds the camera. The distance between the camera and the projected laser line depends on its focal length.
- The incidence angle in the prototype is adjustable in order to study the influence of the shadowing and find the optimal angle.
- It supports all the used hardware, such as the battery, the motors and the electronic circuit.

All the measurements were made with respect to these components. It is important to state that the first prototype represents some compromise from the initial requirements due to some limitations.

5.3.1 Concept embodiment

5.3.1.1 Laser projector holder

The holder clamps around the 12 mm diameter laser pointer and tightens to lock the laser in place with a bolt.

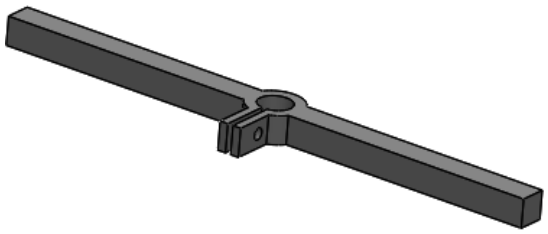

Figure 5.9: The laser holder

The laser holder is mounted at a certain elevation known as the working distance. It is given by:

$$y = \frac{x}{2tan(\frac{\theta}{2})} \tag{5.1}$$

with:

θ: fan angle.
x= laser line length.
y= working distance.

5.3.1.2 Camera projector holder

The camera holder consists of a mounting bracket for the camera, that is attached using four bolts. The system is mounted on a bar, it clamps around the bar and tightens using a bolt. This swiveling system allows us to adjust the position of the camera in order for its projection plan to meet the projected laser line on the pavement.

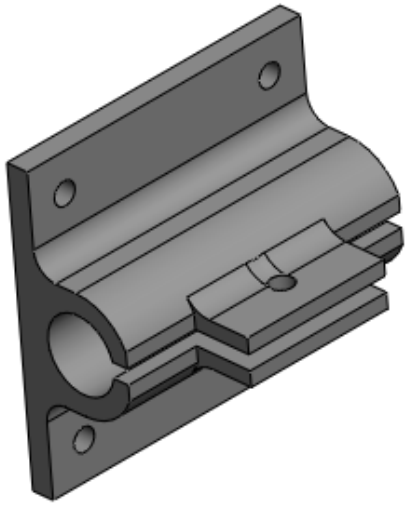

Figure 5.10: The camera holder

5.3.1.3 The sliding system

A sliding system is designed to ensure the variation of the incidence angle. The system holding the camera has a pivot connection in one direction, and moves along the fixed horizontal rail in the other direction as shown in figure 5.11, which ensures the variation of the angle.

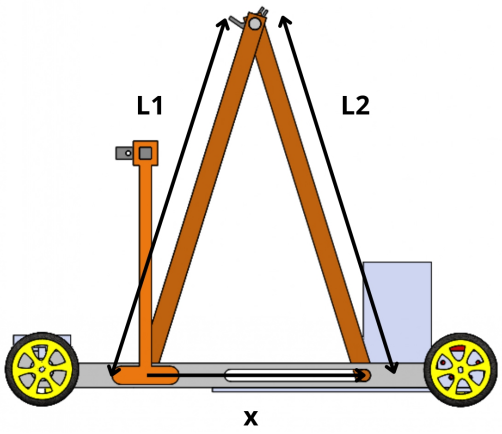

Figure 5.11: The sliding system

When applying the law of cosines, we find that the incidence angle in terms of the system's dimensions is given by the following equation:

$$\theta_{in} = 90 - arccos\left(\frac{L_1^2 - L_2^2 + x^2}{2xL_2}\right) \tag{5.2}$$

for an easier variation of the angle, the two supports are made of equal lengths. The equation is simplified:

$$\theta_{in} = 90 - arccos\left(\frac{x}{2L}\right) \tag{5.3}$$

The length depends on the focal length of the camera, as well as the desired vision field that captures the total length of the laser line.

The relationship is given by:

$$\frac{1}{f} = \frac{1}{Z_o} + \frac{1}{Z_i} \tag{5.4}$$

with:

f: focal length.
Z_o: the length in real life.
Z_i: the length as shown in the camera.

5.3.1.4 The wheels

As it was previously stated, two motors are used to ensure the movement of the back wheels. Motor to wheel connectors are used to ensure the transmission of the movement.

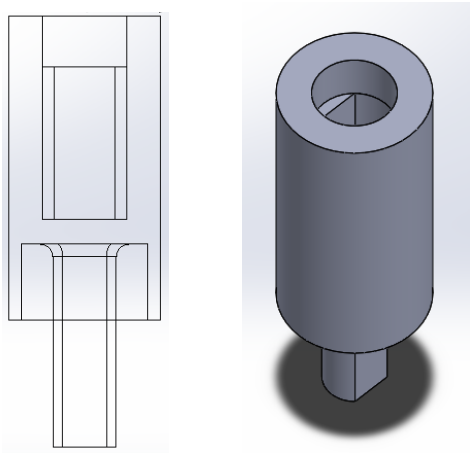

Figure 5.12: The motor to wheels connectors

Bearing are used for an easier movement of the front wheels, since they transfer motion by supporting and guiding the wheels.

The SKF 607-2Z deep groove ball bearings are chosen for our prototype. A miniature connector that couples the bearing and the wheel is designed.

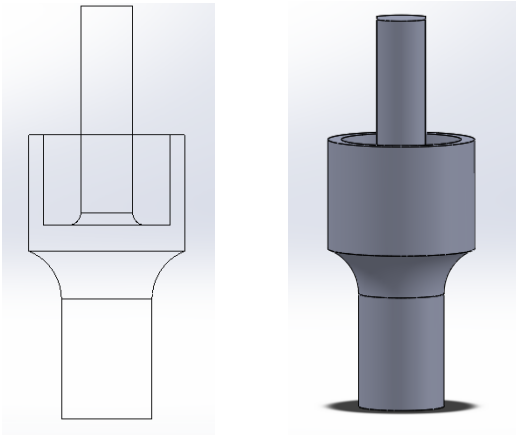

Figure 5.13: The motor to wheels connectors

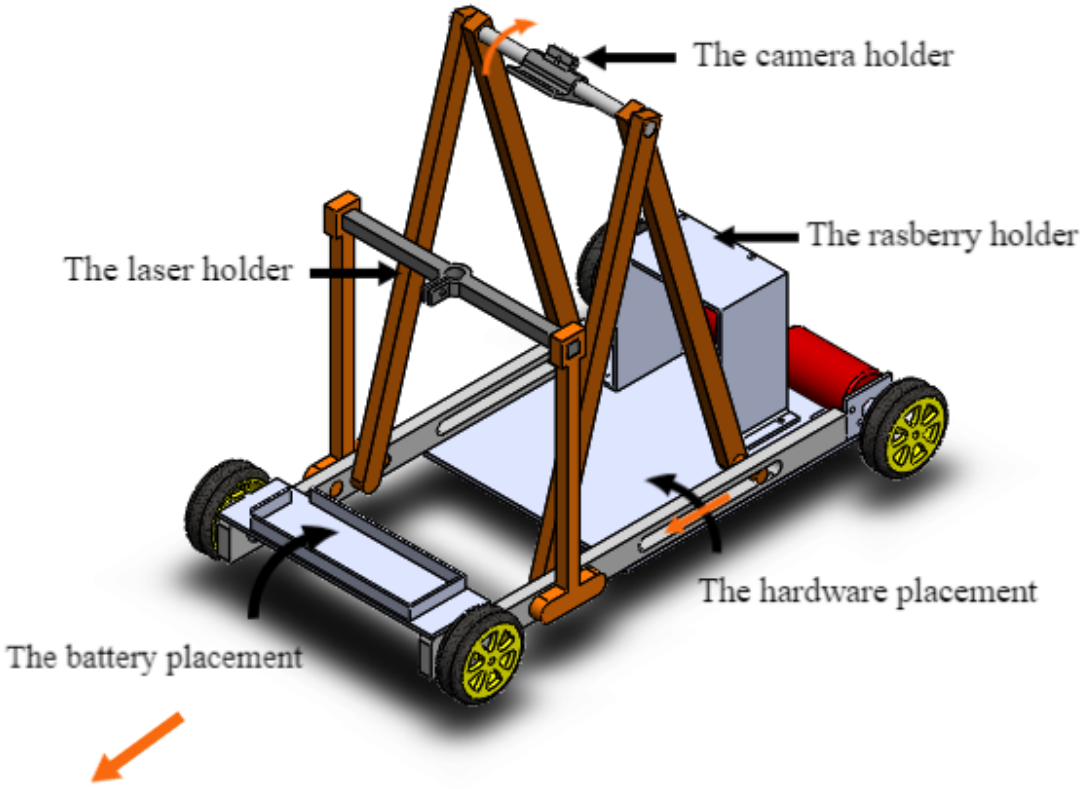

Figure 5.14: The 3D model of our prototype

5.3.2 Manufacturing

The different mechanical components of the prototype are manufactured using a 3D printer. After finalizing the first step of the 3D printing process, which is 3D modeling, the remaining steps are followed:

- Slicing: the designed model is transformed into an STL file, the slicing software that is used is CURA. The software generates a GCode file that the printer reads to build the model. The purpose of slicing is to allow the 3D printer to calculate the amount of filament required as well as the route when printing the model, it

can also automatically create support structures.

- Printing: after the slicing step is complete, the GCode file is uploaded to the printer, and the printing process is launched.
- Post-processing: after printing, the support needs to be removed, and then the different parts of the prototype are assembled.

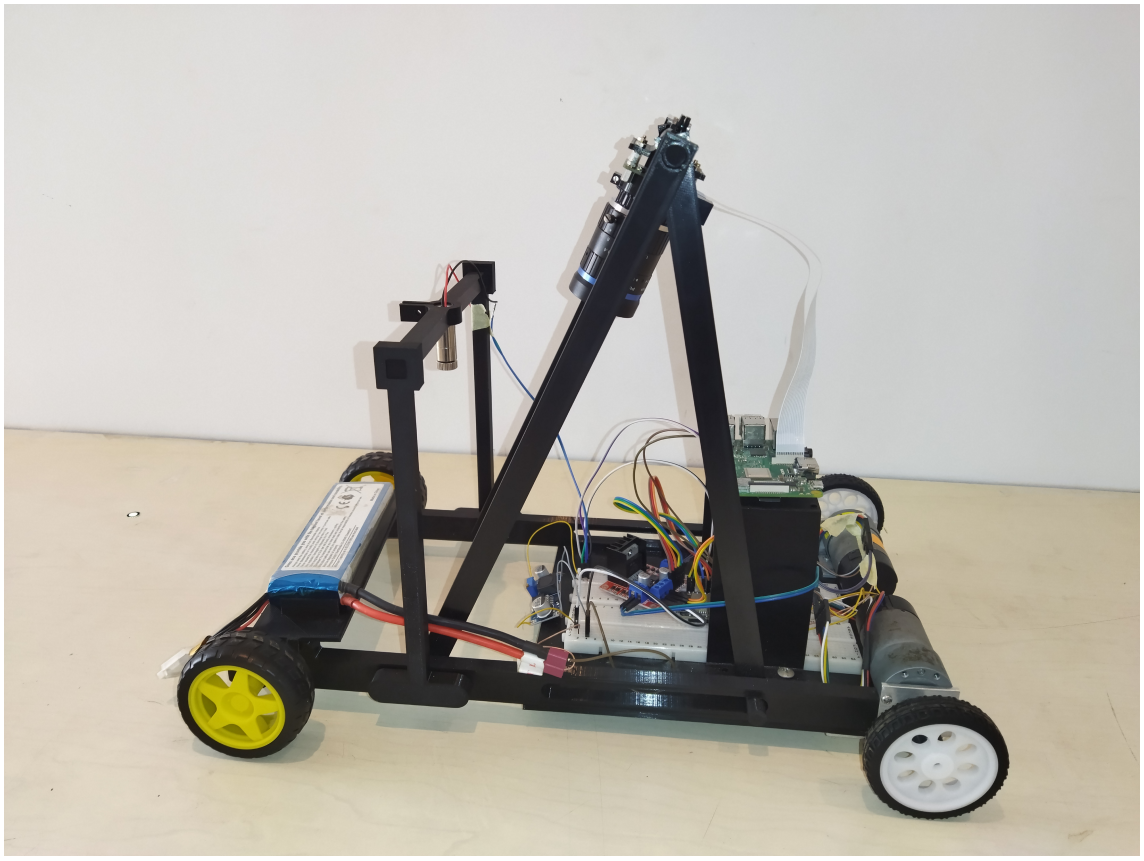

Figure 5.15: The prototype

5.4 Software implementation

In this project we worked on two phases, the first one was the development process where we validated the used algorithms and calculation methods, this phase was approached using Matlab, the second phase (the production phase) relied on Python, and it's open source library to provide a pipeline that applies all the needed steps to take the scans.

The flow chart of the process is described in figure 5.16.

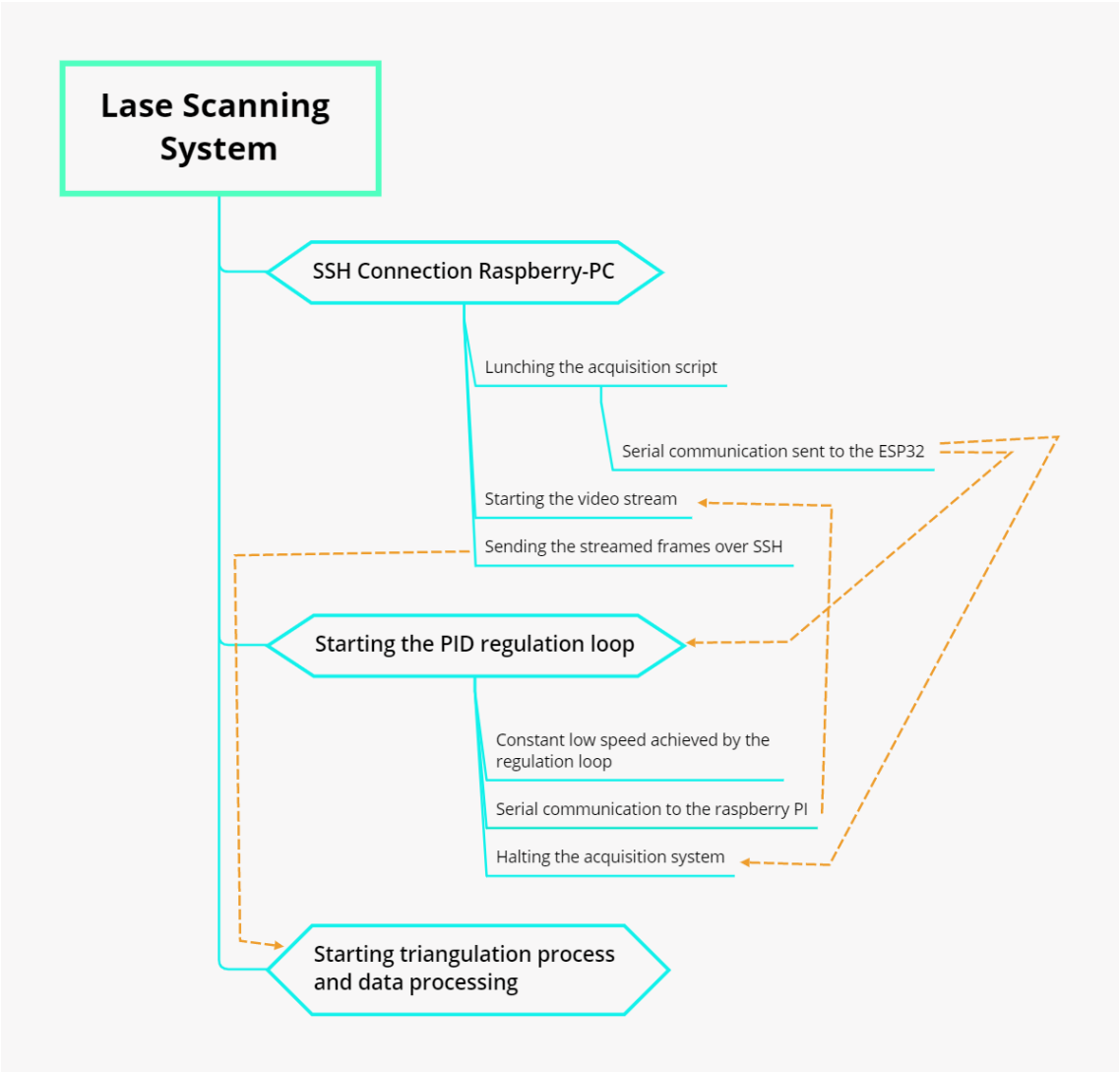

Figure 5.16: Program flow chart

5.5 Calibration in practice

As discussed in chapter **4**, before being capable of doing accurate scans, we first need to pass by a calibration process that identifies the projective model dictated by the chosen camera position and view angle.

To do this step, we 3D printed a rectangle containing circles with known dimensions and positions, this asset is presented in figure 5.17.

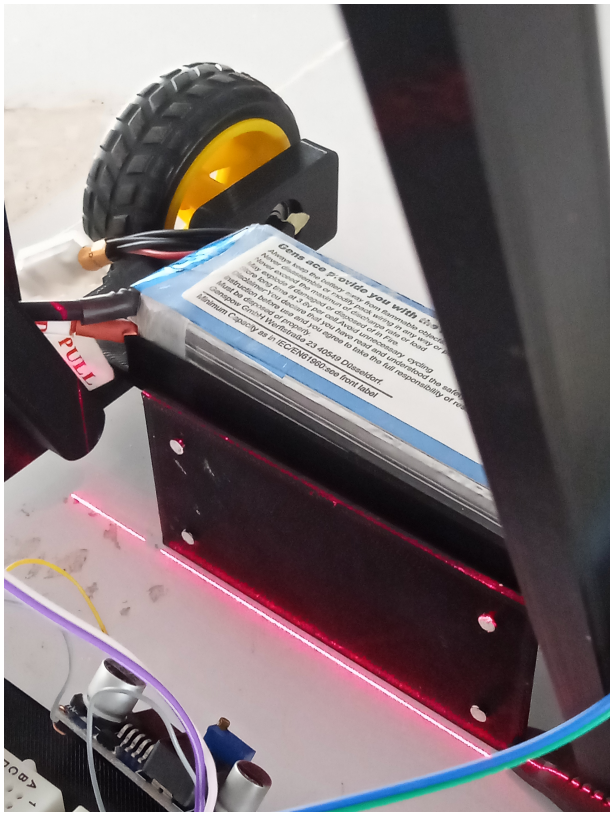

Figure 5.17: Calibration grid

the calibration grid needs to be aligned with the laser line vertical plane, then the white circles are detected and used to estimate the projection matrix discussed in chapter 4. The grid as seen with camera is presented in figure 5.18 after being binarised

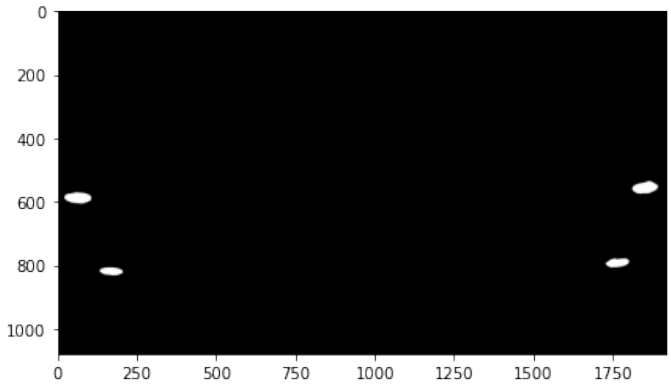

Figure 5.18: Binarised calibration grid

The center of each white circle in the corners is estimated by averaging the white pixels coordinates. The presented system achieved a resolution of 0.05*0.17 mm in the x and z coordinates respectively. The results are discussed in the last chapter.

Conclusion

In this chapter, we discussed the approach we have chosen to satisfy the theoretical need described earlier, we proposed a first prototype designed to be a proof of concept of a laser scanner specialized in surface characterization, figure 5.19 shows the overall process we conducted to arrive to the 3D cloud points of a pavement surface we scanned using our prototyped scanner, using the current configuration we achieved a resolution of 0.04*1*0.17 mm in the x, y and z axis.

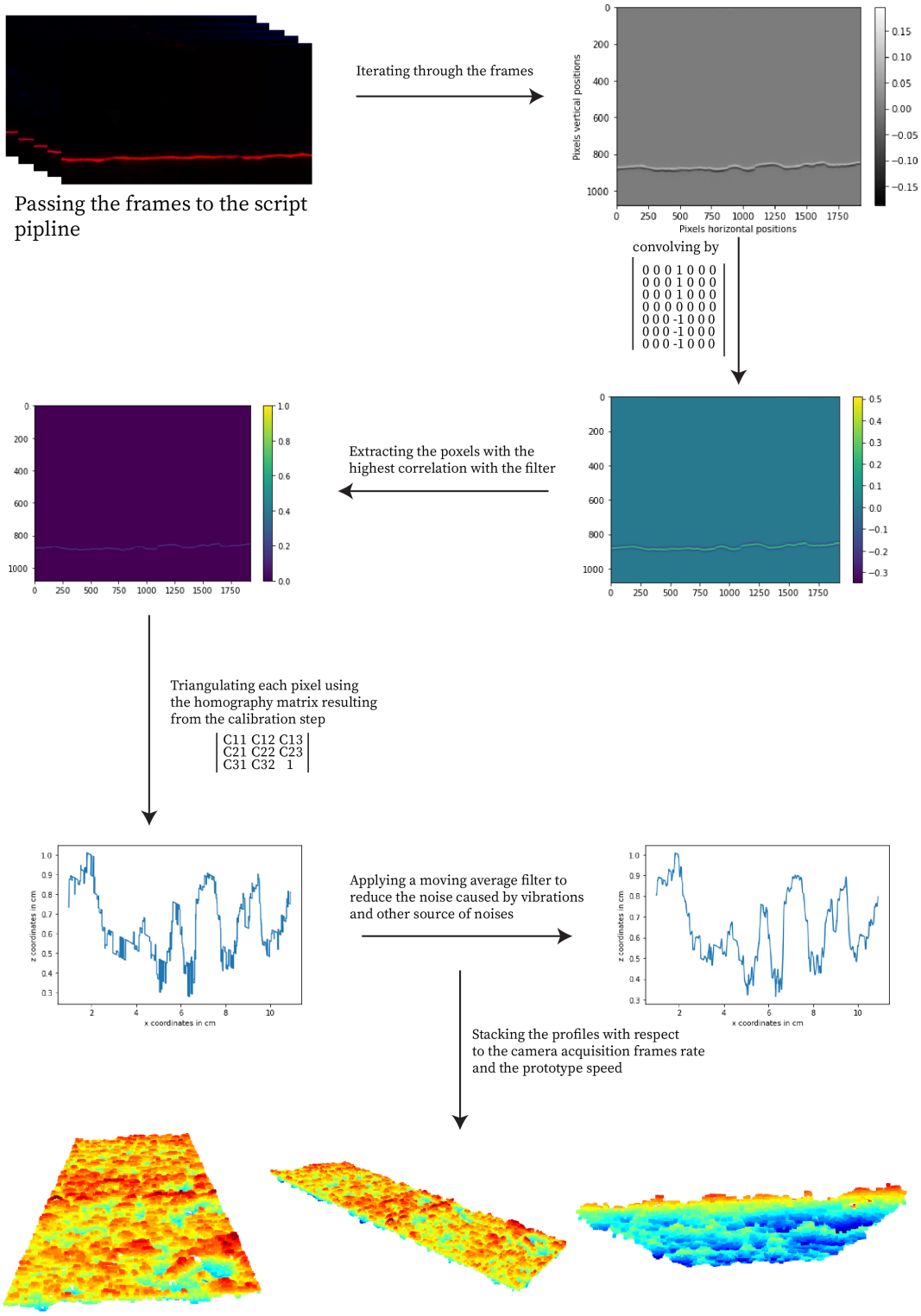

Figure 5.19: Surface scanning process

Chapter 6

Experimental results and validation

Introduction

In this final chapter of our work, we test the built prototype to study its behavior and ensure that it performs as intended.

A series of tests on different geometries are made to validate the resilience of the scanner to different shapes. A test protocol that needs to be followed is established, in order to analyze the different results it gives when scanning pavement surfaces in particular, by comparing them to results given by the traditional sand patch method as well as measurements provided by a high-precision scanner.

6.1 Testing the instrument resilience with different shapes

First, before approaching our pavement surface characterization problem, we aim to validate the information provided by the prototyped instrument using different shapes and patterns, we conduct a visual inspection to see whether the instrument is providing reliable and precise measurements by comparing the provided cloud points with the visual appearance of the object.

6.1.1 Scanning tiles with geometrical patterns

The first trial we have done was to scan a tile present on figure 6.1, it contains visually recognizable patterns that can be distinguished and compared, therefore we present a real image of the tile and then compare it with the scan information, the tile contains some interesting irregularities such as small pebbles, dust and some appearing cracks.

the image in the right is taken for the scanned cloud points, where the color variation represents height (the z value).

Comparing the image with the scanned cloud points shows how precise the instrument is in terms of keeping the visual information. Figure 6.2 shows interesting patterns of irregularities on the surface, such as a stuck chewing-gum in [1] or minimal cracks in [2] and [3] (see figure 6.2) that the scanner was able to detect.

6.1.2 Scanning a measurement instrument (swing arm protractor)

The next step was to scan a very small in dimensions object that has about 2 mm elevation from the ground, the instrument was scanned with a resolution of 0.04*1*0.17 mm in the three axis. Figure 6.3 we show multiple views of the scanned object and the corespondent point cloud.

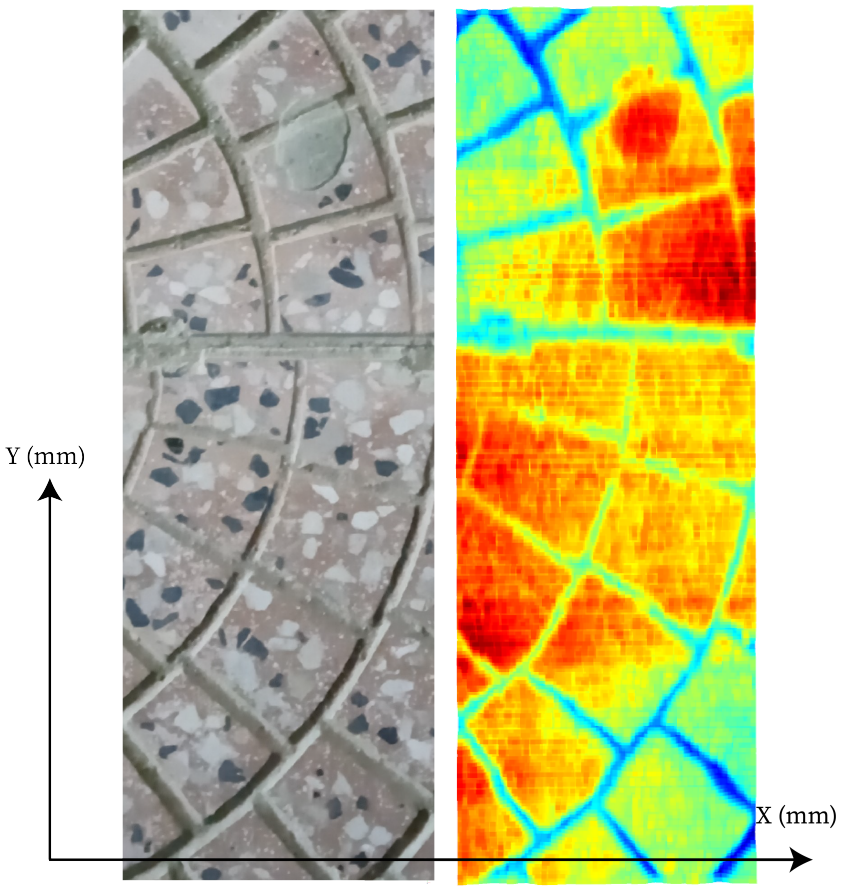

Figure 6.1: A picture and the scanned cloud points of tile surface

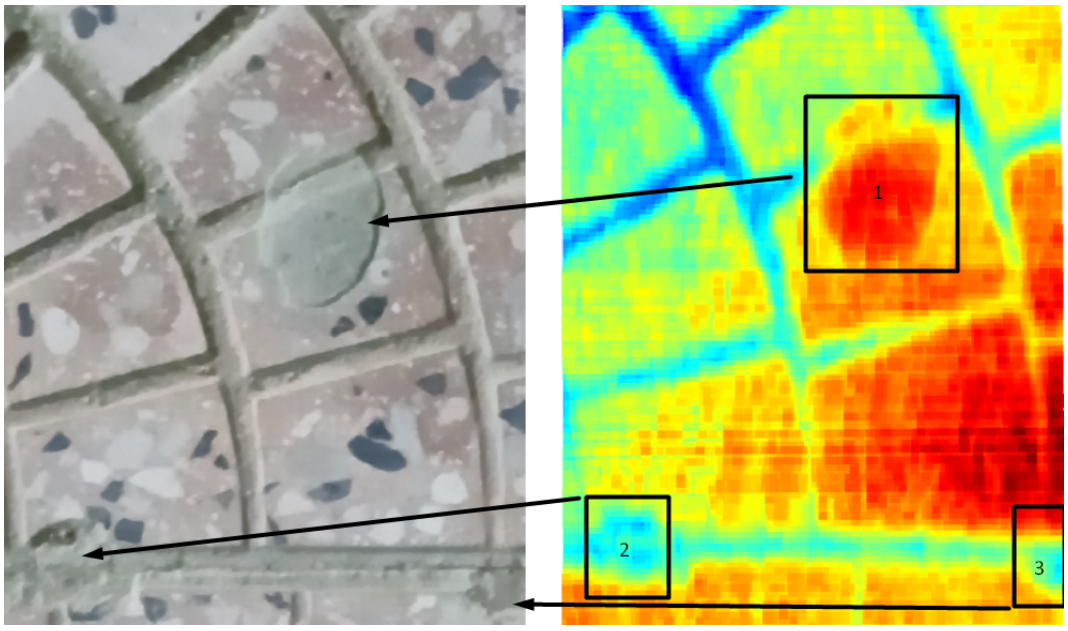

Figure 6.2: Valuable information detected by the scanner

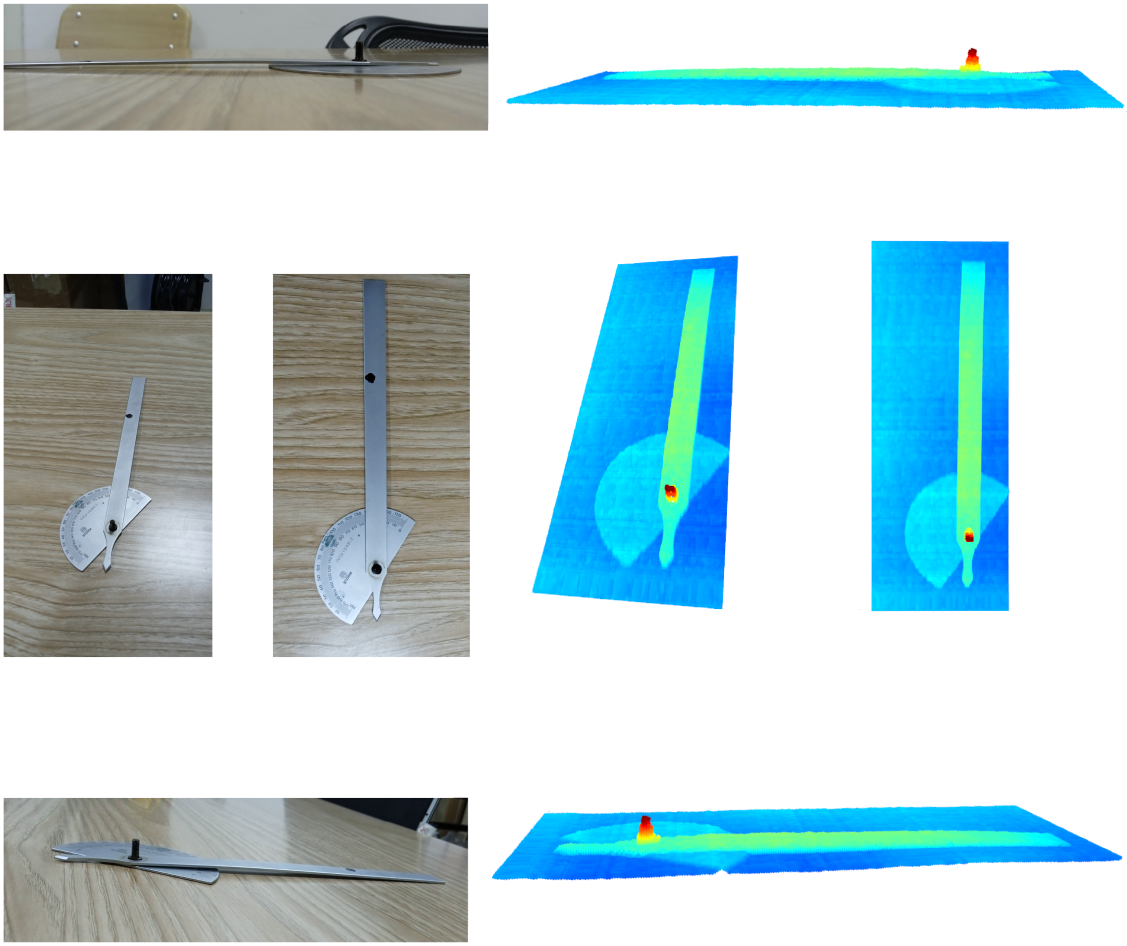

Figure 6.3: Scanning a swing arm protractor

6.2 Test plan

The testing objectives:

The main object of this step of our project is to validate the results given by the built prototype on pavement surfaces and to study the influence of various parameters that can be used to improve future work, the most important points to tackle are:

- Validate the chosen projective approach that allows the transition from pixels to real-life coordinates as well as the calibration process.
- Validate the data processing algorithm and the different methods that were adopted to treat the data.
- Study the influence of the incidence angle on the percentage of dropouts in our data.
- Study the influence of the resolution on the results.

The testing strategy:

In order to achieve our objectives, it is important to develop a strategy. Our strategy can be summarized as follows:

- Scan a portion of the pavement surface using the free X5 scan.
- Scan the same surface using the prototype.
- Do the texture characterization of the same portion using the volumetric method.

The measurements of the three methods will be compared in order to validate our work, the free scan X5 data will be compared to the data given by the prototype, both of these measurements will be compared afterwards to the volumetric method.

Once the validation step is done, we take various measurements, firstly varying the incidence angle in the prototype, and then varying the resolution to study the influence of these two parameters on our results.

The testing steps:

Selection of lots and test sites

- Select lots of traffic lanes and pavement that have different visual appearances.
- Select and record the location of each lot using the Global Positioning System (GPS).
- Mark the test sites.
- Make sure that the test site is dry and free from grease, or paint.
- Sweep off all dust and other loose gravel.
- Take a photo of the chosen site for future reference.

The aim is to find lots with different characteristics:

- The first set of lots includes multi-groove tiles for testing the shadowing. The deepness of the grooves is chosen according to the range of the vertical amplitude of the macrotexture which varies between 0.2 mm and 10 mm.

  The site is scanned with the prototype using different angles. The validation of the acceptable range of the angles is done according to the camera's capacity to detect areas in the grooves.

- The second set of lots includes pavement that looks visually different, this lot will be used for testing and validating the prototype in various conditions.

The validation step

- Choose different sites of the second set of lots.
- Scan the site using the X5 free scan, the data is then stored on a laptop.
- Scan the site using our prototype, the data is then stored on a laptop.
- The captured data of the two measurements is treated. The MTD is then calculated using the developed programs.
- Characterize the surface texture of the site on the exact same area that was scanned, using the volumetric method.

  For the sand patch method, the following apparatus is used:

  - A brass cylinder of known volume (25 cm^3).
  - Standard glass beads.
  - "Sand" spreader - A hard rubber disk or rubber stopper (of 65 mm diameter) for spreading the beads.
  - Steel ruler, at least 300 mm long, readable to 1 mm.

  The following steps are followed:

  - Fill the brass cylinder with beads by dipping into the container and striking off any excess.
  - Tap the base of the filled cylinder on a hard surface three times and top up the cylinder, striking off any excess.
  - Pour the contents of the cylinder onto the road surface into a small pile on the swept test site.
  - Use the sand spreader to gently work the beads down into the surface voids. Keeping the face of the sand spreader flat and applying only horizontal pressure, gently work the beads down into the surface voids in a circular spiral motion from the center outwards.
  - Continue this spreading motion until the diameter of the circle stabilizes, and the beads have completely filled the voids and the sand patch is levelled to the highest points on the surface.
  - Measure the diameter of the circle at 4 evenly spaced diameters and record these measurements.
  - Average the 4 readings to determine the average diameter (D mm) of the circle.
  - Sweep the beads off the road surface and discard.

- A report is written after the test, it includes :

  - The location of the lot, and the location of each test site within the lot.
  - Time, date, and operator undertaking the test.
  - Texture depth for each site, obtained by the sand path method, the X5 scanner and the prototype.

- The error in the measured MTD.
- A picture of the scanned site.
- The incidence angle and the resolution that were used.

6.3 Results

Unfortunately, due to the given time frame, the testing plan is not conducted entirely, however measurements are made on a region of pavement that will be discussed in this section.

- The location of the lot: the road next to the Fablab, Polytechnic School of Algiers.
- The location of the site: 36.72372451980683, 3.1502540516420163
- Date and time : 01/07/2022 at 19h.
- Operator : Abdelaziz.

6.3.1 The freescan X5 laser results

The resolution: 0.25 mm in all three axis.

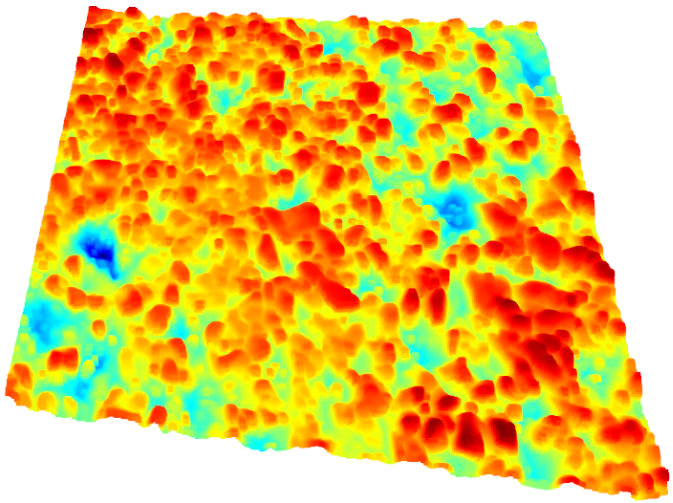

Figure 6.4: The point cloud given by the FreeScan X5

6.3.2 The prototype results

- The angle: 20°.
- The resolution: 0.04*1*0.17 mm.
- The laser line length L_x: 80 mm.
- The length in the y direction L_y: 267 mm.

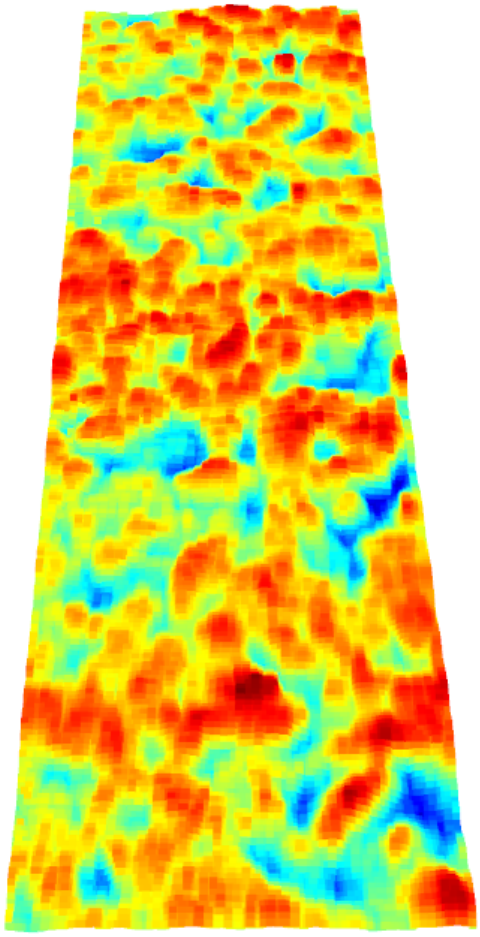

Figure 6.5: The point cloud given by the prototype

6.3.3 The sand patch method results

The detailed steps of the sand patch method are followed, the result is shown in figure 6.6

$$D = \frac{17 + 15 + 16.5 + 15}{4}$$

$$D = 15.75\, cm$$

6.3.4 Comparative discussion

Method	Sand patch	FreeScan X5	Prototype
MTD (mm)	1.28	1.99	2.02

Table 6.1: Summary of the comparative study.

Figure 6.6: The sand patch method

We can observe that the results given by the two scanners are very close, there is a difference of 0.03 mm between the two values. However, the MTD, given by the sand patch method, differs from both of these values.

This difference could be explained by the fact that the examined surfaces are not exactly the same, so the presence of certain anomalies in one surface can lead to a difference in the MTD values. The difference could also be explained by the irregularities in the shape of the circle formed by the glass beads; while the method that relies on the 3D point cloud is based on a perfectly rectangular surface, the surface on which the sand patch method is based on, is not measured with much precision. This is one of the limitations of the classic method for characterizing the pavement surface texture.

We can also notice that even though the FreeScan X5 and the prototype have different resolutions, especially in the Y axis with the FreeScan X5 operating with a resolution of 0.25 mm and the prototype operating with a resolution of 1 mm in the y axis, they give practically the same results. This leads us to think that the influence of resolution is negligible at a certain range.

Conclusion

In this chapter, the results given by the built prototype were presented. It was found that the prototype can scan different geometries and captures their details with precision.

The validation strategy as a final step of the design process was established in the form of a test protocol that relies mainly on a comparative study with the sand patch method as well as the data given by a high precision laser scanner.

The measurement result of the study of one portion of a chosen pavement surface was presented, it was found that the laser scanners give and very close results, as for the sand patch method the result is different. This step showed also that resolution has no significant influence in a certain range.

General Conclusion

Our work constitutes a global engineering design cycle of an innovative 3D data acquisition and non-destructive approach to characterize pavement surface texture, passing by defining the problem to finding the solution, designing a first prototype, and communicating the results it gives. The problem consists of finding an efficient alternative to the already existing methods and technologies. Several solutions were taken into consideration at the earlier stages of the project, and based on the client's specifications, we found that laser triangulation is the most convenient approach for our case study, since it ensures a dense acquisition of the data and can perform at high speed.

The manipulation of the data that was collected in prior work using a laser triangulation system shows certain errors, and since our objective in the short term is to develop a system that gives reliable measurements, a particular focus was given to the data processing step. The simplest and most efficient methods are adopted, and were summarized in the form of a standard algorithm. A new approach to evaluate the MTD to simulate the traditional method was proposed, the results given by the treated data are promising and correspond perfectly with the measurements of the sand patch method.

The built prototype consists mainly of a camera and a laser projector. The mechanical body of the prototype was designed with respect to these two components characteristics. It takes the form of a four wheeled motorized robot that travels at a constant speed. The resolution of the system depends on the resolution and the frame rate of the camera, as well as the speed of travel. The prototype is manufactured with 3D printing. The used hardware allowed us to achieve a resolution of 0.04 * 1 * 0.17 mm, which is a very interesting result considering the expenses spent on the prototype.

In the last chapter a series of tests was carried out, the results show an accurate recreation of 3D replicas of the scanned objects using the prototype. The MTD calculated by the proposed instrument and the professional laser scanner used for comparison exhibit a perfect coherence. The manipulation shows a lack of accuracy of the traditional sand patch method due to the manual work that needs to be done since it was difficult to create a perfectly circular shape, leading to an error in the patch diameter estimation, which introduces an error in the MTD.

Overall, we can conclude that the objectives were mostly met with our prototype. Further work and certain changes need to be done:

- Replacing the current camera with a high speed camera: this can drastically augment the resolution of our laser scanner in the Y axis as well as the speed of scanning. The scanner will be capable of performing the triangulation process while moving at traffic speed, without causing any latencies. However, achieving this objective requires a camera that has a frame rate of around 10 000 per seconds.

- Replacing the current laser with a green light laser: the use of a green light instead of the red one reduces the influence of the daylight interference. In order to enable the usage of the device in daylight, it is preferable to use a more intense laser as well as covering the prototype to shield it from external influence.

- Using a gyroscope to minimize the vibrations in the data caused by the instrument movement, the signals coming from the gyro are recorded so that we can have a real

time information of the absolute position of the camera. This information can be used to remove the noise introduced to the data by the vibrations.

- Changing the manufacturing procedure in order to optimize the time of production and using a different material that is more rigid and resistant to the different constraints to which the prototype is subjected.

Bibliography

[1] E. 13036-1, *Road and airfield surface characteristics — test methods — part 1: Measurement of pavement surface macrotexture depth using a volumetric patch technique*, 2010.

[2] B. Bhushan, "Surface roughness analysis and measurement techniques," in *Modern tribology handbook, two volume set*, CRC press, 2000, pp. 79–150.

[3] P. Ettl, B. Schmidt, M. Schenk, I. László, and G. Häusler, "Roughness parameters and surface deformation measured by coherence radar," *Proc SPIE*, vol. 3407, pp. 133–140, Sep. 1998. DOI: 10.1117/12.323304.

[4] *Characterizing Surface Quality Through 3D Parameters: Why 2D Average Roughness Alone Is No Good*, vol. Volume 5: Education and Globalization, ASME International Mechanical Engineering Congress and Exposition, V005T06A013, Nov. 2017. DOI: 10.1115/IMECE2017-72229. eprint: https://asmedigitalcollection.asme.org/IMECE/proceedings-pdf/IMECE2017/58400/V005T06A013/2499552/v005t06a013-imece2017-72229.pdf.

[5] C. Thigpen, H. Li, S. Handy, and J. Harvey, "Modeling the impact of pavement roughness on bicycle ride quality," *Transportation Research Record: Journal of the Transportation Research Board*, vol. 2520, pp. 67–77, Jan. 2015. DOI: 10.3141/2520-09.

[6] S. Callai and C. Sangiorgi, "A review on acoustic and skid resistance solutions for road pavements," *Infrastructures*, vol. 6, p. 41, Mar. 2021. DOI: 10.3390/infrastructures6030041.

[7] I. 13473-2:2002, *Characterization of pavement texture by use of surface profiles — part 2: Terminology and basic requirements related to pavement texture profile analysis*, 2002.

[8] 1.-1. 2019, *Characterization of pavement texture by use of surface profiles—part 1: Determination of mean profile depth*, 2019.

[9] U. Sandberg, *Influence of road surface texture on traffic characteristics related to environment, economy and safety: A state-of-the-art study regarding measures and measuring methods*. Statens väg-och transportforskningsinstitut., VTI notat 53A-1997, 1998.

[10] J. Kragh, B. Andersen, and J. Oddershede, "Road surface texture-low noise and low rolling resistance," *Report Danish Road Directorate*, no. 188, 2010.

[11] T. Vieira, U. Sandberg, and S. Erlingsson, "Negative texture, positive for the environment: Effects of horizontal grinding of asphalt pavements," *Road Materials and Pavement Design*, vol. 22, no. 1, pp. 1–22, 2021.

[12] Wikipedia, *Whole body vibration — Wikipedia, the free encyclopedia*, http://en.wikipedia.org/w/index.php?title=Whole%20body%20vibration&oldid=1061973337, [Online; accessed 28-April-2022], 2022.

[13] E. Freitas, P. Pereira, M. Antunes, and P. Domingos, "Analysis of test methods for texture depth evaluation applied in portugal," Apr. 2022.

[14] E. David, L. Izeppi, G. Flintsch, *et al.*, "Non-contact methods for detecting hot-mix asphalt nonuniformity," Apr. 2022.

[15] F. Praticò and R. Vaiana, "A study on the relationship between mean texture depth and mean profile depth of asphalt pavements," *Construction and Building Materials*, vol. 101, pp. 72–79, 2015, ISSN: 0950-0618. DOI: https://doi.org/10.1016/j.conbuildmat.2015.10.021.

[16] H. B. KIM, S. W. LEE, T.-J. Hyun, and K. H. Lee, "Measurement of texture depth of pavement using potable laser profiler," *Journal of the Eastern Asia Society for Transportation Studies*, vol. 10, pp. 1576–1589, 2013.

[17] A. E2380/E2380M-15(2019), *Standard test method for measuring pavement texture drainage using an outflow meter*, 2019.

[18] D. D. Gransberg, "Characterizing existing surface condition to evaluate chip seal performance," Tech. Rep., 2007.

[19] A. E1926-08(2021), *Standard practice for computing international roughness index of roads from longitudinal profile measurements*, 2021.

[20] E. 13036-5:2019, *Road and airfield surface characteristics - test methods - part 5: Determination of longitudinal unevenness indices*, 2019.

[21] A. Loizos and C. Plati, "Evolutional process of pavement roughness evaluation benefiting from sensor technology," *International Journal on Smart Sensing and Intelligent Systems*, vol. 1, Jan. 2008. DOI: 10.21307/ijssis-2017-295.

[22] P. Múčka, "International roughness index specifications around the world," *Road Materials and Pavement Design*, vol. 18, no. 4, pp. 929–965, 2017.

[23] M. Faria, F. Oliveira, and G. Pimentel-Junior, "Acoustic emission tests on the analysis of cracked shafts of different crack depths," Dec. 2015. DOI: 10.20906/CPS/COB-2015-1434.

[24] J. Ren, X. Jiang, and J. Yuan, "A chi-squared-transformed subspace of lbp histogram for visual recognition," *IEEE transactions on image processing : a publication of the IEEE Signal Processing Society*, vol. 24, Mar. 2015. DOI: 10.1109/TIP.2015.2409554.

[25] Y. Li, Q. Shi, Y. Li, *et al.*, "High-resolution bone microstructure imaging based on ultrasonic frequency-domain full-waveform inversion∗," *Chinese Physics B*, vol. 30, no. 1, p. 014 302, Jan. 2021. DOI: 10.1088/1674-1056/abc7aa.

[26] A. Q. Bhatti, A. Wahab, and W. Sindi, "An overview of 3d laser scanning techniques and application on digitization of historical structures," *Innovative Infrastructure Solutions*, vol. 6, no. 4, pp. 1–9, 2021.

[27] M. A.-B. Ebrahim, "3d laser scanners' techniques overview," *Int J Sci Res*, vol. 4, no. 10, pp. 323–331, 2015.

[28] A. Abdelhafiz, *Integrating digital photogrammetry and terrestrial laser scanning*. Techn. Univ., Inst. für Geodäsie und Photogrammetrie, 2009.

[29] J. L. Vilaça, J. C. Fonseca, and A. M. Pinho, "Non-contact 3d acquisition system based on stereo vision and laser triangulation," *Machine Vision and Applications*, vol. 21, no. 3, pp. 341–350, 2010.

[30] B. Chen, C. Xiong, W. Li, J. He, and X. Zhang, "Assessing surface texture features of asphalt pavement based on three-dimensional laser scanning technology," *Buildings*, vol. 11, no. 12, p. 623, 2021.

[31] A. Peiravi and B. Taabbodi, "A reliable 3d laser triangulation-based scanner with a new simple but accurate procedure for finding scanner parameters," *Journal of American Science*, vol. 6, no. 5, pp. 80–85, 2010.

[32] J. Forest Collado *et al.*, *New methods for triangulation-based shape acquisition using laser scanners*. Universitat de Girona, 2004.

[33] J. Bloomenthal and J. Rokne, "Homogeneous coordinates," *The Visual Computer*, vol. 11, no. 1, pp. 15–26, 1994.

[34] C. Chen and A. Kak, "Modeling and calibration of a structured light scanner for 3-d robot vision," in *Proceedings. 1987 IEEE International Conference on Robotics and Automation*, IEEE, vol. 4, 1987, pp. 807–815.

[35] K. J. Stout, "The development of methods for the characterisation of roughness in three dimensions," *Commission of the european communities. Luxembourg*, vol. 130, 1993.

[36] E. Mainsah, J. A. Greenwood, and D. G. Chetwynd, *Metrology and properties of engineering surfaces*. Springer Science & Business Media, 2001.

[37] D. E. M. Carrasco, "Enhancing pavement surface macrotexture characterization," Ph.D. dissertation, Virginia Polytechnic Institute and State University, 2015.

[38] N. Dong, J. A. Prozzi, and F. Ni, "Reconstruction of 3d pavement texture on handling dropouts and spikes using multiple data processing methods," *Sensors*, vol. 19, no. 2, p. 278, 2019.

[39] H. Pasindu, S. Bandara, W. Mampearachchi, and T. Fwa, "Road and airfield pavement technology,"

[40] A. Gramacki, *Nonparametric kernel density estimation and its computational aspects*. Springer, 2018, vol. 37.

[41] L. Goubert and K. Samer, "Spike removal from texture profiles: A comparison of two approaches," in *Symposium on Pavement Surface Characteristics (SURF), 8th, 2018, Brisbane, Queensland, Australia*, 2018.

[42] B. Özcan, R. Schwermann, and J. Blankenbach, "A novel camera-based measurement system for roughness determination of concrete surfaces," *Materials*, vol. 14, no. 1, p. 158, 2020.

[43] Q. Liu, "Three-dimensional pavement surface texture measurement and statistical analysis," 2015.

[44] B. Aktaş, D. Gransberg, C. Riemer, and D. Pittenger, "Comparative analysis of macrotexture measurement tests for pavement preservation treatments," *Transportation Research Record: Journal of the Transportation Research Board*, vol. 2209, pp. 34–40, Dec. 2011. DOI: 10.3141/2209-05.